7-24-2017 9:30 AM

Hepatic Drug Metabolism, Uremic Toxins and Bacterial Composition Over Chronic Kidney Disease Progression

Emily Dee Hartjes
The University of Western Ontario

Supervisor
Dr. Brad Urquhart
The University of Western Ontario

Graduate Program in Physiology and Pharmacology
A thesis submitted in partial fulfillment of the requirements for the degree in Master of Science

Abstract

Uremic toxin retention and an altered gut microbiota are suspected to influence cytochrome P450s (CYPs) contributing to the unpredictable pharmacokinetics in chronic kidney disease (CKD). We aim to characterize dysbiosis and uremia to elucidate associations between CYP expression and CKD progression. Rats fed control or CKD-inducing diet were subsequently sacrificed across five time points over 42 days. CYP expression and activity were compared to alterations in the 1) plasma and liver metabolome and 2) bacterial microbiota. CYP3A2 and CYP2C11, respectively, were downregulated in CKD by ≥76% ($p<0.001$) simultaneously or slightly premature to CKD onset defined by creatinine. Metabolite profiles were altered before the gut microbiota and gut-derived uremic toxins including indoxyl sulfate, phenyl sulfate and 4-ethylphenyl sulfate correlated with CYP3A2 or CYP2C11. Identified bacterial genera, Turicibacter and Parabacteroides, characterized CKD and require future study. In conclusion, CYP3A2 and CYP2C11 are downregulated prior to dysbiosis but correlate with select uremic toxins.

Keywords

Uremia, gut microbiota, dysbiosis, cytochrome P450, metabolomics, sequencing

Acknowledgments

This project might not have been about chronic kidney disease if Dr. Brad Urquhart had not so eagerly agreed to have me join the lab. Your enthusiasm about research and teaching has made the lab an enjoyable place of discovery for all your students. Your unwavering support and guidance has never once allowed me to feel like I was pressured, alone or unable to achieve something. This is in part due to your presence in and out of the lab, which is not only impressive but extremely helpful when obstacles like a Mass Spec error seem pitted against you. It is also because you value equality, allowing students to form their own opinions and become independent voices in the scientific community. Even though my aspirations are taking me off the academia path, for now, you have taught me more than how to test hypotheses and be successful in research. You have been a role-model of work-life balance, networking skills I never knew possible, and professionalism while still being human. I truly thank you for all the time and effort you have invested in me.

Next, I would like to thank my lab family whom I've grown very close with over the last year. As I start a new stage in my life, I realize how truly sad I am to be leaving my closest friends. Each of you have taught me so much about friendship, life and science while supporting an amazing place to express ourselves and feel included while at work. I wish you all the best in finding your passion and continue enjoying what you do.

Tom Velenosi requires a shout-out for trying his best to integrate me into the previously male dominated lab group. Thank you for not just showing me the ropes, but also for truly caring about my work's integrity, time spent making mistakes and the overall learning experience. As I go on to teach others, I aim to be as thorough in my explanations and as honest about conclusions as you were with me.

Lastly, the support and understanding I received from my family and other-half Kyle Rupay, has allowed me to overcome the unavoidable stresses of graduate school. Simple gestures like making dinner or telling me to stop doubting myself, made my time out of the lab a de-stressing environment. Down-time spent with you made getting back to work, a challenge rather than a chore.

Ultimately, I want to thank all of those who contributed to my time at Western, in and out of research, that have helped me grow, nail down my values and provide direction for my future.

Author Contributions

Study design and experiments including animal husbandry, sample collection, sample preparation, drug metabolizing enzyme quantification, UPLC/MS operation and DNA extraction for bacterial sequencing was performed by the author Emily Hartjes alongside processing metabolomic and sequencing data, statistical analysis and thesis writing. In-house metabolomics R script was designed by Dr. Thomas Velenosi. Validations of qPCR primers, western blotting antibodies and testosterone assay concentrations were conducted previously by Dr. Thomas Velenosi and Dave Feere. Knowledge and mentorship with respect to data processing of bacterial sequence reads, ALDEx2 analysis and interpretation of microbiota results was provided by Dr. Greg Gloor. Andrew Kucey assisted with animal care and sample collection. Dr. Jeremy Burton and Kait Al provided DNA extraction assistance and materials. Dr. Brad Urquhart assisted in study design, thesis editing and general supervision.

Table of Contents

List of Tables

List of Figures

List of Appendices

Abbreviations

AKI	Acute Kidney Injury
ADE	Adverse Drug Event
ADR	Adverse Drug Reaction
ANOVA	Analysis of Variance
ADH	Antidiuretic Hormone
ABC	ATP Binding Cassette
ANP	Atrial Natriuretic Peptide
BCA	Bicinchoninic Acid
CVD	Cardiovascular Disease
CKD	Chronic Kidney Disease
CKD-EPI	Chronic Kidney Disease Epidemiology Collaboration
CAR	Constitutive Androstane Receptor
CONT	Control
CYP	Cytochrome P-450
POR	Cytochrome P450 Oxidoreductase
DN	Diabetic Nephropathy
DME	Drug Metabolizing Enzyme
ESI	Electrospray ionization
ESRD	End-Stage Renal Disease
EOG	Equol-4/7-O-glucouronide
eGFR	Estimated Glomerular Filtration Rate
EDTA	Ethylenediaminetetraacetic Acid
EPS	4-Ethylphenyl Sulfate
FDR	False Discovery Rate
FMO	Flavin-containing Monooxygenase
FMT	Fecal Microbial Transplantation
GI	Gastrointestinal
GFR	Glomerular Filtration Rate
GST	Glutathione S-transferase
GH	Growth Hormone
HNF-4α	Hepatocyte Nuclear Factor Alpha
HRP	Horseradish Peroxidase
HMDB	Human Metabolome Database
HMP	Human Microbiome Project
HILIC	Hydrophilic Interaction Liquid Chromatography
IS	Indoxyl Sulfate
IBD	Irritable Bowel Disease
IPO	Isotopologue Parameter Optimization
LCA	Lithocholic Acid
MS	Mass Spectrometry
Vmax	Maximal Enzyme Velocity
mRNA	Messenger RNA
Km	Michaelis-Menten constant

miRNA	Micro RNA
MDRD	Modification of Diet in Renal Disease
NGS	Next-Generation Sequencing
NADPH	Nicotinamide Adenine Dinucleotide Phosphate
Nf-kB	Nuclear Factor Kappa-light-chain-enhancer of Activated B Cells
NMR	Nuclear Magnetic Resonance
OTU	Operational Taxonomic Unit
OAT	Organic Anion Transporter
OPLS-DA	Orthogonal Partial Least Squares Discriminant Analysis
PTH	Parathyroid Hormone
PPARα	Peroxisome Proliferator-Activated Receptor Alpha
PS	Phenyl Sulfate
PCR	Polymerase Chain Reaction
PXR	Pregnane X Receptor
PCA	Principle Component Analysis
QTof/MS	Quadrupole Time-of-flight Mass Spectrometer
qPCR	Quantitative Polymerase Chain Reaction
RAAS	Renin-angiotensin-aldosterone System
RXR	Retinoid X Receptor
RPLC	Reverse Phase Liquid Chromatography
rRNA	Ribosomal RNA
SCFA	Short-Chain Fatty Acid
SNP	Single Nucleotide Polymorphism
SDS	Sodium Dodecyl Sulfate
SLC	Solute Carrier
SEM	Standard Error of the Mean
SULT	Sulfotransferase
TEMED	Tetramethylethylenediamine
TMAO	Trimethylamine-N-oxide
UGT	UDP-glucuronosyltransferase
UPLC	Ultra-Performance Liquid Chromatography
VIP	Variable Importance in Projection
VDR	Vitamin D Receptor

Chapter 1

1 Introduction

1.1 Preface

Understanding biological systems is quickly becoming a multidimensional and multidisciplinary effort. With the wealth of technological advances in biological methodology, study of whole-organism physiology has become a reality. The combination of "omics" methods such as metabolomics and sequencing of the microbiome has provided the opportunity to compare whole-system host physiological processes. Our era of public databases and data sharing allows blinded discovery of complex biological fingerprints without requiring the identity of any individual sequence or metabolite. This exploratory and hypothesis-forming science supports big questions about phenotype and disease states with relation to dependent bodily systems such as the gut microbiome and host metabolome (Nicholson *et al.*, 2005). In this thesis, detectable host gut bacteria and metabolomic profiles are characterized and related to altered drug metabolism over the progression of chronic kidney disease (CKD).

1.2 Renal Physiology

The kidney is an essential organ responsible for excretion of harmful biological waste products while simultaneously maintaining water, electrolyte, nutrient and pH balance (Reese *et al.*, 2011). Nephrons, the functional units of the kidney, filter water, urea and all other molecules excluding large proteins and red blood cells at the glomerulus. Immediately following filtration, reabsorption back into the bloodstream begins in the proximal tubule where active transport of sodium stimulates the reabsorption of water, chloride, glucose and amino acids (Reese *et al.*, 2011). Most water reabsorption occurs in the descending limb of the loop of Henle, effectively concentrating the urine. Further reabsorption of sodium and chloride ions occurs in the water impermeable ascending limb. The distal tubule performs fine adjustments in salt and ion concentrations by activation of

the renin-angiotensin-aldosterone system (RAAS) (Reese *et al.*, 2011). In short, macula densa cells detect decreased sodium levels of the filtrate in the distal tubule and signal to juxtaglomerular cells of the afferent or efferent arteriole to produce renin. Renin released into the bloodstream sends a signalling cascade through angiotensinogen, angiotensin I, angiotensin II and finally aldosterone to increase the reabsorption of sodium at the distal tubule. The filtrate then reaches the collecting duct where it may be further influenced by antidiuretic hormone (ADH) or atrial natriuretic peptide (ANP) depending on the persisting imbalance of either nutrients or arterial pressure, respectively (Reese *et al.*, 2011). Urea, a small molecule responsible for removing harmful ammonia is recycled from the collecting duct filtrate and used to increase the osmolarity at the earlier descending loop of Henle allowing for more water to be reabsorbed (Reese *et al.*, 2011). After the urea helps reabsorb water, it returns to the final filtrate and is excreted in the urine. Besides maintaining water, pH and electrolyte balance, the kidney eliminates toxic metabolites, controls blood pressure and produces renin, erythropoietin, prostaglandins and activated vitamin D (Reese *et al.*, 2011).

1.3 Chronic Kidney Disease

1.3.1 Prevalence

Chronic kidney disease (CKD) is a progressive and irreversible loss of kidney function heavily associated with age, obesity and diabetes (Levey *et al.*, 2003; O'Hare *et al.*, 2007; Zhou *et al.*, 2008; Kopple, 2010; Hahr & Molitch, 2015). An estimated three million Canadians (12.5%) are affected by renal insufficiency or complete renal failure but inconsistencies in identifying earlier stages of CKD suggest prevalence may be even higher (Jha *et al.*, 2013; Arora *et al.*, 2013). In 2015, the number of Canadians aged 65 years or older (16.1%) was higher than those aged 0-14 for the first time in history, and projections suggest this will increase to 20.1% by 2024 (Statistics Canada, 2015). In addition to an aging population, a staggering 24.8% of Canadians over 18 years of age have a body mass index classified as obese which increased by 17.5% from 2003 (OECD, 2011). As a result, the prevalence of insulin resistance in the form of diabetes mellitus, the most common cause of CKD, is also expected to increase (Hahr & Molitch, 2015; Wouters *et al.*, 2016).

Thus, the national health care burden of CKD is extensive and projected to increase along with these associated demographics (Manns *et al.*, 2007). Alongside Canada, 16% of the global population is affected by CKD in other aging or obese countries such as Taiwan, USA, Japan, Portugal, Belgium and South Korea (Jha *et al.*, 2013). More recently, developing countries such as Nepal, Sri Lanka, Mexico and many locations in India are experiencing prevalent CKD because of insufficient health care and access to renal therapies (Abraham *et al.*, 2016).

1.3.2 Causes & Comorbidities

There is no singular blanketing CKD pathophysiology due to the many causes and comorbidities across individuals. Kidney damage is most commonly mediated by hypertension or diabetic nephropathy although acute kidney injury (AKI), lupus nephritis or genetic variations such as polycystic kidney disease may translate into CKD later in life (Levey *et al.*, 2003).

Hypertension is both a stimulus and consequence of CKD. Persistently increased blood pressure can induce thickening and subsequent narrowing of the arterioles entering the glomerulus. This decreases the glomerular pressure reducing the amount of filtrate entering the proximal tubule and sequentially decreases urine output (Hall *et al.*, 2014). A healthy kidney experiencing reduced glomerular pressure produces renin to retain sodium and water to increase blood volume and heart rate. The injured kidney will also activate the RAAS system but this increases the blood flow through narrow arteries promoting fluid retention (Sereno *et al.*, 2016). Thus, an increased fluid volume worsens glomerular pressure, further contributing to hypertension and leading to edema, cardiovascular stress and heart disease (Tedla *et al.*, 2011). Additionally, lack of blood flow to the kidney can cause glomerulosclerosis or hardening of the capillaries required for filtration. This triggers ischemia and eventually nephron death (Sugiyama *et al.*, 1996; Tedla *et al.*, 2011).

Diabetic nephropathy (DN) is an anticipated outcome for 40% of diabetics (Gross *et al.*, 2005; Hahr & Molitch, 2015). Although controversial, some research suggests that strictly maintaining glucose levels reduces the rate at which pathologies such as mesangial cell expansion and proliferation, podocyte death and glomerulosclerosis manifest. However,

other factors such as hormone regulation and inflammation are also suspected to have a role in DN onset (Schena, 2005). DN can be organized into four severity classes, the final being glomerulosclerosis which eventually leads to nephron death (Tervaert *et al.*, 2010).

1.3.3 Detection & Progression

CKD is an irreversible disease because following nephron death, undamaged nephrons acquire the added filtration load in a condition called glomerular hyperfiltration (Kopple, 2010). This usually occurs in early stages of CKD when the kidney has reduced but adequate function. Unfortunately, overworked nephrons eventually succumb to glomerulosclerosis, vascular sclerosis and tubulointerstitial fibrosis responsible for the transition into late-stage CKD.

To eliminate variance caused by multiple pathologies, the National Kidney Foundation has clinically defined CKD as a progressive loss of renal function by measuring glomerular filtration rate (GFR). The GFR is the volume of filtrate produced by glomeruli over time and surface area expressed in units of ml/min/1.73m^2. Normal GFR ranges between 120-130 ml/min/1.73m^2, but this decreases with age by about 1ml/min/1.73m^2 per year (Levey *et al.*, 2003). An estimated GFR (eGFR) is arguably the least invasive and most effective method of CKD assessment. It relates patient age, sex, race and body mass with a measurement of the disease marker creatinine by a common eGFR calculation. Creatinine is a normal by-product of non-enzymatic creatine degradation that remains relatively constant from day to day (Wyss & Kaddurah-Daouk, 2000). Creatinine remains the biomarker of choice because of its unhindered filtration through the glomerulus and minimal reabsorption (Lopez-Giacoman, 2015). However, creatinine has limited accuracy not only because it is dependent on diet and muscle mass but it is also secreted via the proximal tubule. In severe CKD, hypersecretion of creatinine can exaggerate the estimate of GFR (Shemesh *et al.*, 1985). Examples of eGFR calculations are the Modification of Diet in Renal Disease (MDRD) equation and Chronic Kidney Disease Epidemiology Collaboration (CKD-EPI) equation, the latter of which is newer and has received more support for its improved accuracy over the MDRD method (Stevens *et al.*, 2010; Arora *et al.*, 2013).

Changes in GFR can be preceded by proteinuria which is known to indicate CKD risk earlier than GFR, especially in diabetic patients (Gross *et al.*, 2005). Proteinuria is the amount of albumin or any other protein normally unable to escape the bloodstream that is allowed to enter the urine due to structural epithelial malfunctions at the glomerulus (Satchell & Tooke, 2008). Albuminuria is solely the loss of albumin. Microalbuminuria is considered moderately increased and macroalbuminuria severely increased levels of albumin (Hahr & Molitch, 2015). Albuminuria is commonly expressed as a ratio of albumin to creatinine where a level under 30mg/g is normal, 30-200mg/g is indicative of early to moderate CKD and a level over 200mg/g is indicative of late-stage CKD (Levey *et al.*, 2003).

Kidney disease has five clinically identified stages defined by the National Kidney Foundation (Levey *et al.*, 2003) (Figure 1.1). Stage 1 represents kidney damage detectable by albuminuria but expressing a normal GFR >90ml/min/1.73m^2. Stage 2 is kidney damage with GFR between 60-89ml/min/1.73m^2. To be categorized as having moderate CKD, a patient must have a GFR <60ml/min/1.73m^2 or kidney damage that has persisted for over three months. This definition can also be classified as Stage 3 with a GFR between 30-59ml/min/1.73m^2. Severe CKD begins in Stage 4 with a GFR between 15-29ml/min/1.73m^2 and requires extensive pharmaceutical interventions to combat comorbidities such as hypertension, diabetes and cardiovascular diseases (CVD). End-stage renal disease (ESRD) specifically refers to patients requiring renal replacement therapies such as dialysis or kidney transplantation to sustain life and generally include Stage 5 CKD patients with kidney failure or a GFR <15ml/min/1.73m^2. Dialysis modalities include hemodialysis or peritoneal dialysis where the blood of a patient is filtered through a dialysis membrane simulating the filtering function of a kidney (Luo *et al.*, 2011).

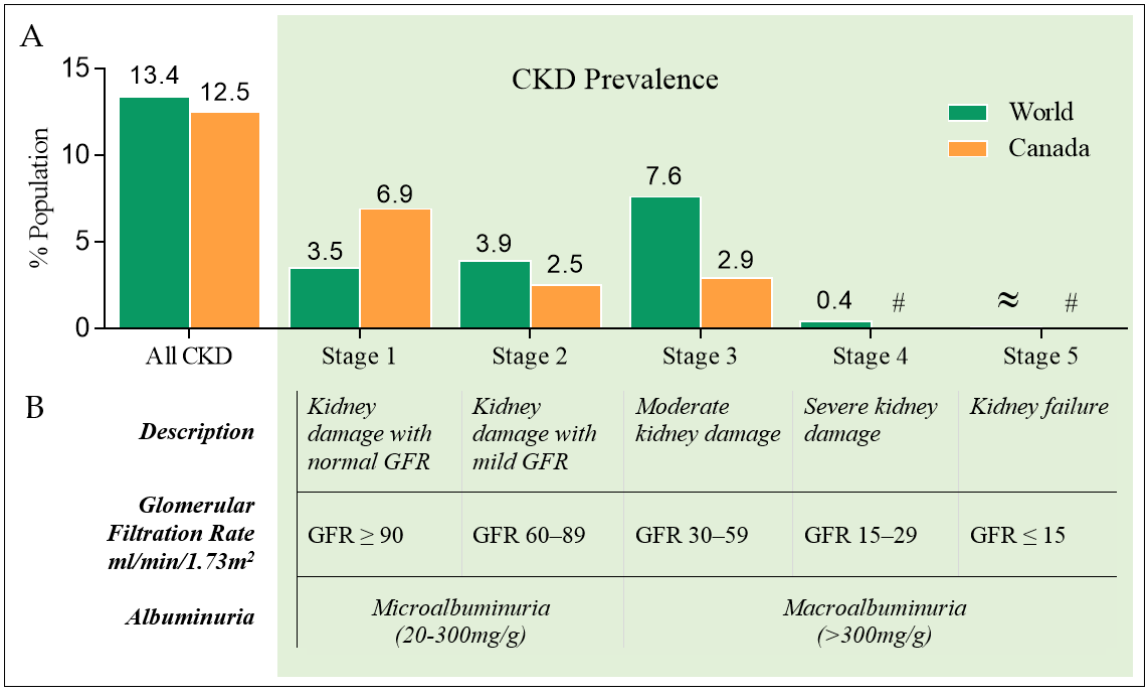

Figure 1.1. Prevalence and clinical stages of CKD. A) Canadian and worldwide prevalence of all CKD and CKD stages 1-5. B) Description, GFR and albuminuria guidelines with respect to CKD stages 1-5. # Prevalence estimate cannot be reported due to low sample size and variability (coefficient of variation > 33.3%); ≈ 0.1% world population. Adapted from (Levey *et al.*, 2003; Smink *et al.*, 2012; Arora *et al.*, 2013; Hill *et al.*, 2016).

1.3.4 Clinical Manifestations & Uremia

Nephron loss causes a host of nutrient imbalances that can prove fatal if left untreated. Metabolic acidosis and hypocalcaemia will cause bone decalcification and osteodystrophy if left unchecked (KDIGO Work Group, 2009). Even more dangerous is the imbalance of potassium, sodium and water that can lead to hyperkalemia, peripheral edema, hypertension and heart disease (KDIGO Work Group, 2009). The leading cause of death in CKD is CVD inflicted by hypertension and largely unknown mechanisms that may be related to vitamin D deficiency, anemia, uremia, dyslipidemia, low-grade inflammation or hormone imbalances (Gansevoort *et al.*, 2013). Currently, there is no cure for CKD and therapeutics focus on the treatment of comorbidities with the aim of delaying disease progression into ESRD.

Uremic syndrome however, remains a clinically challenging symptom to alleviate and drives the progression of CKD into ESRD (Meyer & Hostetter, 2007). Uremic syndrome manifests when harmful molecules called uremic toxins are permitted to circulate in the plasma at abnormally high concentrations regardless of dialysis interventions (Lisowska-Myjak, 2014). Uremia is the pathological environment of the blood plasma in CKD patients experiencing retention of urea and other organic compounds due to a loss of renal clearance (Meyer & Hostetter, 2007). The state of uremia has been associated with the activation of the immune response and gut microbial alterations (Vitetta & Gobe, 2013), cardiovascular events (Ito & Yoshida, 2014), bone toxicity (Barreto *et al.*, 2009*a*), neurological disorders (Bugnicourt *et al.*, 2013) and a host of other manifestations affecting every organ of the body (Vanholder & De Smet, 1999; Lisowska-Myjak, 2014). As of 2012, concentrations of 88 uremic toxins were identified as abnormal in CKD patients and can be sorted into three classes dependent on molecular size and protein binding (Duranton *et al.*, 2012). Free water-soluble metabolites such as creatinine and urea have the lowest molecular mass (<0.5kDa) and are largely removable by dialysis. Middle molecules range from 0.5-60kDa and include small proteins, hormones and cytokines. Protein-bound uremic toxins are often of low molecular weight but are bound to larger protein carriers in circulation. Dialysis membranes will not allow the removal of albumin; thus, uremic toxins bound to albumin are especially difficult to remove from the plasma. Out of the over 88 recognized uremic

toxins, 25% are protein-bound and have proven clinically challenging to eliminate with traditional dialysis strategies (Duranton *et al.*, 2012).

1.3.5 Animal Models of CKD

Models of CKD in rats include 5/6th nephrectomy, diabetic nephropathy and adenine-induced CKD. The most common 5/6th nephrectomy method surgically removes the top and bottom thirds of one kidney and the entire contralateral kidney effectively simulating the loss in kidney function although potentially inducing post-surgery stress (Ali *et al.*, 2013). Diabetic nephropathy models of diabetes-induced kidney disease usually use the administration of streptozotocin to cause pancreatic β cell death. Additionally, the diabetic nephropathy model although most exemplary of human CKD caused by diabetes, requires a timely experimental period to successfully cause CKD that may not occur simultaneously across all animals. The newer adenine-induced model of CKD is a less invasive orally administered model suggested to provide a more consistent rate of CKD onset than the 5/6th nephrectomy (Terai *et al.*, 2008). The adenine model of CKD also shows the best promise as a progressive CKD model suitable for temporal evaluation due to its timely onset in comparison with the diabetic model. Additionally, the adenine model has been used to study alterations in DMEs of the liver in the past, providing a clear example of severe CKD after 42 days of oral administration (Feere *et al.*, 2015; Velenosi *et al.*, 2016). Mechanistically, adenine and its metabolite 2,8-dihydroxyadenine precipitate when concentrated at the kidney. This mechanically damages the kidney tubules comparable to that inflicted by kidney stones and is thus a tubular model of kidney damage (Engle *et al.*, 1996; Morishita *et al.*, 2011; Succar *et al.*, 2017).

1.4 Hepatic Physiology

Where the kidney is made up of functional units, the liver is made up of cells lining hepatic sinusoids organized around hepatic veins. Parenchymal hepatocytes make up the majority of the liver volume alongside non-parenchymal sinusoidal endothelial, stellate and Kupffer cells which together are responsible for the multitude of hepatic functions (Porth, 2011).

Select roles of the liver are important with respect to CKD and kidney physiology. Firstly, the liver is responsible for the continuation of the RAAS signalling pathway by production of angiotensinogen, the hormone stimulated in response to the release of renin by the kidney (Reese *et al.*, 2011). Secondly, the liver's ability to produce carrier proteins synthesized with the purpose of transporting signalling molecules is relevant in CKD. Albumin, a highly versatile carrier protein responsible for much of the endogenous and xenobiotic transport within the plasma, is the most abundant plasma protein produced by the liver (Berg *et al.*, 2012). Since it cannot pass through the glomerulus, albumin can retain bound molecules in the plasma, preventing their excretion via the kidney and is particularly exaggerated in CKD (Meyer & Hostetter, 2007). The liver is also known for its major roles in metabolism. The liver not only handles lipid, carbohydrate and amino acid synthesis and degradation but also xenobiotic metabolism (Porth, 2011). An endogenous example is the catabolic degradation of amino acids by aminotransferases which release ammonia that is excreted as urea through the kidney (Berg *et al.*, 2012). Next, exogenous metabolism by specific enzymes produced in the liver will be explicitly discussed.

1.5 Drug Metabolizing Enzymes

Approximately 75% of all exogenous molecules require metabolic transformation into active metabolites or waste products before being excreted (Williams *et al.*, 2004). The functional units are drug metabolizing enzymes (DMEs) and can be categorized into three groups. Phase I and II DMEs are responsible for the direct biotransformation of endogenous and exogenous molecules usually by increasing hydrophilicity to ease distribution and excretion. The cytochrome P450 superfamily dominates Phase I and are found ubiquitously, but concentrated in the intestine, lungs, kidney and most abundantly in hepatocytes. Phase II DMEs consist of multiple conjugating enzyme superfamilies such as sulfotransferases (SULT), UDP-glucuronosyltransferases (UGT) and glutathione S-transferases (GST) amongst others. Phase III comprises membrane transport proteins belonging to the ATP binding cassette (ABC) family or solute carrier (SLC) family (Xu *et al.*, 2005). Together, DMEs build the framework for drug absorption, distribution, metabolism and excretion (Sheweita, 2000; Williams *et al.*, 2004).

1.5.1 Cytochrome P450s

CYP enzymes are heme-containing membrane-bound proteins found primarily in the endoplasmic reticulum of cells. The common mono-oxygenase is essential for accepting an oxygen moiety in a process where electrons, provided by an NADPH-dependent P450 oxidoreductase (POR), are required for CYP function (Johnson & Stout, 2005). The enzymatic goal is to transform lipid-soluble molecules via oxidation into more water-soluble products. However, the promiscuous substrate-binding nature of CYP enzymes mean a single CYP enzyme is capable of multiple reactions utilizing various forms of oxidation and reduction (Gad, 2009). The substrate specificity is so broad that ~75% of all hepatic xenobiotic metabolism is mediated by CYP enzymes (Williams *et al.*, 2004; Wienkers & Heath, 2005).

There are 57 CYP enzyme genes identified in humans categorized into 18 families determined by their amino acid composition. For example, the enzyme CYP3A4 is broken down into four components: CYP referring to the cytochrome P450 superfamily, gene family #3, subfamily A, and individual isoform #4. CYPs can also be organized with respect to the number of drugs or endogenous molecules they are capable of metabolizing. Subfamilies CYP1, CYP2 and CYP3 predominately metabolize xenobiotics while most other families primarily carry out specific endogenous metabolism of hormones, vitamins and bile acids (Gad, 2009).

Out of the 57 CYP genes, the *CYP3A* family, *CYP2C9*, *CYP2D6*, *CYP2C19* and the *CYP1A* family are responsible for ~95% of all CYP mediated drug metabolizing activity (Wienkers & Heath, 2005). Specifically, single enzymes CYP3A4 and CYP2C9 are responsible for the metabolism of ~43% of all clinically used drugs, thereby making them well-studied in the literature and the focus of this work (Zanger & Schwab, 2013). To study human CYP enzymes, gene sequence, evolutionary divergence and gene clustering information is used to determine the orthologous pairs between human and non-human species. Therefore, *CYP3A4* and *CYP2C9* genes are usually represented as *CYP3A2* and *CYP2C11* in rat models or *Cyp3a11* and *Cyp2c29/Cyp2c37* in mouse models, respectively (Nelson *et al.*, 2004; Pan *et al.*, 2016).

1.5.2 Induction & Regulation

CYP enzyme expression and activity is not only determined by a number of factors including genetic polymorphisms, sex and age, but also by continually fluctuating bioavailability of substrate (Zanger & Schwab, 2013). Evidence for genetic polymorphisms of CYP3A4 are slowly emerging, but remain elusive in comparison to CYP2C9 which has multiple single nucleotide polymorphisms (SNPs). The two most common in European ancestry are CYP2C9*2 and CYP2C9*3 while CYP2C9*5 is considered rare (Schwarz *et al.*, 2008). Warfarin, a known CYP2C9 substrate and anticoagulant drug used in CKD, must be administered at a fraction of a normal dose if an individual expresses CYP2C9*2 or CYP2C9*3 to avoid drug toxicity and adverse effects like bleeding (Gong *et al.*, 2011; Klein & Zanger, 2013; Vear *et al.*, 2014). Females tend to have higher levels of CYP3A4 than males, but age slowly decreases activity in both sexes (Sotaniemi *et al.*, 1995). CYP2C9 is relatively static across sexes but increases as juveniles mature (Yang *et al.*, 2010; Zanger & Schwab, 2013; Vear *et al.*, 2014).

Substrate bioavailability regulates the expression and activity of CYPs by utilizing a plethora of induction pathways. Specifically, CYP3A4 and CYP2C9 can be regulated at the transcriptional level by substrate induction of either pregnane X receptor (PXR) or constitutive androstane receptor (CAR) (Tirona *et al.*, 2003; Chen *et al.*, 2005). PXR and CAR are nuclear receptors containing both a ligand-binding and DNA-binding domain. Upon ligand-binding, PXR or CAR translocate into the nucleus to form a heterodimer with retinoid X receptor (RXR) before binding to the proximal promotor region of the CYP3A or CYP2C gene to upregulate its production (Kliewer *et al.*, 2002). To optimize CYP2C9 induction, hepatocyte nuclear factor 4 alpha (HNF-4α) is also required to bind to a promotor of the CYP2C9 gene (Jover *et al.*, 2009). HNF-4α, along with a list of other constitutive elements promote or inhibit CYP3A4 expression in the absence of inducers (Honkakoski & Negishi, 2000; Tirona *et al.*, 2003; Zanger & Schwab, 2013). In addition to the PXR/CAR induction mechanisms, peroxisome proliferator-activated receptor alpha (PPARα) (Thomas *et al.*, 2013), glucocorticoid and vitamin D receptor (VDR) pathways (Wang *et al.*, 2013) are slowly being recognized as influencers of CYP3A4 and CYP2C9 expression (Zanger & Schwab, 2013). More recently, microRNA (miRNA) has shown to

influence CYP3A4 directly and indirectly through nuclear receptors PXR, HNF-4α and VDR (Pan *et al.*, 2009; Wei *et al.*, 2014). Besides miRNA, mechanisms of post-transcriptional or post-translational regulation of CYP3A4 and CYP2C9 are largely understudied.

Disease states and associated inflammation are suspected to alter DMEs via changes in levels of hormones, regulatory cytokines and other metabolites. Specifically, disease modulation of CYP enzymes is usually a downregulation of activity or expression and occurs by alteration of basal and inducible transcriptional mechanisms. Inflammation activates the NF-κB pathway and inhibits RXR, thus acting as an antagonist for PXR, CAR and other transcription factors responsible for CYP induction (Jover *et al.*, 2002; Zhou *et al.*, 2006; Morgan, 2009). Models of diabetes mellitus suggest a unique induction of CYP3A4 activity and PXR expression by the increased levels of free fatty acids present in the serum (Kim & Novak, 2007; Hu *et al.*, 2014). A model of nutritionally induced obesity in mice and rats exhibited increased liver triacylglycerol levels as well as decreased liver Cyp3a11 and Cyp2c29, although nuclear factors and inflammatory factors were unchanged (Yoshinari *et al.*, 2006). The accumulation of normally excreted metabolites is a common theme in the suspected cause of disease-associated CYP regulation (Fisher *et al.*, 2009).

Most drugs are substrates for CYP enzymes (Williams *et al.*, 2004; Wienkers & Heath, 2005). Pharmaceutically, this creates the dangerous potential for drug interactions. Rifampicin is a classic example of a PXR ligand that induces both CYP3A4 and CYP2C9 expression (Goodwin *et al.*, 1999). A drug co-administered with rifampicin requiring CYP3A4 or CYP2C9 metabolism will be extensively metabolized resulting in decreased plasma concentration and reduced efficacy (Lynch *et al.*, 2007). In the case of a prodrug such as losartan used to treat hypertension, activation will be inhibited if the CYP enzyme responsible for the activation is inhibited by a co-administered drug (Lynch *et al.*, 2007). This same idea can apply to dietary molecules that influence CYPs. A clinically relevant example is the CYP3A4 inhibition by grapefruit juice. When grapefruit juice is co-administered with drugs dependent on CYP3A4 metabolism, the result is abnormally high bioavailability (Bailey *et al.*, 1998). Drug interactions in combination with the multiple influences of CYP expression result in high intra- and inter-individual variability in

pharmacokinetics. The clinical outcome can be drug toxicity in the form of adverse drug reactions (ADR) or drug ineffectiveness. This will be discussed in the context of CKD in section 1.5.4.

1.5.3 Altered Drug Metabolism in CKD

It is evident that renal drug clearance is hindered by CKD due to a reduced GFR. However, it was not until 2009 that non-renal, hepatic drug clearance became clinically relevant for kidney disease patients in the Guidance for Industry and not until 2011 that KDIGO (Kidney Disease: Improving Global Outcomes) identified non-renal clearance as a usually forgotten aspect of pharmacokinetic studies necessary for dose recommendations (Matzke *et al.*, 2011). Reviewed by Nolin and colleagues in 2008, eleven drugs known to be metabolized by hepatic CYP3A4 showed altered clinical pharmacokinetics in CKD patients (Nolin *et al.*, 2008). More recently, eight drugs extensively metabolized by CYP3A4 and another three drugs metabolized via CYP2C9 presented reduced non-renal clearance in CKD (Ladda & Goralski, 2016). Aliskiren, carvedilol, erythromycin and telithromycin are a few CYP3A4 xenobiotic substrates that are commonly administered and exhibit altered pharmacokinetics in CKD patients (Ladda & Goralski, 2016). CYP2C9 is the major metabolizer of warfarin, a drug commonly used in CKD as a blood thinner to reduce the risk of stroke or atrial fibrillation associated with cardiovascular diseases. A 50% reduction in warfarin metabolism in CKD is suspected to be caused by inhibited or decreased CYP2C9 (Nolin *et al.*, 2008). This is further supported by Gong and colleagues who established that renal function is a determinant of warfarin dosing although warfarin is excreted through non-renal pathways suggesting altered DMEs are responsible for warfarin pharmacokinetic changes in CKD (Gong *et al.*, 2011). Over 75 drugs exhibit reduced non-renal clearance in CKD patients (Yeung *et al.*, 2014). However, it remains largely undecided whether levels of DMEs are altered in humans and responsible for the altered pharmacokinetics seen in CKD (Nolin, 2015). Early human studies utilized the erythromycin breath test to identify impaired CYP3A4 metabolism in ESRD patients (Dowling *et al.*, 2003; Nolin *et al.*, 2006). Simply, radiolabeled carbon dioxide end-product is measured from the breath of subjects given a known dose of radiolabeled erythromycin, a known CYP3A4 specific substrate. When further studies showed DME transporters also

influence erythromycin disposition *in vitro*, the breath test was scrutinized for its indication of CYP3A4 activity and blamed for subsequent contradictory results (Frassetto *et al.*, 2007; Ladda & Goralski, 2016). Interestingly, using a specific probe drug suggests human CYP3A4 activity may not be significantly changed in CKD (Nolin *et al.*, 2009; Thomson *et al.*, 2015). Moreover, the most recent meta-analysis study suggested there was only modest downregulation of human CYP3A4 in comparison to other CYP enzymes over CKD progression (Yoshida *et al.*, 2016). However, extensive animal models of severe CKD show severely decreased gene expression, protein expression and enzymatic activity of CYP enzymes including CYP3A2 and CYP2C11 as well as Phase II and DME transporters (Leblond *et al.*, 2001; Velenosi *et al.*, 2012; Ladda & Goralski, 2016). Therefore, the hypothesis remains that altered pharmacokinetics in humans with CKD stems from altered DME expression or activity. Research today focuses on the mechanisms regulating CYPs in animal models of CKD to further elucidate their function with respect to disease.

1.5.4 Pharmacy & Outcomes in CKD

Altered CYP function is particularly worrisome in CKD patients because this population is elderly, receiving polypharmacy and potentially on dialysis (Sharif-Askari *et al.*, 2014; Ladda & Goralski, 2016). These factors increase the risk of a CKD patient experiencing an adverse drug event (ADE) or ADR inflicted by a medical intervention, usually by the administration of a drug (Bates *et al.*, 1995; Edwards & Aronson, 2000; Munar & Singh, 2007). ADEs are often due to inappropriate dosing that either enhances the activity of the drug and exceeds the intended therapeutic range or fails to meet the therapeutic range potentially reducing efficacy and allowing the symptom to persist.

As there is no cure for CKD, co-morbidities that exist in moderate to severe CKD are primarily treated with medications. In total, patients require an average of 7-12 drugs daily to manage associated comorbidities and the likely causes of CKD (Talbert, 1994). In a study of 512 CKD patients, the risk of ADR was increased when patients were taking over 8 medications, of which anticoagulant drugs including warfarin caused the highest incidence (Sharif-Askari *et al.*, 2014). Secondly, if the patient is on dialysis, a drug's

pharmacokinetics can differ pre- and post-dialysis, further complicating the appropriate dose (Velenosi & Urquhart, 2014). Thirdly, most CKD patients are over 65 years of age and are likely to be taking additional medications aside from those required to treat kidney disease specific comorbidities. As such, the elderly population alone increases the risk of ADEs (Sharif-Askari *et al.*, 2014; Davies & O'Mahony, 2015). Thus, dosing considerations in each CKD patient requires an individual drug plan and continuous monitoring (Corsonello *et al.*, 2005; Matzke *et al.*, 2011). Ultimately, the combination of unavoidable polypharmacy and unpredictable drug metabolism is the suspected driver of ADEs and ADRs seen in CKD patients (Manley *et al.*, 2005).

It is therefore important to assess the probable causes of pharmacokinetic alterations in CKD. In the following sections, suspected factors contributing to changes in DME regulation in CKD will be discussed including the intestinal microbiome and uremia.

1.6 The Microbiome

The microbiome is the entire community of bacterial species and their corresponding genes that co-exist within the human host gastrointestinal (GI), urogenital and respiratory systems as well as on the exterior surfaces of the skin (Cho & Blaser, 2012; Ursell *et al.*, 2012). Compared to the human genome, the microbiome is approximately 150 times larger and contains many genes that aid in symbiotic functions humans are incapable of carrying out on their own (Qin *et al.*, 2010). Bacterial acquisition occurs in infants during and immediately following birth (Lloyd-Price *et al.*, 2016). During childhood through to adulthood the microbiome is continually shaped in response to a regular diet and environmental insults. These are largely associated with geography and race/ethnicity, and by two years of age, a "core microbiome" or stable abundance of each major bacterial group is established (Huttenhower *et al.*, 2012; Ursell *et al.*, 2014; Lloyd-Price *et al.*, 2016). However, the microbiome is far from static and small short-term changes can occur within hours of a dietary alteration, largely not affecting the core microbiome (David *et al.*, 2013).

1.6.1 Microbiota Methodology

A decade ago, bacterial species analysis was performed primarily by culture and PCR methods limited by the knowledge of individual bacterial species and associated primers. However, there are thousands of species residing in a single fecal sample and a large proportion of bacteria are unculturable with current techniques making it increasingly difficult to assess the bacterial composition or "microbiota" as a complete community (Stewart, 2012). Culture-independent methods like Sanger sequencing, although developed in the 1970s (Sanger *et al.*, 1977) was a long and laborious process and was rarely utilized for sequencing the microbiota (Hiergeist *et al.*, 2015). Around 2005, the first high-throughput next generation sequencing (NGS) techniques improved the cost and efficiency of sequencing, promoting an interest in the microbiome (Gloor *et al.*, 2010; Hiergeist *et al.*, 2015). However, in addition to high error rates per-read, the first NGS methods (e.g. pyrosequencing) remained expensive and unattainable for many research groups (Gloor *et al.*, 2010). Within the last 10 years NGS methods such as Illumina MiSeq have provided the ability to assess the microbiota with higher throughput and accuracy at an attainable cost (Caporaso *et al.*, 2012; Ramezani *et al.*, 2015). Phylogenetic microarrays are another popular method of bacterial sequencing and both NGS and phyloarrays involve a reference gene. Usually the 16S small ribosomal subunit rRNA gene is used due to its combination of both highly conserved regions used for primer design applicable across all bacterial species and the adjacent variable regions utilized for species identification (Janda & Abbott, 2007). Unlike phyloarrays that are limited to the known 16S sequences applied to the plate, NGS methods allow all 16S genes within a sample to be sequenced regardless of previous identification (Vaziri *et al.*, 2012). This is important because unidentified bacteria are necessary to understand species richness and diversity indices that are otherwise skewed without them.

Although methodology is constantly improving, gene sequencing results still heavily rely on the sequencing method used. In this work, the Illumina MiSeq platform was used to perform paired-end sequencing of the 16S rRNA gene focusing on the V4 variable region for maximum fecal bacteria coverage (Gloor *et al.*, 2010). Through a process called bridge amplification, clusters of DNA are formed on a flow-cell within the sequencer.

Sequencing-by-synthesis and dye-terminated primer extension uses fluorescent signals to indicate what nucleotide is being added along the amplicon as it is made. Final instrument outputs are called reads and after data processing are matched with their most likely bacterial sequence. The final product is called an operational taxonomic unit (OTU) and generally needs to match the expected bacterial sequence with 97% accuracy (Cho & Blaser, 2012; Ursell *et al.*, 2012). OTUs are quantifiable and used to understand the relative abundance of each species and diversity indices of a sample. Today, large scale endeavours such as the Human Microbiome Project (HMP) and the European project (MetaHIT) provide the foundation for bacterial databases (Turnbaugh *et al.*, 2007; Cho & Blaser, 2012; Huttenhower *et al.*, 2012).

Due to the vast number of bacteria at varying levels of identification and the large proportion yet to be identified, bacterial classification is usually presented as the most confirmed tier of the taxonomy ladder. Taxa are arranged in the ecological order of kingdom, phylum, class, order, family, genus, species followed by strain if applicable. Nomenclature for kingdom through genus taxa are capitalized and only species or strain names are italicized (e.g. Escherichia *coli*; *E. coli*).

1.6.2 Gut Microbiota & Host Physiology

The gut microbiota is the collection of bacteria residing in the lumen or mucosal layer of the upper to lower intestine and comprises up to 5000 bacterial species (Nieuwdorp *et al.*, 2014; Ramezani *et al.*, 2015). Ninety percent of the residential bacteria are dominated by phyla Firmicutes and Bacteroidetes and further split into five most prevalent genera Bacteroides, Clostridium, Lactobacillus, Escherichia and Bifidobacterium (Nicholson *et al.*, 2005; Eckburg *et al.*, 2005; Huttenhower *et al.*, 2012; Goodrich *et al.*, 2014; Mafra & Fouque, 2015). It is suggested with some controversy that global intestinal enterotypes or common diversity profiles exist in the human population (Arumugam *et al.*, 2011; Knights *et al.*, 2014; Moeller & Ochman, 2014). It is agreed however, that different species reside in the upper GI tract than those found in the colon and most are obligate anaerobes responsible for digestion, immune functions and gut physiology (Eckburg *et al.*, 2005; Turnbaugh *et al.*, 2007). Gut bacteria found in the lumen elicit the metabolism of dietary

fibres, sugars, alcohols and carbohydrates unable to be metabolized by the host (Nieuwdorp *et al.*, 2014). Dietary fibre and some carbohydrates are largely indigestible until bacterial fermentation to short-chain fatty acids (SCFAs) such as acetate, propionate, and butyrate (den Besten *et al.*, 2013). Commensal, or harmless co-existing bacteria, residing in the intestinal mucosal layer also support immune function of the host by ultimately inhibiting intestinal wall inflammation and subsequent bacterial translocation that could cause infection. Some bacteria produce anti-microbial peptides to fend off pathogenic microbes while others stimulate immune cell maturation of the host (Belkaid & Hand, 2014; Yip *et al.*, 2015). SCFAs produced by bacteria limit the proliferation of effector $CD4^+$ T cells and stimulate macrophage suppression of pro-inflammatory molecules (Felizardo *et al.*, 2016). Gut bacteria also determine host physiology. Studies utilizing germ-free mice raised in sterile environments, show reduced intestinal angiogenesis and ensuing malformed villi (Belkaid & Hand, 2014).

Ties between gut bacteria and host physiology spark questions regarding health and disease. Healthy fluctuations in symbiotic gut bacterial abundances are difficult to assess as most research focuses on deleterious disease states. In a large cohort of 1106 human stool samples, the largest influencers of gut composition were medications, blood parameters (e.g. red blood cell count, uric acid, hemoglobin), bowel properties (e.g. Bristol stool score, time since previous relief), health and diet (Falony *et al.*, 2016). Dysbiosis is the altered bacterial composition associated with a non-infectious disease state (Lloyd-Price *et al.*, 2016). Many diseases including inflammatory bowel disease, obesity, cardiovascular disease, asthma and more recently cancer exhibit dysbiosis (Cho & Blaser, 2012; Carding *et al.*, 2015; Lloyd-Price *et al.*, 2016). Often the probable cause of dysbiosis is indistinguishable from its added clinical manifestations (Vanholder & Glorieux, 2015). Luckily, a dignified method of bacterial replacement, usually in the form of fecal microbial transplantation (FMT), is used to assess the deleterious effects of diseased bacterial compositions by giving dysbiotic bacterial culture to a healthy individual (Manichanh *et al.*, 2010). FMT gained popularity after multiple studies showed inducible adiposity when intestinal bacteria from obese mice were introduced to lean counterparts (Turnbaugh *et al.*, 2008). In humans, FMT from healthy, lean individuals into obese individuals improved peripheral insulin sensitivity (Vrieze *et al.*, 2012). Even increased susceptibility to

atherosclerosis was seen in mice receiving FMT from mice with atherosclerosis-induced dysbiosis (Gregory *et al.*, 2015). Thus, the gut microbial community is capable of driving disease states.

1.6.3 Dysbiosis in CKD

In the 1106 stool sample cohort described above, one of the largest associated factors of altered bacterial composition was GFR and thus it comes as no surprise that CKD patients exhibit a differing bacterial composition from healthy individuals (Falony *et al.*, 2016). Actinobacteria, Firmicutes (especially subphylum Clostridia), and Proteobacteria phyla of CKD patients contain changes in specific bacterial genera when assessed using phylogenetic microarray (Vaziri *et al.*, 2012). Similar to the microarray results, bacterial sequencing showed altered Actinobacteria, Bacteroidetes, Firmicutes (Clostridia), Proteobacteria and Verrucomicrobia in ESRD patients (Wong *et al.*, 2014). Unfortunately, the only study assessing early renal decline in humans showed bacterial alterations occurred solely in the Clostridiales order within the phylum Firmicutes (Barrios *et al.*, 2015). Rat feces show similar overall composition to those of humans with Actinobacteria, Bacteroidetes, Firmicutes, and Proteobacteria among the phyla with the highest abundances (Vaziri *et al.*, 2012). When subjected to severe CKD, rat models show decreases in both Firmicutes and Bacteroidetes and decreased overall diversity (Vaziri *et al.*, 2012). Obesity, a risk factor for CKD, is shown to have decreased levels of Bacteroidetes when compared as a proportion to Firmicutes in obese mice (Ley *et al.*, 2005). A summary of specific gut bacterial alterations in CKD has been reviewed (Ramezani *et al.*, 2015).

Although still unclear, most studies suggest the altered gut composition is a result of CKD pathophysiology; however, once established, the altered gut composition has a supportive role in CKD progression. CKD patients experience reduced gut motility, dietary changes, and a host of pharmaceutical insults which all have explainable impacts on the host gut microbial composition. For example, clinicians may recommend the removal of some fruits, vegetables or fibre from the diet to combat hyperkalemia which is one contributing factor to the reduced abundance of SCFA-producing bacteria in CKD (Wong *et al.*, 2014;

Vaziri, 2016). Less obvious is the uremia-associated gut wall inflammation suspected to effect bacterial changes in CKD patients. The gut wall integrity is compromised in CKD shown by gap-junction alterations likely brought on by inflammation (Lau *et al.*, 2016). The gut wall then becomes permeable to uremic toxins including urea, a substrate for bacteria with urease activity, which converts urea to ammonia. Ammonia is spontaneously transformed into ammonium hydroxide increasing the luminal pH and further damaging the gut lumen (Felizardo *et al.*, 2016; Vaziri, 2016). This increase in pH naturally selects for species capable of surviving in alkaline environments exhibited by Wong and colleagues who demonstrated that bacteria established in ESRD patients favoured a uremic environment (Vaziri *et al.*, 2013; Wong *et al.*, 2014).

Alternatively, manifestations including systemic ramifications of dysbiosis are evident in CKD by endotoxin and bacterial DNA fragments found in the bloodstream. Not only would a leaky gut lumen explain dysbiosis, but also elucidate the parallel movement of bacteria into the blood-stream presented as endotoxemia in CKD and CVD patients (Feroze *et al.*, 2012; Lau *et al.*, 2016). Appealing to the idea of targeting dysbiosis as a therapy, pro- and prebiotics are being investigated as novel dysbiosis treatments (Koppe *et al.*, 2015). A recent clinical trial demonstrated positive effects in reducing select uremic toxins in pre-dialysis CKD patients after a 6 week symbiotic therapy comprised of pre- and probiotics (Rossi *et al.*, 2016). Although minor improvements have been suggested in overall CKD health, pro- or prebiotic treatment with intent to improve DME function has yet to be studied.

1.6.4 Gut-Derived Uremic Toxins

Gut-derived uremic toxins are uremic toxins produced by the commensal gut community under disease circumstances. An elegant study of germ-free versus conventionally raised mice first established that gut bacteria were required to produce host plasma metabolites such as indoxyl sulfate (IS) and phenyl sulfate (PS) (Wikoff *et al.*, 2009). Out of the over 88 uremic toxins identified in CKD, IS and PS are two highly retained, protein-bound, gut-derived uremic toxins difficult to remove via dialysis (Duranton *et al.*, 2012). Thereafter, a feasible connection between uremia and the altered gut microbiota in CKD was formed

(Meyer & Hostetter, 2012). In addition to indole and phenol metabolites, other by-products of bacterial metabolism include branched-chain fatty acids, SCFAs, ammonia, choline, hydrogen sulfide, amines [e.g. trimethylamine-N-oxide (TMAO)] mercaptanes and carbon dioxide (Macfarlane & Macfarlane, 2012).

Indoxyl sulfate begins as dietary tryptophan, transformed into indole by tryptophanase-possessing gut bacteria including species within the genera Bacteroides, Bifidobacterium, Clostridium, Lactobacillus and Parabacteroides (Zhang & Davies, 2016). Indole circulates in the plasma until it is shuttled to the liver to be hydroxylated by CYP enzymes and sulfated by SULTs before returning to the plasma as indoxyl sulfate (Figure 1.2). Phenyl sulfate begins as dietary tyrosine before being sulfated in the liver. Bacteria capable of phenol metabolism belong to the Bacteroides, Bifidobacterium, Lactobacillus, Enterobacter, and Clostridium genera (Ramezani *et al.*, 2015). Both IS and PS are normally excreted via the proximal kidney tubule, but are retained if kidney function is inhibited by reduced GFR or CKD-associated inhibition of transporters (Niwa, 2013). In a study of bacterial functionality in human ESRD, 12 of 19 microbial families with an increased abundance compared to healthy individuals possessed urease activity. Another four possessed the ability to produce indole. Two of four families that showed a decrease due to ESRD were capable of SCFA production (Wong *et al.*, 2014). This data highlights the influence of CKD-induced uremia on the gut through altering the luminal environment and selecting for uremic toxin-producing bacteria, ultimately furthering disease progression through added uremic toxin production (Figure 1.2). Although biological manifestations of each gut-derived uremic toxin are unique and still being elucidated, IS has been of particular interest due to its association with overall mortality and multiple comorbidities through mechanisms of endothelial dysfunction, renal and cardiac fibrosis, immune activation and regulation of various other proteins with functions across all organ systems (Barreto *et al.*, 2009*b*; Vanholder *et al.*, 2014; Ramezani *et al.*, 2015). With uremic toxins like IS so heavily linked to CKD progression and comorbidities, therapeutic options like pro- and prebiotics are suspected to improve the gut microbiota and systematically reduce uremia (Koppe *et al.*, 2015).

1.6.5 Metabolomics

Metabolomics is the study of the entire metabolic profile of a biological matrix utilizing high-throughput diagnostic tools such as mass spectrometry (MS) or nuclear magnetic resonance (NMR) spectroscopy. Endogenous as well as exogenous metabolites including uremic toxins, food metabolites, hormones and other small molecular weight molecules can be studied by metabolomics. The field is indispensable for understanding the final outputs of cellular processes and provides a picture of cellular mechanisms when analyzed alongside gene expression. In this work, metabolomics using MS coupled with advanced chromatography tools were used to measure metabolites present in plasma and liver homogenates.

In short, MS involves the ionization of a sample to obtain a mass-to-charge (*m/z*) ratio at a specific retention time unique to each molecule within a sample. To effectively measure many metabolites in a complex biological sample, ultra-performance liquid chromatography (UPLC) is often used in conjunction with MS to first separate metabolites by hydrophobicity before entering the mass spectrometer for ionization. The electrospray ionization (ESI) utilized in this work, uses high voltage to form an aerosol from a liquid sample. The aerosol is the point at which the molecules of the sample are ionized either in positive or negative ionization mode determined by either the addition or removal of a hydrogen ion, respectively. Whether a molecule ionizes better in positive or negative mode is determined by its molecular composition so generally both modes are used to capture as many metabolites as possible. After ionization, the metabolites travel parallel and in the center of four quadrupoles where brief alterations in the applied current alters the movement of the metabolites travelling through them. The mass of the metabolite ultimately determines if it reaches the other end of the quadrupole without being pushed or pulled out of the center. Systematically, by altering the window of current applied to the quadrupole, each *m/z* ratio is scanned at high mass accuracy. Following the quadrupole, the metabolites enter the collision cell where the parent metabolite may be broken into smaller fragments for additional information during identification later in analysis. In this work, the MS was run using the MS^e Waters method that continuously switches from MS to MS/MS data acquisition using a low collision energy for production of parent molecules,

and ramping high collision energy, for production of fragments. The parent molecule is also called function 1 and the fragmentation data is called function 2. These fragments then enter the final time-of-flight (TOF) chamber which further separates the fragments by mass but using the time it takes for the ionized molecule to hit a detector after accelerating all molecules with the same force. Thus, the measured time required for the metabolite to reach the detector is dependent on the mass of the molecule. Ultimately this provides the m/z ratio, retention time and fragmentation pattern for each detected metabolite within a sample.

Using this instrument, both targeted and untargeted metabolomics can be conducted. Untargeted metabolomics refers to detection and measurement of metabolites within a sample without defining metabolites of interest prior to the experiment and is particularly useful for understanding the uremic milieu of CKD (Zhao, 2013).

Due to the large metadata output from metabolomics analysis, complex statistical analysis must be utilized (Saccenti *et al.*, 2014). Principle component analysis (PCA) is a common multivariate method of displaying samples with respect to their relative metabolite compositions in a map-like format for visual verification of differing compositions. PCA was also used to visualize patterns of OTUs from the microbiota sequencing data. Metabolite features such as the accurate mass, retention time and fragmentation pattern captured via MS can be used to identify the metabolite when referenced to an online database such as the Human Metabolome Database (HMDB; www.hmdb.ca/) (Wishart *et al.*, 2013).

1.7 Mechanistic DME Regulation in CKD

The mechanisms suggested for CYP downregulation in CKD are minimally understood, but have implicated uremia and uremic toxins, bacterial gut alterations, hormone alterations and associated inflammation. The next subsections break down two mechanistic pathways of DME alteration in CKD, uremia (section 1.7.1) and dysbiosis (section 1.7.2).

1.7.1 Uremia & DMEs

Since the discovery of uremic toxins, uremia has been considered a top candidate for the primary influencer of CYP enzyme manipulation in CKD because multiple mechanisms spanning pre-transcription to direct inhibition have been suggested (Velenosi *et al.*, 2014; Volpe *et al.*, 2014; Nolin, 2015). In addition to IS and PS, uremia provides a vast number of metabolites, many of which are unsuccessfully removed by dialysis and inflict pathological effects on other organs including the liver and cardiovascular systems (Niwa, 2013; Lin *et al.*, 2015). The proposed mechanisms of uremia on DME expression include i) reduced nuclear receptor binding and epigenetic histone deacetylation (Velenosi *et al.*, 2014), ii) NF-κB modulation via inflammatory cytokines or parathyroid hormone (PTH) (Michaud *et al.*, 2006, 2008) and iii) direct inhibition by various uremic toxins (Guévin *et al.*, 2002; Sun *et al.*, 2004; Barnes *et al.*, 2014; Volpe *et al.*, 2014). However, uremic toxins may not be the sole regulator of DMEs. Preliminary studies using intestinal adsorbent AST-120 in rats with severe CKD show effective removal of uremic toxins without recovery of CYP3A2 or CYP2C11 function (Velenosi, 2015). In addition, most of the mechanistic studies described above, do not sufficiently provide support for 100% of the observed DME alteration.

1.7.2 Bacteria & DMEs

The altered gut composition of CKD is suggested to influence DME regulation. Two mechanisms are described here. The first is through increased production of uremic toxins. In short, increases in uremic toxin-producing bacteria are suspected to increase the load of uremic toxins, which are responsible for DME downregulation through mechanisms relating to the increased concentration of uremic toxins themselves (see section 1.7.1). Thus, removal of uremic-toxin producing bacteria may lessen the strain of uremia in CKD (Koppe *et al.*, 2015), but this notion has yet to be evaluated in the context of DME alteration.

It is also possible that bacterial species are required for DME regulation independent of uremia. When bacterial species are lost due to CKD, associated dysbiosis may result in

faulty DME regulation. This mechanism was first hypothesized after recognizing the antibiotic ciprofloxacin diminished the intestinal diversity and impacted CYP expression (Toda *et al.*, 2009). However, at the time, it was unclear if this decreased CYP expression was due to the drug acting as a direct inhibitor of CYP expression or killing the necessary bacteria for CYP function. Shortly thereafter, germ-free mice lacking gut bacteria showed reduced drug metabolizing Cyp3a11 and Cyp2c29 expression; however the microbiota was recovered upon colonization with gut bacteria from conventionally raised mice (Toda *et al.*, 2009; Claus *et al.*, 2011). An extensive gene expression study further showed that germ-free mice without gut bacteria have 87% downregulation of Cyp3a11 but unaffected Cyp2c29 (Selwyn *et al.*, 2015).

Displacement of commensal bacteria in a dysbiotic state may remove the normally applied suppression of the inflammatory response. Essentially, bacterial SCFAs are implicated with many immunomodulatory effects including T cell inactivation, downregulation of TNFα/β, IL-6 and IL-1β, and inhibition of macrophage NF-κB nuclear translocation required for its activation (Lührs *et al.*, 2002). As previously demonstrated, inflammation through activation of the NF-κB pathway can block DME expression via inducible PXR regulation (Gu *et al.*, 2006). Mechanistically, molecules derived from bacteria like lithocholic acid (LCA) promote PXR activation responsible for CYP induction (Staudinger *et al.*, 2001; Toda *et al.*, 2009). Thus, one of the ways dysbiosis might affect drug metabolism is through loss of beneficial bacteria or beneficial molecules produced by bacteria required for DME induction.

It is important to note however, that dysbiosis is suspected to be caused by deleterious effects of uremic toxins on the gut wall. This highlights the proposed positive feedback manifestation of dysbiosis and uremia in CKD (Figure 1.2) (Vanholder & Glorieux, 2015). Assessment of both dysbiosis and uremia along the progression of CKD is suspected to shed light onto which factor may be primarily influential in DME alteration.

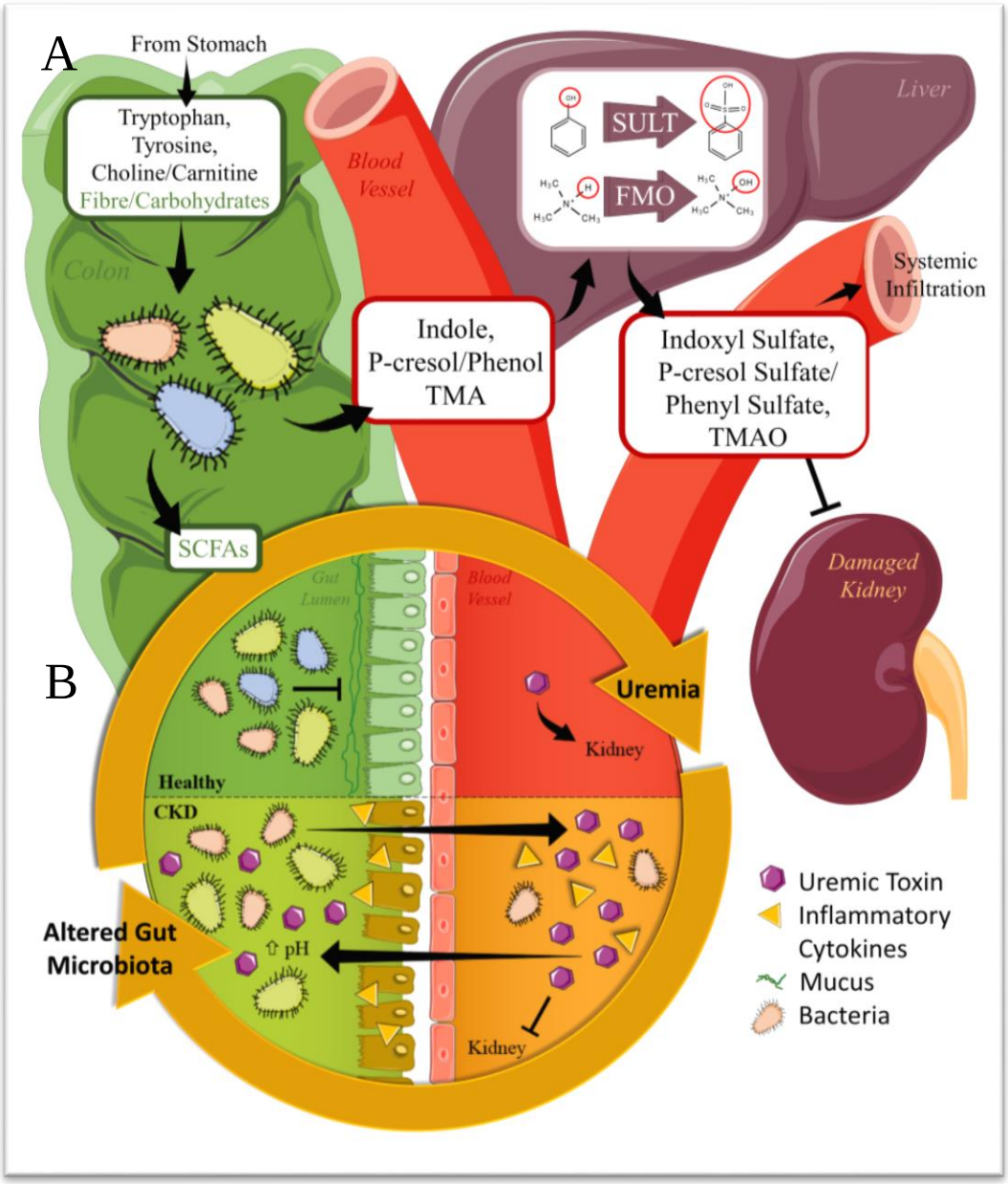

Figure 1.2. Pathophysiological summary of uremia and dysbiosis in CKD. A) Pathway of uremic toxins: IS, PS, p-cresol sulfate and TMAO. B) The cyclic gut-kidney relationship. Uremic toxins and associated inflammation are suspected to impede the integrity of the gut lumen allowing urea and other toxins to cross the leaky intestinal barrier and increase the luminal pH promoting growth of uremic-toxin-producing bacteria and overall dysbiosis. This promotes further production of uremic toxins associated with disease progression and CKD comorbidities. Images were modified from Servier Medical Art (www.servier.co.uk/medical-art-gallery).

1.8 Hypothesis & Objectives

1.8.1 Rationale

Currently the literature demonstrates non-renal drug clearance is altered in CKD. It is less clear why proteins such as DMEs are altered. Suggested mechanisms include alterations of the gut microbiota or uremic toxins. Thus, studies are needed to link gut-derived uremic toxins (e.g. IS) and gut bacteria with DMEs. Human DME orthologs have been studied in rat models of CKD but these studies focus only on severe or late-stage CKD leaving a gap in our understanding of when CKD factors and DME expression changes (Leblond *et al.*, 2001; Velenosi *et al.*, 2012; Ladda & Goralski, 2016). Additionally, very few studies have looked at both bacterial alterations and metabolomics within one CKD cohort, none of which have focused on DMEs (Ursell *et al.*, 2014; Nallu *et al.*, 2016). To our knowledge, no studies have assessed the effect of CKD on hepatic DMEs over disease progression in attempt to understand when uremic toxins are changing relative to DME alterations. Additionally, this thesis will be the first to encompass metabolomics, 16S bacterial sequencing and DME analysis over CKD progression.

1.8.2 Hypothesis & Objectives

Although both the uremic and microbial environments are altered in CKD patients, their roles in DME regulation remain unclear. The pathophysiological factors of uremia and dysbiosis have never been tested temporally over the progression of CKD. The basic principle of causality dictates that for a factor (e.g. uremia or dysbiosis) to be causative, it must exist or apply the effect before the outcome (e.g. DME regulation) in time (Otero *et al.*, 2014). Elucidating the series of events that occur over CKD progression may provide support for current hypotheses, which suggest uremic toxins or bacterial alterations are causal factors in DME regulation. Alternatively, results may fail to support current hypotheses by finding DME changes occur before the suspected causal factors. Thus, this thesis aims to reveal the timing in which each pathophysiological factor changes in the attempt to support the hypothesis that uremic toxins and/or bacterial alterations are mechanistically involved in the regulation of DMEs in CKD. Specifically, we aim to

characterize plasma and liver uremic toxins, the gut microbial composition and DME fluctuation over the progression of an adenine-fed rat model of CKD. We hypothesize that adenine-induced CKD will cause uremia and gut microbial changes detectable prior to the anticipated downregulation of CYP3A2 and CYP2C11 DMEs.

Chapter 2

2 Materials & Methods

2.1 Animal Model & Study Design

Animal work was approved by the Western University Animal Care Committee and experiments were conducted in accordance with the Canadian Council on Animal Care (Appendix A). Sixty-six male Wistar rats (initially 150g) were obtained from Charles River Laboratories, Inc. (Wilmington, MA) and randomized into six groups defined by time of sacrifice (day 0, 3, 7, 14, 28 and 42). Each time point consists of a minimum six control and six CKD rats along with six control rats on day 0. Rats were housed in a conventional animal care facility with a 12h light cycle. Rats were paired with a same-group cage mate to minimize coprophagy alterations of the gut microbiota. All rats were acclimated for seven days prior to starting either 0.5% adenine supplemented Teklad 22/5 Rodent Diet (Harlan Laboratories Inc., Madison, WI) for CKD rats or standard chow pair fed to match caloric intake for control rats (Prolab® RMH 3000, LabDiet, St. Louis, MO). Water was provided *ad libitum* to both groups. Body weights were monitored daily (Table 3.1) until sacrifice via isoflurane anesthetization followed by decapitation. Blood was collected in heparinized tubes. Liver was snap-frozen in liquid nitrogen. Caecal samples were obtained on a sterile, single culture swab (BD, Sparks, MD) touched to an open incision at the enlarged proximal end of the rat caecum. All samples were stored at -80°C until further analysis excluding the right kidneys which were stored in 10% formalin until histological embedding.

2.2 Disease Markers & Histology

Conventional CKD markers urea (mmol/L) and creatinine (µmol/L) were measured in rat plasma using standard methods by the Pathology and Laboratory Medicine group (PaLM, London, ON; www.lhsc.on.ca/palm/). Kidney tissue and histological images were prepared as previously described (Feere *et al.*, 2015). Briefly, kidneys were fixed in 10% formalin

(Anachemia Canada Co., Montreal, QC) before undergoing tissue slide preparation at the Department of Pathology (Western University, ON). Light microscopy and photographs of prepared haematoxylin and eosin (H&E) stained slides were obtained under identical exposure, saturation and contrast on a Leica DM1000 light microscope paired with a Leica DFC295 colour camera and Leica Application Suite v3.8.0 software.

2.3 Real-Time PCR

In preparation for quantitative (real-time) PCR, total mRNA was extracted from rat liver using TRIzol reagent (Life Technologies, Burlington, ON) following the manufacturers protocol before quantification and purity testing using a Nanodrop 2000 (ThermoScientific, West Palm Beach, FL). One µg of total RNA underwent reverse transcription (Bio-Rad C1000) for cDNA synthesis using qScript cDNA Supermix (Quanta Biosciences, Gaithersburg, MD). Amplified cDNA was diluted 1:40 before running 5µL in triplicate on a 384-well plate with 7µL mastermix containing primers and PerfeCTa SYBR green fastmix (Quanta Biosciences, Gaithersburg, MD). Rat primers for CYP3A2 (forward) [5'-GCTCTTGATGCATGGTTAAAGATTTG-3'] and (reverse) [5'-ATCACA GACCTTGCCAACTCCTT-3'] and CYP2C11 (forward) [5'-CCCTGAG GACTTTTGGGATGGGC-3'] and (reverse) [5'-AGGGGCACCTTTGCTCTTCCTC-3'] (Invitrogen) were previously validated by cycle threshold (Ct) and melt-curve analysis (Velenosi *et al.*, 2014). β-Actin was used as the housekeeping gene (forward) [5'-ACGAGGCCCAGAGCAAGA-3'] and (reverse) [5'-TTGGTTACAATGCCGTGTTCA-3'], samples were run on a Bio-Rad CFX384 Real-Time System (Hercules, CA, USA) and relative RNA expression was assessed through the ΔΔCt method (Livak & Schmittgen, 2001; Rao *et al.*, 2013).

2.4 Western Blotting

2.4.1 Microsomal Isolation & BCA Assay

Hepatic microsomal fractions were prepared by differential centrifugation followed by Pierce BCA assay as previously described (Feere *et al.*, 2015). Briefly, approximately 1/6 of each rat liver was homogenized using a T10 Basic Ultra-TURRAX (Sigma Aldrich, St.

Louis, MO) on ice in 1mL of buffer [1.15% KCl + 1mM ethylenediaminetetraacetic acid (EDTA)] for 5 min. Samples were centrifuged at 4°C in an ultracentrifuge (Beckman Coulter Optima L-90K, Fullerton, CA), first at 9000×g for 20 min to collect the supernatant which was further spun at 105,000×g for 1 hour. Total microsomal pellet was suspended in 500µL storage buffer (0.1M potassium phosphate buffer + 20% glycerol, pH=7.4) and subsequently separated into two aliquots of approximately equal amounts before storing at -80°C. A Pierce BCA Protein Assay kit (Thermo Scientific) was used to assess total protein content from diluted microsomal fractions (1:100) in a 96-well plate. Concentrations of 1000, 500, 250, 125, 62.5, 0 µg/mL protein standard (Sigma Aldrich) provided a sufficient standard curve to measure all samples by chemiluminescence on a plate reader (SpectraMax-M5). The original microsomal fraction was aliquoted to 5µg/µL total protein and stored at -80°C until western blot analysis.

2.4.2 Gel Electrophoresis & Blotting

Western blot analysis was performed as previously depicted with minor alterations (Feere *et al.*, 2015). Electrophoresis was optimized on a 15-well 10% polyacrylamide resolving gel with 4% stacking gel containing 0.1% sodium dodecyl sulfate (SDS) and polymerized using ammonium persulfate and tetramethylethylenediamine (TEMED) (Bio Basic Inc, Markham, ON). A total of 4µL loading volume contained 4.8µg of protein per well. The samples were diluted in sample buffer (10% SDS, 26% glycerol and 0.5% bromophenol blue) and reduced with beta-mercaptoethanol at 80°C for 20 min. The gel was run at 60V for 20 min followed by 120V for 45mins in Bio-Rad Running Buffer. Protein was transferred to a nitrocellulose membrane for 1.5 hours with 120V in Bio-Rad Transfer Buffer. The membrane was washed with PBS + 0.1% tween (PBS-T) before blocking with PBS-T + 5% skim milk powder + 0.6% bovine serum albumin (BSA) for 1 hour followed by three washes of PBS-T. Primary CYP3A2 rabbit anti-rat antibodies (Millipore, Temecula, CA) were diluted 1:8000 with PBS-T + 0.6% BSA. CYP2C11 mouse anti-rat antibody (Millipore, Temecula, CA) was diluted 1:5000 with PBS-T + 5% skim milk powder. β-Actin housekeeping primary antibody, conjugated to horseradish peroxidase (HRP), was made in mouse (Sigma Aldrich), diluted 1:50000 with PBS-T + 0.6% BSA and made fresh before each use. After 4°C overnight incubation with primary antibody and

subsequent PBS-T washes, secondary antibody (rabbit or mouse) linked to HRP (Santa Cruz Biotechnology Inc., Santa Cruz, CA) at 1:10000 dilution in PBS-T + 0.6% BSA were incubated with the blots for no longer than 1 hour. Imaging was performed on the Bio-Rad VersaDoc Imaging System (Hercules, CA) and accompanying QuantityOne (v4.6.3) software after final washing steps and 1 min incubation of 1 mL chemiluminescent agent Luminata Forte western blot HRP substrate (Millipore, Billerica, MA). After imaging of CYP3A2, the blot was washed, stripped of protein (Restore Western Blot Stripping Buffer, ThermoScientific, Rockford, IL) and washed with PBS-T once more before the application of the β-Actin or CYP2C11 primary antibody before repeating the washes and imaging steps. Densitometry data was normalized to β-actin, presented as a percent of day 0 control samples and standardized across blots by a communal pooled sample run on every blot. Western blot analysis was completed in duplicate for both CYP3A2 and CYP2C11.

2.5 Enzymatic Activity

Enzymatic activity was analyzed by incubating microsomal fractions with testosterone, a known substrate of CYP3A2 and CYP2C11 (Chovan *et al.*, 2007). The respective products 6βOH-testosterone and 16αOH-testosterone were measured via mass spectrometry (MS) in a 96-well plate assay adapted from (Feere *et al.*, 2015). In a final volume of 75µL, 0.2mg/mL microsomal protein and reaction buffer (50 mM potassium phosphate with 2 mM MgCl2 pH 7.4) was incubated with 1µL testosterone (Steraloids Inc., Newport, RI) substrate at concentrations of 12.5, 25, 75, 200 and 400µM for 10 min at 37°C. Reaction volume is completed by incubation with 1mM NADPH (Sigma Aldrich) and shaken at 37°C for exactly 20 min before sequestration using 225µL ice-cold acetonitrile with 80ng/mL flurazepam as an internal standard (Cerilliant, Round Rock, TX). Plates were shaken, centrifuged at 4000×g for 10 min, supernatant diluted 1 in 5 with milliQ water and stored at 4°C no longer than 24 hours until analysis. Enzymatic products were separated on an ultra-performance liquid chromatography (UPLC) Phenomenex Kinetex phenyl-hexyl column (1.7µm particle size, 50mm × 2.1 mm) maintained at 40°C in a Waters ACQUITY UPLC I-Class System (Milford, MA). Mobile phase flow was set to 0.5 ml/min and consisted of UPLC-grade water (A) and acetonitrile (B) both containing 0.1% formic acid with a gradient as follows: 0–0.5 mins, 25% B; 0.5–2 mins 25–35% B; 2–2.5 mins

35–80% B; 2.5–3.5 mins held at 80% B; 3.5 mins 25% B. Analytes were detected using quadrupole time-of-flight mass spectrometry (UPLC-QTof/MS) on a Waters Xevo^{TM} G2S-QTof/MS and Waters ACQUITY I-Class UPLC with parameters as previously described (Feere *et al.*, 2015). The positive mode mass-to-charge ratio (*m/z*) for 6βOH-testosterone and 16αOH-testosterone (*m/z* = 305.2117) were quantified using standard curves of purchased 6βOH-testosterone (0.04–50μM) and 16αOH-testosterone (0.09–100μM) (Steraloids Inc., Newport, RI) using QuanLynx v4.1 software. Michaelis-Menten curves generated with GraphPad Prism (v5.0 for Windows; GraphPad Software Inc., San Diego, CA) were used to find the maximum enzymatic reaction rate (V_{max}), Michaelis-Menten constant (K_m) and average intrinsic clearance (V_{max}/K_m) for each group.

2.6 Untargeted Metabolomics

2.6.1 Sample & Batch Preparation

Plasma and liver biological matrices each run on two different chromatography columns totaling four metabolomics runs. The first column, a Waters ACQUITY UPLC HSS T3 (1.8μm particle size, 100 mm × 2.1 mm) reverse-phase liquid chromatography (RPLC) column best encompasses hydrophobic molecules while the second hydrophilic interaction liquid chromatography (HILIC) column, a Waters ACQUITY BEH Amide (1.7μm particle size, 100 mm × 2.1 mm), best separates hydrophilic molecules. Plasma and liver samples were prepared as previously described (Velenosi *et al.*, 2016) by adding 3:1 ice-cold acetonitrile with 2.5μM chlorpropamide internal standard (Sigma Aldrich) to 100μL of rat plasma or 200mg ± 5mg homogenized liver sample. Samples were vortexed, incubated at -20°C for 20 min then centrifuged at 14,000×g for 5 min. Supernatant was either diluted 1:5 in water for RPLC or directly injected for HILIC. Sample injection order was randomized and a quality control sample made from pooled samples was run every ten injections to monitor instrument drift. All samples were run in a single batch for each biological matrix and column.

2.6.2 Chromatography & Mass Spectrometry

Both RPLC and HILIC columns were maintained as previously stated (Velenosi *et al.*, 2016) at 45°C and mobile phase flow set to 0.45 ml/min consisting of UPLC-grade water (A) and acetonitrile (B), both containing 0.1% formic acid. A gradient of 0-2 min 60% B; 2-6 min 85% B; 6-8 min 99% B; 8-10 min 1% B was used. The HILIC column followed a gradient of 0–0.5 mins 99% B; 0.5–6 mins 99–50% B; 6–8 mins 50–30% B; 8–8.5 mins 30–99% B. Samples were run separately in succession for both positive and negative electrospray ionization (ESI) modes on the UPLC-QTof/MS instrument described in section 2.5. Mass spectrometer method consisted of capillary voltage 2kV, cone voltage 40V, source temperature at 150°C, desolvation gas flow 1200L/h at 600°C, and cone gas flow 50L/h. Data acquisition was conducted in centroid mode using the MS^e method as described in section 1.6.5, with 0.05s scan time over a range of 50-1200 *m/z* with collision energy of 0V for MS (function 1) and ramped from 15V-50V for MS/MS (function 2) fragmentation. For mass accuracy, lockspray solution leucine-enkephalin (500ng/mL) was used as the lockmass and set at a flow rate of 10µL/min, measured every 10s and averaged over 3 scans. Data was collected by MassLynx v4.1 software (Waters). In anticipation of detecting previously identified uremic toxins IS, PS and 4-ethylphenyl sulfate, a standard curve of these metabolites was added to the front and back of both RPLC runs in plasma and liver.

2.6.3 Data Processing

Data processing for each run and ESI mode was performed separately in R studio (v3.2.3). MassLynx data files were converted from raw to mzData files using convert.waters.raw package v1.0 (github.com/stanstrup/convert.waters.raw). Pooled samples were used to find the optimal peak picking parameters, retention time corrections and grouping parameters simultaneously with the isotopologue parameter optimization (IPO) package v1.0.0 (github.com/rietho/IPO/blob/master/vignettes/IPO.Rmd). Minimum peak width ranged from 2 to 5 seconds, maximum peak width ranged from 10 to 20 seconds and a static ppm of 15 were used as starting parameters for the IPO process. The resulting IPO parameters unique for each mode were inputted into the XCMS package v1.50.1 (Smith *et al.*, 2006) to pick appropriate peaks, integrate the area under the curve and replace zero values for all

samples within the dataset. The CAMERA package v1.32.0 was used to annotate possible isotopes and adducts (Kuhl *et al.*, 2012). XCMS and CAMERA packages were used to integrate positive and negative ESI modes before normalizing to internal standard chlorpropamide and applying a threshold of 30% variability of the quality control. Through an in-house R script positive and negative modes were combined to make one dataset ready for statistical software with masses identified in both modes retained in the mode with greater intensity (Urquhart Laboratory, *unpublished*).

2.6.4 Metabolite Identification

The accurate monoisotopic mass (*m/z*) and fragmentation spectrum of each metabolite was used to identify potential metabolite matches within the METLIN, MassBank or Human Metabolome Database (HMDB) (Wishart *et al.*, 2013). This was carried out by first searching the parent *m/z* ratio in the corresponding ionization mode across all possible adducts with a molecular weight tolerance of ±0.01Da. The MOL file for each suspected metabolite was downloaded from the HMDB website and uploaded using MassFragment, a MassLynx software add-on, to compare expected fragmentation patterns with the experimental fragmentation pattern. Fragmentation profiles of metabolites representing the most experimental fragments were purchased for identity confirmation.

A categorical system of metabolite identification has been adapted from previously defined levels 1 through 4 (Salek *et al.*, 2013). To confirm a suspected metabolite's identity, a purchased standard was run and compared to a sample known to have the unidentified signal. If the retention time, accurate mass and fragmentation pattern matched across the experimental sample and purchased standard, it was considered "level 1 identified". Level 2 identified metabolites exhibited HMDB and METLIN database matches with delta $\leq$ 5ppm and conformation to at least one of the following criteria: a matching online database fragmentation spectrum, or matching *m/z* ratio in a publication where it was similarly identified. Level 2 identification is typically used when analytical standards are unavailable or the cost prohibits level 1 identification. Level 3 identified metabolites required only a HMDB and METLIN match with delta $\leq$ 5ppm. Metabolites with multiple matches, zero matches or deltas $\geq$ 5ppm were considered unknown.

Metabolite standards were obtained as follows: indoxyl sulfate from Gold Biotechnology (Olivette, MO), phenyl sulfate and 4-ethyl phenyl sulfate were synthesized as previously described (Velenosi *et al.*, 2016), allantoin, L-carnitine, 2,8-dihydroxyadenine and equol 4/7 glucuronide were purchased from Toronto Research Chemicals (Toronto, ON), creatinine from Sigma Aldrich and pantothenic acid from Supelco (Bellefonte, PA).

2.7 Gut Microbial Sequencing

2.7.1 Illumina Sequencing

DNA was extracted from caecum swabs using the PowerSoil-96 Well DNA isolation kit from MoBio using convenience modifications of the Earth Microbiome Project protocol (Gilbert *et al.*, 2014). Unique barcoded primers named 515F and 806R (Caporaso *et al.*, 2011; Gilbert *et al.*, 2014) amplified the V4 variable region of the 16S rRNA gene. A total of 12 forward and 24 reverse primers barcodes were used to provide 288 unique primer combinations. The primers are as follows: forward primer [5'-ACACTCTTT CCCTACACGACGCTCTTCCGATCTnnnn(8)GTGCCAGCMGCCGCGGTAA-3'] and reverse primer [5'-CGGTCTCGGCATTCCTGCTGAACGCTCTTCCGATCTnnnn (8)GGACTACHVGGGTWTCTAAT-3'] where the 5' end is the Illumina adaptor sequence, the nnnn indicates four random nucleotides, (8) represents one of the 36 barcoded sequences eight nucleotides in length and the 3' end is the primer region for V4 (Supplementary Table 1. Appendix B) (Gloor *et al.*, 2010). Amplification was carried out in 42µL total volume with 20µL primer mix (3.2pmol/µL per primer), 20µL GoTaq Hot Start Mastermix (Thermo Scientific) and 2µL template DNA then run for 2 min at 95°C followed by 25 cycles of 1 min at 95°C; 1 min at 52°C and 1 min at 72°C excluding a final elongation. Barcoded PCR products were quantified with a Qubit dsDNA assay kit on a Qubit 2.0 (Life Technologies), normalized by amount of DNA, pooled then purified with a PCR clean-up column. The cleaned DNA is amplified once more with primers OLJ139 [5'AATGATACGGCGACCACCGAGATCTACACTCTTTCCCTACACGA3'] and OLJ140 [5'CAAGCAGAAGACGGCATACGAGATCGGTCTCGGCATT CCTGCTGAAC3'] (Majerczyk *et al.*, 2010) before paired-end, high-throughput

sequencing on the Illumina MiSeq platform at the London Regional Genomics Centre (LRGC, lrgc.ca, London, ON).

2.7.2 Data Processing

Paired reads, each 220bp long were processed with the Illumina_SOP protocol accessed through Github with minor convenience revisions (https://github.com/ggloor/miseq_bin). After demultiplexing, raw reads were first overlapped with a minimum 30 nucleotides using Pandaseq (v2.5) (Masella *et al.*, 2012) then filtered with in-house Perl and UNIX scripts to ensure exact barcode matching and primer matching with up to two allowable mismatches (Gloor *et al.*, 2010). OTUs were clustered using the uSearch (v7.0.1090) script (Edgar, 2010) at 97% identity and the most abundant sequence was applied for annotation via the mothur script (Schloss *et al.*, 2009) to search the Silva 16S rRNA gene reference database (Silva.nr_v119) (Quast *et al.*, 2013; Yilmaz *et al.*, 2014). In mothur, a bootstrap cut-off of 70% was used for taxonomical identification and redundancy. A total of 1199 OTUs were retained across all samples (Supplementary Table 2. Appendix B). Due to study time-period differences, only days 3, 14, 28 and 42 could be used for sequencing analysis. In R studio (v3.2.3) the zCompositions (v1.0.3-1) package (Martín-Fernández *et al.*, 2003) was used for zero-replacement before data was centre-log ratio (clr) transformed for compatibility with downstream univariate and multivariate statistics (Gloor & Reid, 2016; Gloor *et al.*, 2016*b*).

2.8 Statistical Analysis

2.8.1 Disease Markers, Real-Time PCR, Western Blotting & Enzymatic Activity Assay

DME measurements and disease markers urea and creatinine are presented as mean ± SEM and analyzed by 2-way ANOVA paired with Sidak's multiple comparisons test. $*p < 0.05$ compared to matching day control indicates significance.

2.8.2 Untargeted Metabolomics

Principal component analysis (PCA) was used to evaluate the initial separation between CKD and control over time for each of the four analytical runs using MassLynx software

and the EZInfo v2.0 package (Umetrics, Umeå, Sweden). Placement of each sample within a PCA plot is determined by the entire detectable metabolite composition within each sample with relation to all other samples. Samples within close proximity are considered "clustered" and represent samples with similar compositions. Data for each of the four runs was Pareto scaled to remove emphasis on metabolites with large magnitude of variance. Outliers were removed utilizing a Hotelling's analysis with a maximum allowable T^2 range of 35 (Wiklund, 2008). Pooled samples are confirmed to show little variance and a clear separation is identified between control and condition before applying statistics. Each statistical method: multivariate, univariate and correlations to each DME, was performed independently on the same metabolomics dataset for each of the four runs with the aim to isolate metabolites related to CYP alterations. Each of the 1] multivariate, 2] univariate and 3] correlation analyses are described below.

1] Multivariate analysis was performed on all four runs, on all 5 days in comparison with same day control. EZInfo was used to generate orthogonal partial least squares discriminant analysis (OPLS-DA) of the original PCA (Figure 2.1). OPLS-DA, unlike PCA, is a supervised comparison between known groups. To assess multivariate OPLS-DA sufficiency, each comparison received goodness of fit values R^2 and Q^2. R^2 is the goodness of fit estimated for the model and Q^2 is the level of prediction accuracy the model infers if the experiment were to be repeated. The values are dependent and thus can be expressed as a ratio (R^2/Q^2) with the expectation that $R^2/Q^2 < 2$ or $Q^2 > 0.5$ (Triba *et al.*, 2015). The metabolites characteristic of treatment were then plotted as an S-plot with axis of "p(corr)[1]" representing the treatment difference and "p[1]" representing the magnitude of the metabolite's influence. Strict thresholds were applied (VIP > 0.8; p(corr)[1] > 0.4 or < -0.4) by finding the variable importance in projection (VIP) and the p(corr)[1] axis as a general measure of magnitude and difference between treatments (Farrés *et al.*, 2015) (Figure 2.1). Only metabolites that met or exceeded the S-plot thresholds on two or more consecutive time points were retained for comparison with univariate and correlative analyses.

2] Univariate analysis on the original metabolomics datasets were used to assess the relative concentration of each metabolite over time and course of the disease. Open access

online software MetaboAnalyst 3.0 was used to perform a p-value corrected (FDR = 0.05) independent 2-way ANOVA on each metabolite via the “Time Series” and “Two-factor independent samples” applications (Wishart *et al.*, 2013). No additional data filtering, normalization or transformation was performed. Pareto scaling was applied for consistency. Significance ($p<0.05$) was required for both “*Time*” and “*Disease*” to retain the metabolite for comparison with multivariate and correlative analyses.

3] Spearman correlations were conducted between each metabolite and the mRNA, protein or enzymatic activity levels of each enzyme. Spearman correlation analysis of metabolomics results have been conducted in the past to compare metabolites to other metabolites (Camacho *et al.*, 2005), metabolites to bacterial abundances (Theriot *et al.*, 2014; McMillan *et al.*, 2015), and metabolites to gene expression (Bartel *et al.*, 2015; Auslander *et al.*, 2016). Original processed metabolomics dataset for each run was matched by sample to the corresponding DME dataset and a correlation coefficient (r) obtained before comparison to the final multivariate and univariate subsets. R-values were manually filtered with high stringency ($r > 0.65$ or $r < -0.65$) since more than 50% of the dataset satisfied $p<0.0001$. After filtering, correlation analysis provided the smallest subset of the three analysis methods. Metabolites on this list that did not also satisfy univariate analysis were removed from the correlation subset. Metabolites that did not satisfy multivariate analysis are indicated but retained to capture biologically relevant changes independent of magnitude.

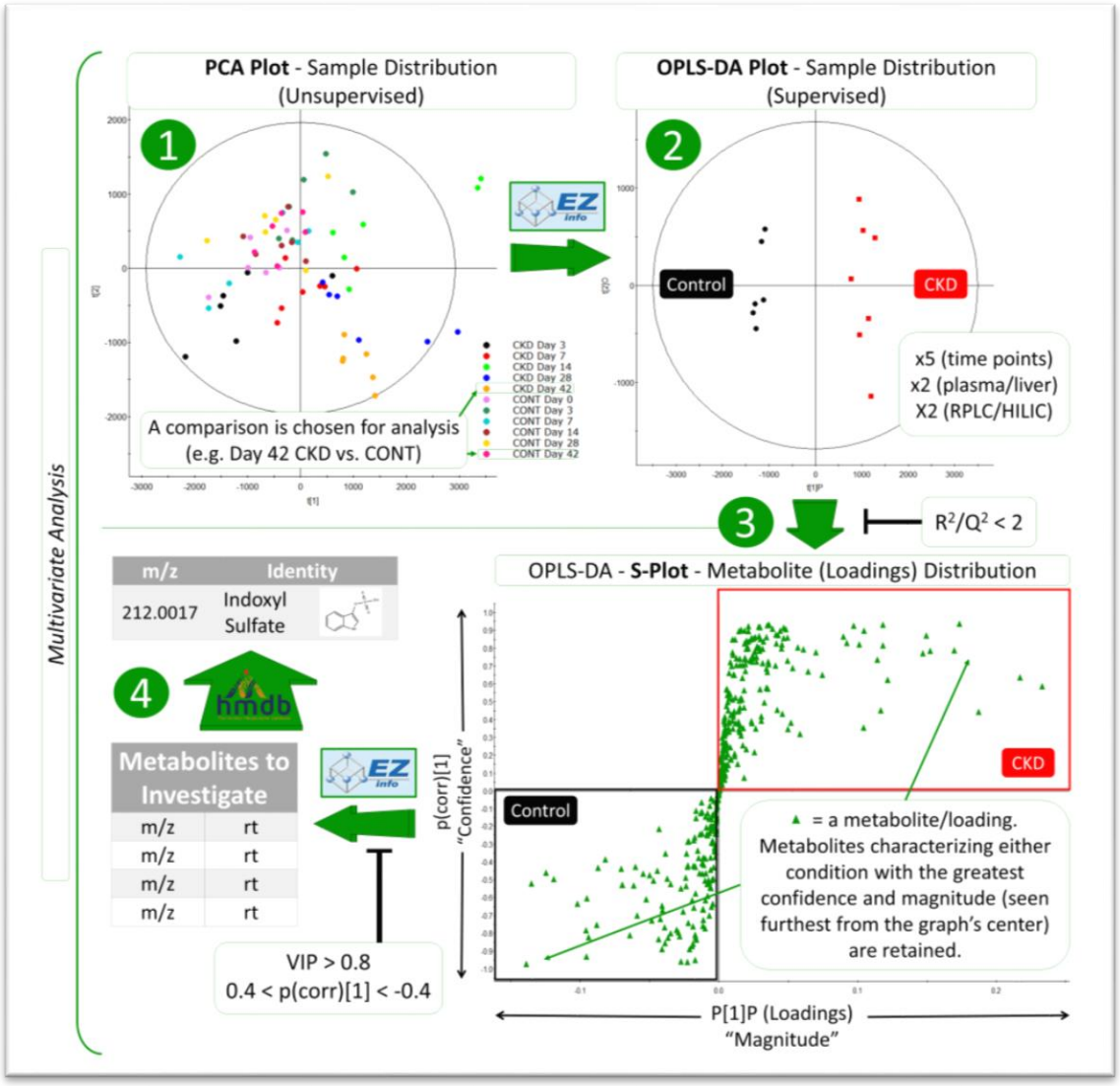

Figure 2.1. Example of multivariate analysis workflow utilizing OPLS-DA and S-plots. A PCA is made using EZInfo software (1), comparisons are chosen for OPLS-DA, an OPLS-DA plot of sample distribution is made and R^2 and Q^2 thresholds are applied (2). Successful OPLS-DA plots are further analyzed by observing metabolite contributions towards either condition by S-plot (3) where VIP and p(corr)[1] thresholds are applied. From the S-plot, a list of *m/z* ratios and retention times (4) in addition to fragmentation pattern are searched within online databases such as HMDB in attempt to identify the metabolite.

2.8.3 Caecal Microbiota

Multivariate PCA was performed in EZInfo as described for untargeted metabolomics except no scaling was utilized to emphasize large variations. Although applied infrequently in the microbiology field (Hong *et al.*, 2011; Stewart *et al.*, 2015), R^2 and Q^2 values are important for understanding the variability in the PCA and were calculated for consistency with metabolomics analysis. To obtain univariate differences between CKD and control groups, the effect size and overlap for each bacterial taxonomic group was calculated for each time point individually using the R package ALDEx2 (v1.2.0) (bioconductor.org/packages/release/bioc/html/ALDEx2.html) (Fernandes *et al.*, 2014; Gloor *et al.*, 2016*a*). Severe thresholds were applied to both effect size (> 1.5 or < -1.5) and overlap (< 6.5%) for each bacterial abundance (Macklaim *et al.*, 2013; Halsey *et al.*, 2015; Gloor *et al.*, 2016*a*). OTUs that met or exceeded the thresholds were graphed and significance was defined as satisfying the effect size and overlap thresholds with 95% confidence. Where applicable, genera were manually searched for species and strain information by Targeted Loci Nucleotide BLAST application through NCBI (blast.ncbi.nlm.nih.gov/Blast.cgi).

Chapter 3

3 Results

3.1 Model Validation

First, I validated the adenine-fed CKD model by measuring plasma CKD markers urea and creatinine alongside kidney histological analysis across all time points. CKD markers urea and creatinine both showed significant increase in CKD rat plasma by day 14 (Figure 3.1.A-B). This increase continued to a 9-fold and 11-fold difference between CKD and control for urea and creatinine, respectively, on day 42. Kidney histology showed enlarged tubules, inflammatory cells and fibrosis by day 14 through to day 42 (Figure 3.1.C-H). Animal weights did not change between groups (Table 3.1).

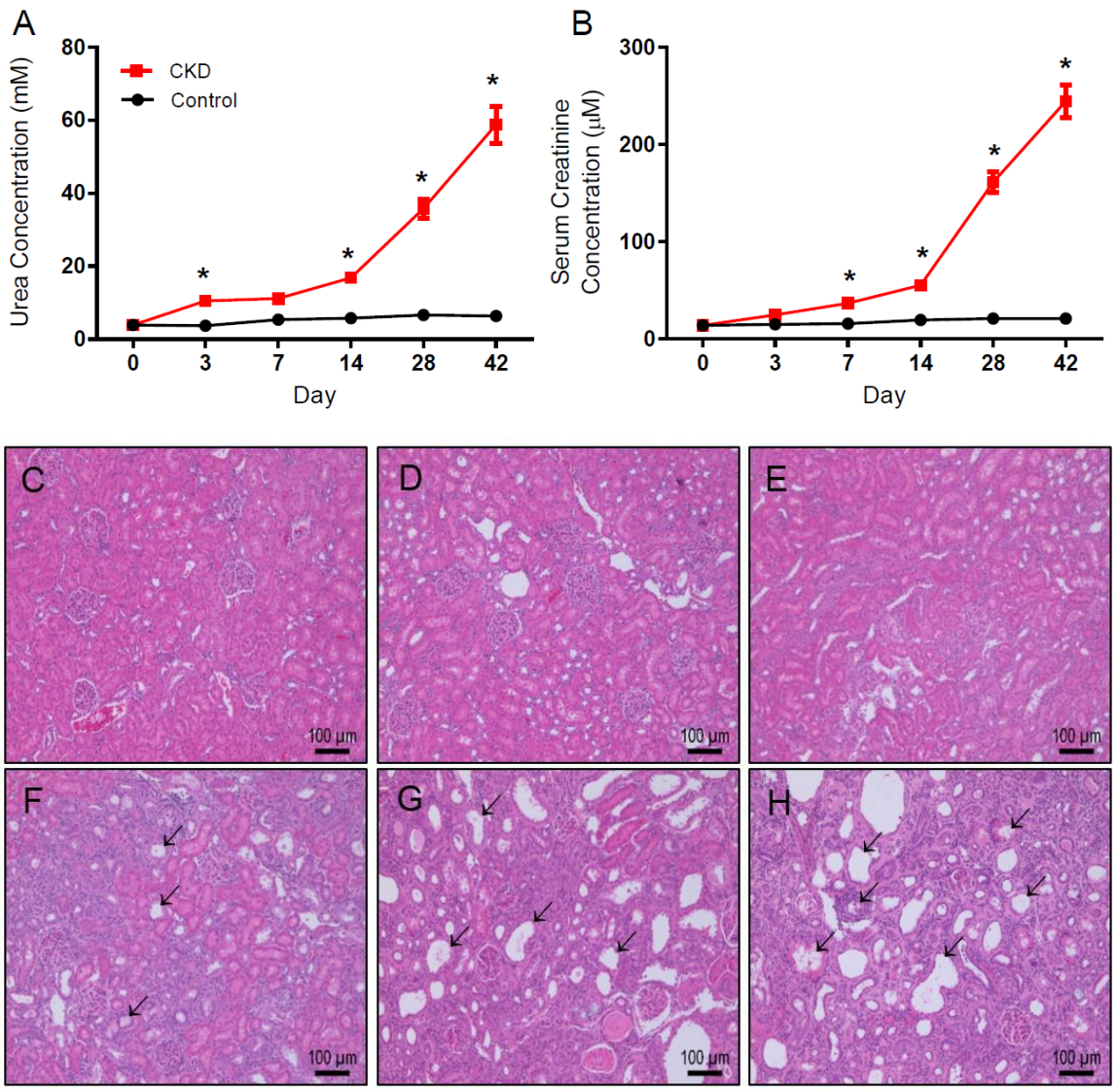

Figure 3.1. Assessment of CKD in Wistar rats orally administered 0.5% adenine over 42 days. (A) Plasma urea (mM) and (B) serum creatinine (µM) concentrations of control and CKD rats presented as mean ± SEM. *$p < 0.05$ when compared to matching day control; n ≥ 6. H&E stained rat kidney sections from day 42 control (C) and CKD days 3 (D), 7 (E), 14 (F), 28 (G) and 42 (H). Arrows indicate enlarged nephron tubules and areas of fluid retention. Inflammatory cells and areas of atrophy are evident on days 14, 28 and 42.

Table 3.1. Weight in grams of control and CKD rats over 42 days.

		Control	CKD
Weight (g)	Day 0	206.5 ± 1.4 (n=41)	207.1 ± 1.8 (n=36)
	Day 3	188.6 ± 1.1 (n=41)	186.1 ± 1.5 (n=36)
	Day 7	201.0 ± 1.5 (n=24)	202.4 ± 1.9 (n=26)
	Day 14	227.3 ± 2.0 (n=18)	227.9 ± 3.3 (n=19)
	Day 28	257.3 ± 2.6 (n=12)	258.3 ± 5.0 (n=13)
	Day 42	274.5 ± 8.4 (n=6)	254.7 ± 12.7 (n=7)

3.2 Hepatic CYP3A2 & CYP2C11 mRNA Expression over CKD Progression

Having confirmed the adenine-fed rats were developing CKD, the mRNA expression of DMEs CYP3A2 and CYP2C11 were assessed in the liver. CYP3A2 mRNA expression was minimally decreased on day 3, recovered on day 7, then declined substantially by day 14 (-83%, $p<0.001$) which persisted to day 42 (-99%, $p<0.001$) (Figure 3.2.A). CYP2C11 mRNA expression was unchanged on day 3 but largely increased in the control group on day 7 leaving CKD rats well below normal (-76%, $p<0.001$) (Figure 3.2.B). On day 14 (-84%, $p<0.001$), day 28 (-96%, $p<0.001$), and day 42 (-98%, $p<0.001$) the CKD CYP2C11 mRNA expression remained low in comparison to control.

3.3 Hepatic CYP3A2 & CYP2C11 Protein Expression over CKD Progression

To ascertain whether protein expression was changed with respect to mRNA expression, CYP3A2 and CYP2C11 protein quantification was carried out by western blotting. Decreases in CYP3A2 protein levels were seen on day 14 (-63%, $p<0.001$), day 28 (-86%, $p<0.001$) and day 42 (-85%, $p<0.01$) (Figure 3.2.C). CYP2C11 protein quantification also shows depletion in CKD but starting on day 7 (-42%, $p<0.05$) through to day 42 (-83%, $p<0.001$) (Figure 3.2.D). A non-specific CYP3A2 band was not quantified.

3.4 Hepatic CYP3A2 & CYP2C11 Enzymatic Activity over CKD Progression

Sequentially, CYP3A2 and CYP2C11 enzymatic activity was assessed from liver microsomes. CYP3A2 intrinsic activity in CKD rats decreased on day 3, recovered on day 7 and fell again 3.6-fold by day 14, 13-fold by day 28 and nearly 14-fold lower than controls by day 42 (Figure 3.2.E). The intrinsic activity of CYP2C11 showed a 4.6-fold difference between CKD and control as early as day 7 and up to 12.8-fold difference by day 42 (Figure 3.2.F). V_{max}, K_m and intrinsic clearance are summarized (Table 3.2).

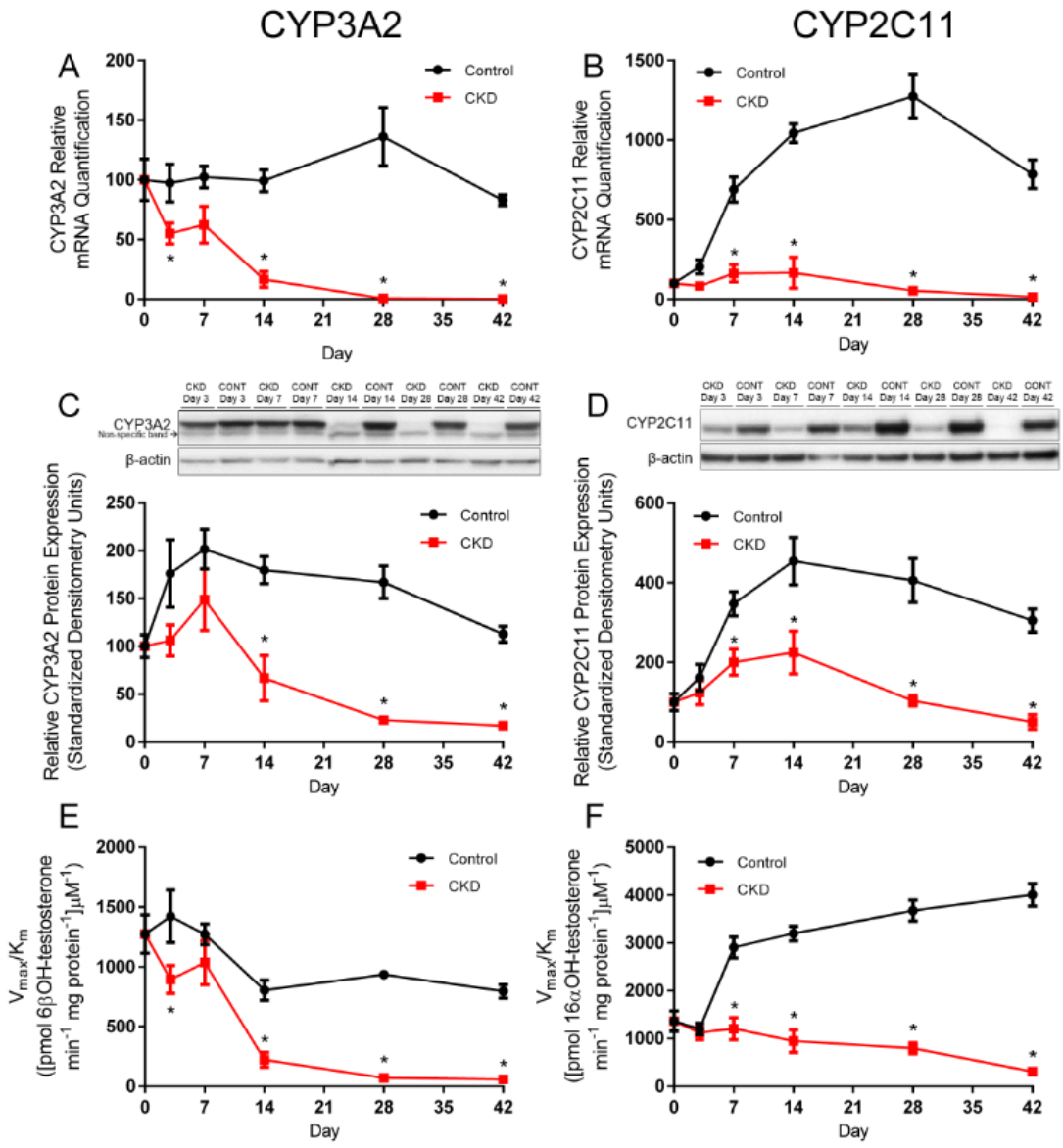

Figure 3.2. Relative mRNA expression, protein expression and enzymatic activity levels of CYP3A2 and CYP2C11. CYP3A2 (A) and CYP2C11 (B) mRNA expression and protein expression, CYP3A2 (C) and CYP2C11 (D), with representative western blots. Values were relative to β-actin represented as the mean ± SEM, normalized to control day 0 and arbitrarily defined as 100%. A non-specific band in CYP3A2 immunoblot was not quantified. Enzymatic activity of CYP3A2 (D) and CYP2C11 (E) in control and CKD rats represented as the mean intrinsic clearance V_{max}/K_m [(pmol/min/mg protein)/µM] of testosterone metabolite ± SEM. *$p < 0.05$ when compared to matching day control; $n \geq 6$.

Table 3.2. CYP3A2 and CYP2C11 enzymatic activity over CKD progression. 6βOH-testosterone (CYP3A2) and 16αOH-testosterone (CYP2C11) production of liver microsomes measured following incubation with NADPH and testosterone. *p<0.05 compared to matching day control; n ≥ 6.

	6βOH-testosterone (CYP3A2)					
	V_{max}[a]		K_m[a]		Intrinsic Clearance (V_{max}/K_m)[a]	
	Control	CKD	Control	CKD	Control	CKD
Day 0	35938±2841	35938±2841	29.5±9.02	29.5±9.02	1275±393.87	1275±393.87
Day 3	56184±5640	**26425±2097***	40.1±14.46	29.8±9.13	1422±540.42	**894±288.25***
Day 7	49912±1806	42396±4911	40.2±5.218	42.7±17.48	1272±214.04	1036±489.05
Day 14	38223±2797	**12804±1983***	49.4±12.34	59.4±29.88	804±207.09	**222±152.72***
Day 28	61702±3069	**10102±1289***	66.6±10.43	**141.6±44.74***	936±86.36	**71±21.50***
Day 42	45706±2266	**7849±1297***	58.5±9.46	**135.6±56.32***	795±139.12	**58±24.76***
	16αOH-testosterone (CYP2C11)					
	V_{max}[a]		K_m[a]		Intrinsic Clearance (V_{max}/K_m)[a]	
	Control	CKD	Control	CKD	Control	CKD
Day 0	17983±1210	17983±1210	14.2±4.56	14.2±4.56	1365±518.05	1365±518.05
Day 3	25892±2353	15453±1195	21.8±8.28	13.8±5.13	1202±298.73	1123±357.65
Day 7	41420±2488	27114±3431	14.3±4.09	23.5±12.17	2907±541.70	**1206±607.94***
Day 14	51824±2556	**17521±2406***	16.9±3.75	18.6±11.18	3199±377.15	**948±523.91***
Day 28	72358±2064	**16236±1548***	20.1±2.45	21.2±8.52	3679±548.84	**797±273.19***
Day 42	62571±3147	**6658±513***	16.2±3.71	22.6±7.21	4005±570.00	**312±179.33***

[a]V_{max}, K_m and intrinsic clearance (V_{max}/K_m) were obtained by Michaelis-Menten kinetics.

3.5 Plasma & Liver Metabolomics

Having demonstrated changes in mRNA, protein levels and enzymatic activity in the CYP enzymes, I next performed an untargeted metabolomics analysis by MS to assess changes in metabolite composition. Principle component analysis (PCA) clearly separated CKD and control for both rat plasma and liver samples (Figure 3.3). Early disease stages are arbitrarily defined as day 3-14 and late stages days 28 and 42. A loadings biplot for each run shows the position of each loading/metabolite (Figure 3.4). OPLS-DA plots were generated for each of the twenty comparisons across all four runs. OPLS-DA plots comparing control versus CKD at each time point for the plasma RPLC run provide an example for the other three runs (Figure 3.5). R^2 and Q^2 parameters were used to accompany the interpretation of OPLS-DA plots and R^2/Q^2 ratio < 2 represent results with high reproducibility between control and CKD on each day (Table 3.3). Metabolites in rat plasma were well separated from control as early as day 3 when using RPLC (Figure 3.3.A). Liver RPLC showed far less separation between control and CKD before day 28 (Figure 3.3.B). The HILIC column showed separation back to day 7 except for poor Q^2 values on day 14 in both plasma and liver samples (Figure 3.3.C-D).

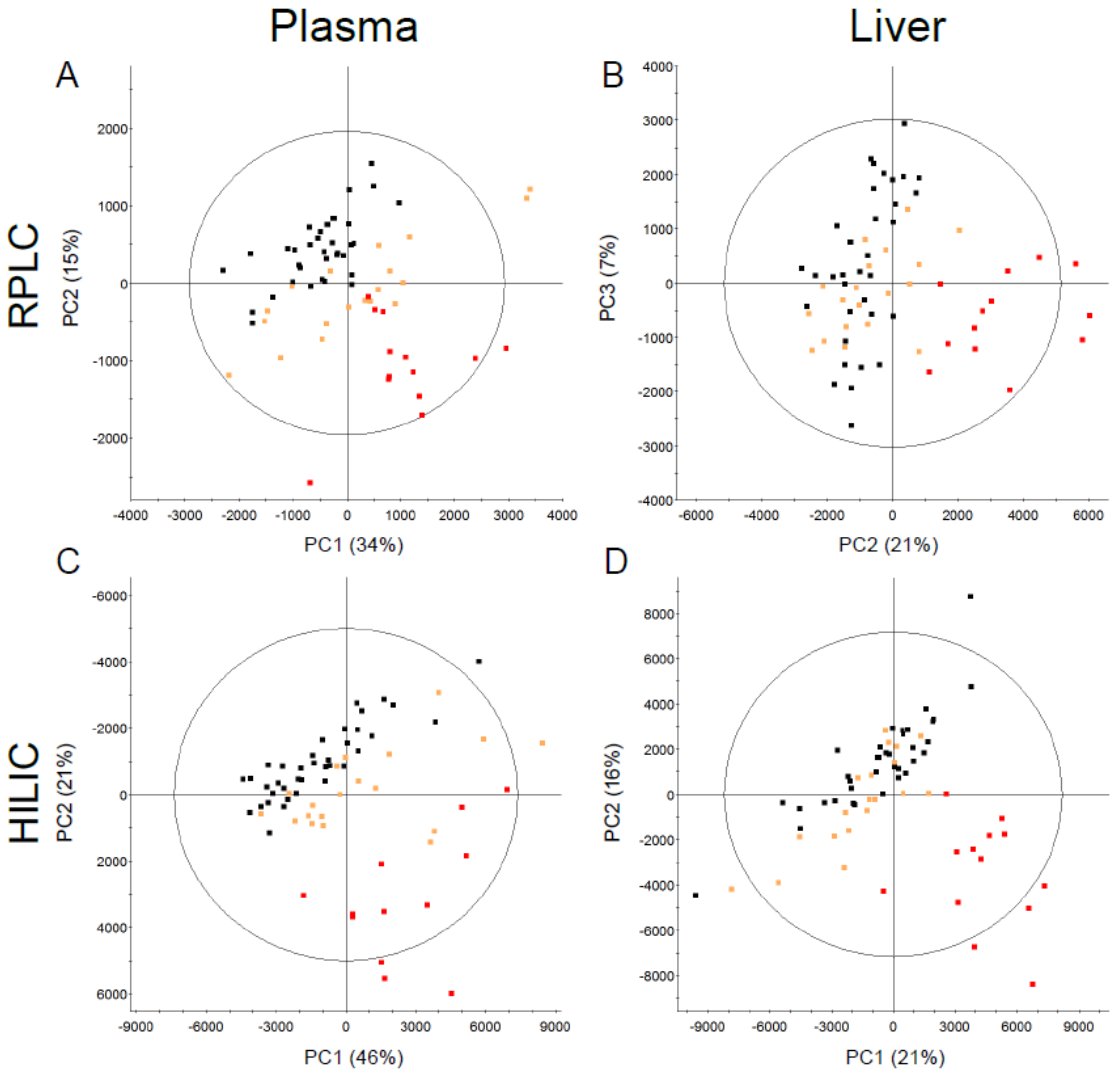

Figure 3.3. Unsupervised principle component analysis (PCA) plots of rat plasma (A) and liver (B) metabolome separated by RPLC. PCA of plasma (C) and liver (D) metabolome separated by HILIC. Each point is either control (■), early stage CKD defined by day 3, 7 and 14 (■), or late stage CKD defined by days 28 and 42 (■). Each axis is either the first [1], second [2] or third [3] principle component showing the two components representing the largest variation between groups and displayed as a percentage of component contribution. Placement of each sample is determined by the metabolite composition within each sample and clustered samples share similar compositions. Data is centered and Pareto-scaled. Select rat samples were removed as outliers (A) no outliers, (B) a day 3 and day 42 control, (C) a day 28 CKD sample, and (D) a day 7 control sample.

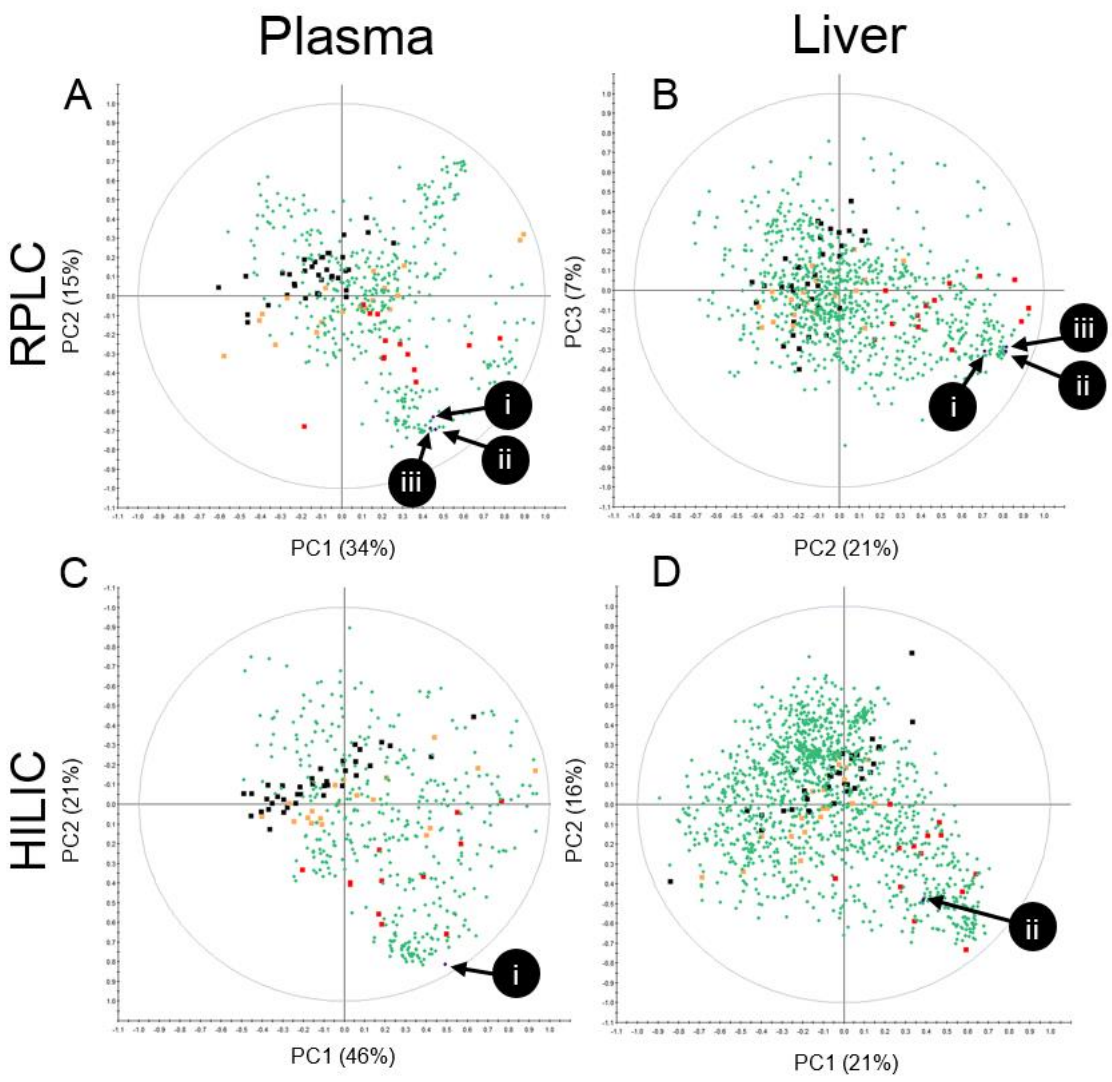

Figure 3.4. Loadings biplot of rat plasma (A) and liver (B) metabolome separated by RPLC and plasma (C) and liver (D) metabolome separated by HILIC. Each point is either a sample control (■), early stage CKD defined by day 3, 7 and 14 (■), late stage CKD defined by days 28 and 42 (■), or a metabolite loading (●). Metabolites PS (i), EPS (ii) and IS (iii) are indicated. Each axis is either the first [1], second [2] or third [3] principle component showing the two components representing the largest variation between groups and displayed as a percentage of component contribution. Data is centered and Pareto-scaled. Select rat samples were removed as outliers (A) no outliers, (B) a day 3 and day 42 control, (C) a day 28 CKD sample, and (D) a day 7 control sample.

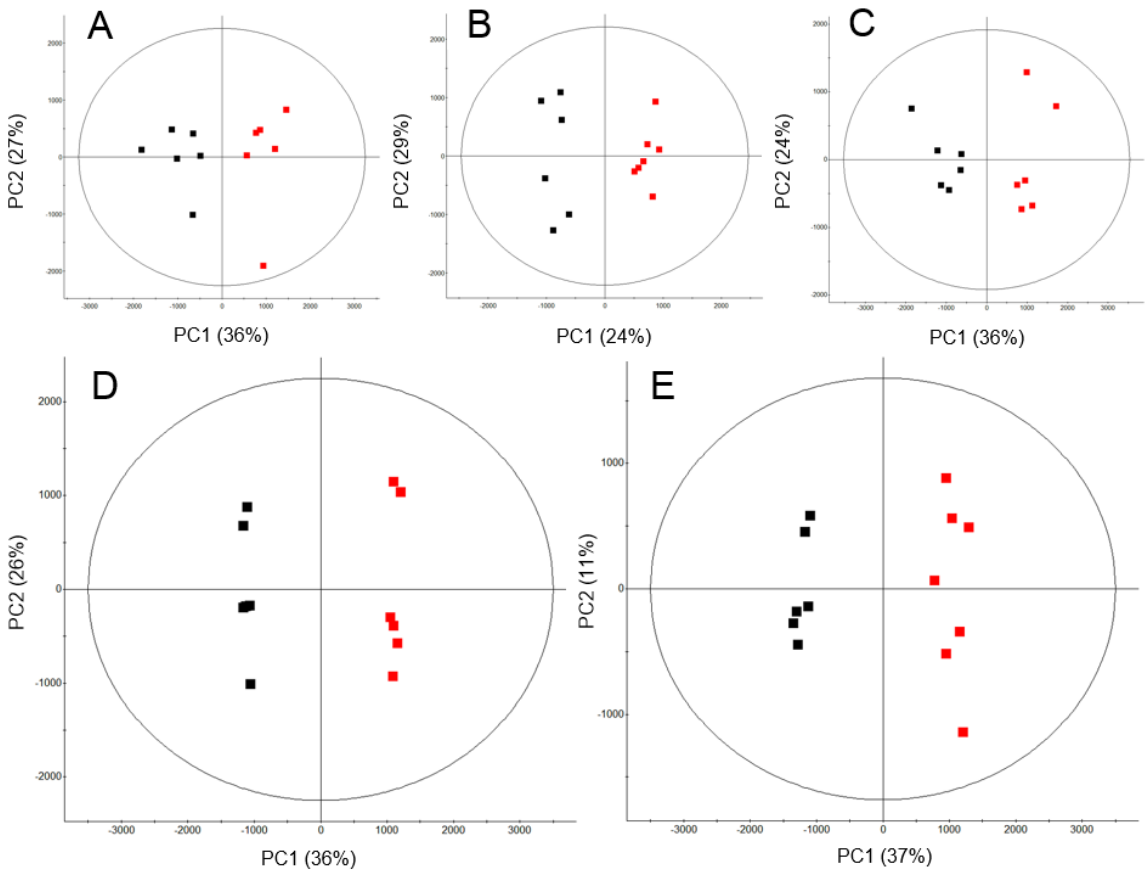

Figure 3.5. OPLS-DA plots generated from the PCA of rat plasma separated by RPLC for day 3 (A), day 7 (B), day 14 (C), day 28 (D) and day 42 (E). Each point is a control (■) or CKD (■) sample. Each axis is the first [1] and second [2] principle component representing the largest variation between supervised groups and displayed as a percentage of component contribution.

Table 3.3. Multivariate OPLS-DA parameters R^2 and Q^2. R^2 and Q^2 values for plasma and liver metabolomics using RPLC and HILIC across all time points.

	Rat Plasma							
	RPLC				**HILIC**			
Day 42	Comp No.	R^2	Q^2	R^2/Q^2	Comp No.	R^2	Q^2	R^2/Q^2
	[1]	0.9859	0.9175	1.0745	[1]	0.9821	0.5936	1.6546
	[2]	0.9859	0.9493	1.0385	[2]	0.9821	0.8064	1.2180
					[3]	0.9821	0.8677	1.1319
Day 28	Comp No.	R^2	Q^2	R^2/Q^2	Comp No.	R^2	Q^2	R^2/Q^2
	[1]	0.9982	0.6410	1.5572	[1]	0.9734	0.8402	1.1586
	[2]	0.9982	0.8176	1.2210	[2]	0.9734	0.9491	1.0255
Day 14	Comp No.	R^2	Q^2	R^2/Q^2	Comp No.	R^2	Q^2	R^2/Q^2
	[1]	0.8940	0.5438	1.6439	[1]	0.7248	**0.2872ǂ**	**2.5240ǂ**
	[2]	0.8940	0.5203	1.7181	[2]	0.7248	0.5121	1.4152
Day 7	Comp No.	R^2	Q^2	R^2/Q^2	Comp No.	R^2	Q^2	R^2/Q^2
	[1]	0.9628	0.5418	1.7770	[1]	0.9169	0.5979	1.5336
	[2]	0.9628	0.7150	1.3466	[2]	0.9169	0.8431	1.0876
Day 3	Comp No.	R^2	Q^2	R^2/Q^2	Comp No.	R^2	Q^2	R^2/Q^2
	[1]	0.8680	0.5969	1.4542	[1]	0.9873	**0.2812ǂ**	**3.5112ǂ**
	[2]	0.8680	0.5420	1.6016	[2]	0.9873	0.6354	1.5538
					[3]	0.9873	0.7510	1.3146
	Rat Liver							
	RPLC				**HILIC**			
Day 42	Comp No.	R^2	Q^2	R^2/Q^2	Comp No.	R^2	Q^2	R^2/Q^2
	[1]	0.9753	0.7750	1.2585	[1]	0.9832	0.8722	1.1273
	[2]	0.9753	0.8708	1.1200	[2]	0.9832	0.9194	1.0694
	[3]	0.9753	0.9214	1.0585				
Day 28	Comp No.	R^2	Q^2	R^2/Q^2	Comp No.	R^2	Q^2	R^2/Q^2
	[1]	0.9691	0.7830	1.2377	[1]	0.9900	0.9034	1.0958
	[2]	0.9691	0.9284	1.0438	[2]	0.9900	0.9286	1.0661
Day 14	Comp No.	R^2	Q^2	R^2/Q^2	Comp No.	R^2	Q^2	R^2/Q^2
	[1]	0.8357	**0.0070*ǂ**	**118.877*ǂ**	[1]	0.9712	**0.4582ǂ**	**2.1194ǂ**
	[2]	0.8357	**0.2953ǂ**	**2.8298ǂ**	[2]	0.9712	0.6679	1.4541
					[3]	0.9712	0.7677	1.2651
Day 7	Comp No.	R^2	Q^2	R^2/Q^2	Comp No.	R^2	Q^2	R^2/Q^2
	[1]	0.9973	**0.3534ǂ**	**2.8218ǂ**	[1]	0.9512	0.5142	1.8498
	[2]	0.9973	0.7233	1.3787	[2]	0.9512	0.7394	1.2864
	[3]	0.9973	0.8425	1.1837				
Day 3	Comp No.	R^2	Q^2	R^2/Q^2	Comp No.	R^2	Q^2	R^2/Q^2
	[1]	0.8938	0.5384	1.6601	[1]	0.9512	0.5142	1.8498
	[2]	0.8938	0.5749	1.5548	[2]	0.9512	0.7394	1.2864
					[3]	0.9873	0.7510	1.3146

ǂ Values indicate poor predictability. *Abnormal values, considered poor predictability. Comp No. = principle component number.

3.6 DME & Uremic Toxins

After establishing changes in the metabolomic profile by PCA, metabolites were correlated to CYP mRNA, protein and enzymatic activity after satisfying multivariate and univariate analysis. 204 *m/z* ratios were identified across all four runs that correlated with either CYP3A2 or CYP2C11 (Supplementary Table 3. Appendix B). Of these 204 *m/z* ratios, 9 metabolites were identified at identification level 1 using purchased standards. These metabolites include: Allantoin, L-carnitine, creatinine, 2,8-dihydroxyadenine, equol-4/7-O-glucuronide, 4-ethylphenyl sulfate, IS, pantothenic acid (vitamin B5) and PS (Table 3.4). IS, PS and 4-ethylphenyl sulfate concentrations across both plasma and liver samples using RPLC were quantified via standard curve. All three metabolites show significantly increased concentrations ($p<0.0001$) on days 28 and 42 for both plasma and liver tissue (Figure 3.6).

Table 3.4. Metabolites classified level 1 from CKD and control rat plasma and liver untargeted metabolomics.

ID Level	Mass Error (ppm)[a]	Mass (*m/z*)	t_R (min)	Empirical Formula (Adduct)	Identity	Matrix[b]	Column	ESI Mode	CYP3A2 Correlation (r value)[c]	CYP2C11 Correlation (r value)[c]	Satisfies Multivariate Analysis[d]
1	2	181.0328	0.57	C4H6N4O3 (M+Na)	Allantoin	P	RPLC	(+)	-0.7254	-0.7073	FALSE
1	5	157.0359	0.56	C4H6N4O3 (M-H)	Allantoin	L	RPLC	(-)	-0.7284	-0.7920	FALSE
		157.0360	0.57			P	RPLC	(-)	-0.7391	-0.7921	FALSE
1	1	162.1123	0.53	C7H15NO3 (M+H)	L-Carnitine	P	RPLC	(+)	0.6694	0.8657	TRUE
1	0	114.0662	3.24	C4H7N3O (M+H)	Creatinine	P	HILIC	(+)	-0.7029	-0.6590	TRUE
1	1	168.0515	4.56	C5H5N5O2 (M+H)	2,8-Dihydroxyadenine	P	HILIC	(+)	-0.7336	-0.6860	FALSE
1	2	417.1182	1.85	C21H22O9 (M-H)	Equol 4/7-O-Glucuronide	L	RPLC	(-)	-0.7265	-0.8050	TRUE
1	3	201.0221	1.06	C8H10O4S (M-H)	4-Ethylphenyl Sulfate	L	HILIC	(-)	-0.6689	n/a	TRUE
		201.0221	2.13			L	RPLC	(-)	-0.7387	n/a	TRUE
		201.0221	2.10			P	RPLC	(-)	-0.6813	n/a	TRUE
1	3	212.0016	1.65	C8H7NO4S (M-H)	Indoxyl Sulfate	L	RPLC	(-)	-0.7201	n/a	TRUE
		212.0017	1.65			P	RPLC	(-)	-0.7072	n/a	TRUE
1	0	220.1179	2.23	C9H17NO5 (M+H)	Pantothenic Acid	P	HILIC	(+)	n/a	-0.7160	TRUE
1	3	172.9909	1.27	C6H6O4S (M-H)	Phenyl Sulfate	L	HILIC	(-)	-0.6914	-0.6770	TRUE
		172.9906	1.59			L	RPLC	(-)	-0.726	-0.6840	TRUE
		172.9907	1.38			P	HILIC	(-)	-0.6848	-0.6500	TRUE
		172.9906	1.57			P	RPLC	(-)	-0.6902	n/a	TRUE

[a]Mass error was obtained using the 4th decimal place *m/z* from the Human Metabolome Database (HMDB). [b]P = Plasma; L = Liver. [c]Metabolites satisfying univariate analysis and Spearman correlation to same-sample CYP3A2 or CYP2C11 data with correlation coefficients (r value) listed. 2-way independent ANOVA was conducted via MetaboAnalyst v3.0 (Wishart *et al.*, 2013) using FDR<0.05 to correct for multiple comparisons and satisfaction required p<0.05 across both *"Time"* and *"Disease"*. [d]Multivariate analysis required VIP > 0.8 and 0.4 < p(corr)[1] < -0.4 indicating adequate separation by OPLA-DA and S-plot.

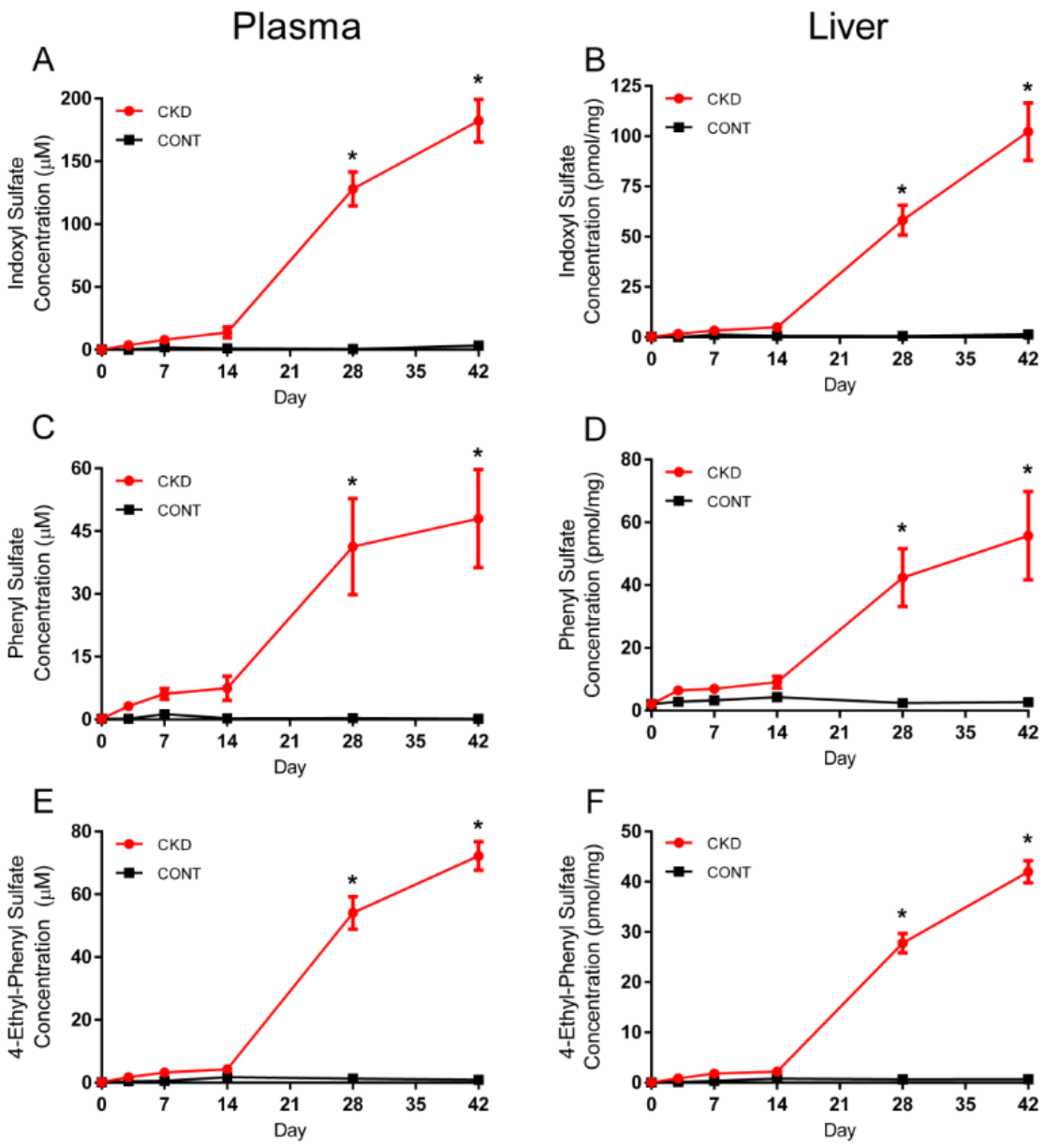

Figure 3.6. Quantitative analysis of metabolites IS, PS and EPS. Plasma IS (A), PS (C), EPS (E) (μM) and liver IS (B), PS (D) and EPS (F) (pmol/mg liver tissue) concentrations obtained via untargeted metabolomics. Results are presented as mean ± SEM, $*p < 0.0001$ when compared to same day control; n≥6.

3.7 Caecal Microbiota

To understand if the gut microbiota was changing in parallel with metabolite changes, next-generation Illumina sequencing was used to assess the bacterial composition of the caecum. Following data processing of Illumina sequencing reads, 1199 bacterial OTUs were identified (Supplementary Table 2. Appendix B). Unsupervised PCA analysis separated caecum samples primarily by time, regardless of disease state along the first principle component (Figure 3.7.A). The PCA also clearly separated CKD and control groups at day 28 and 42 on the second principle component (day 28: $R^2 = 0.97$; $Q^2 = 0.71$ and day 42: $R^2 = 0.98$; $Q^2 = 0.70$) (Figure 3.7.B). The ALDEx2 R package (Fernandes *et al.*, 2014; Gloor *et al.*, 2016*a*) was used to compare the relative bacterial abundances responsible for the observed clustering on each day. Using effect size and overlap statistical thresholds, relative abundance of each OTU was tabulated and assessed for trends (Table 3.5). Only two bacterial OTUs changed between control and CKD on two or more consecutive days with respect to effect size and overlap. The first OTU was from the phylum Firmicutes and genus Turicibacter and was significantly higher in CKD rats compared to control animals on days 14, 28 and 42 (Figure 3.8.A) with an increasing trend associated with disease progression. The second OTU from phylum Bacteroidetes and genus Parabacteroides showed a significant decrease in control rats over time, but CKD rats did not show a similar decrease on days 28 and 42 (Figure 3.8.B).

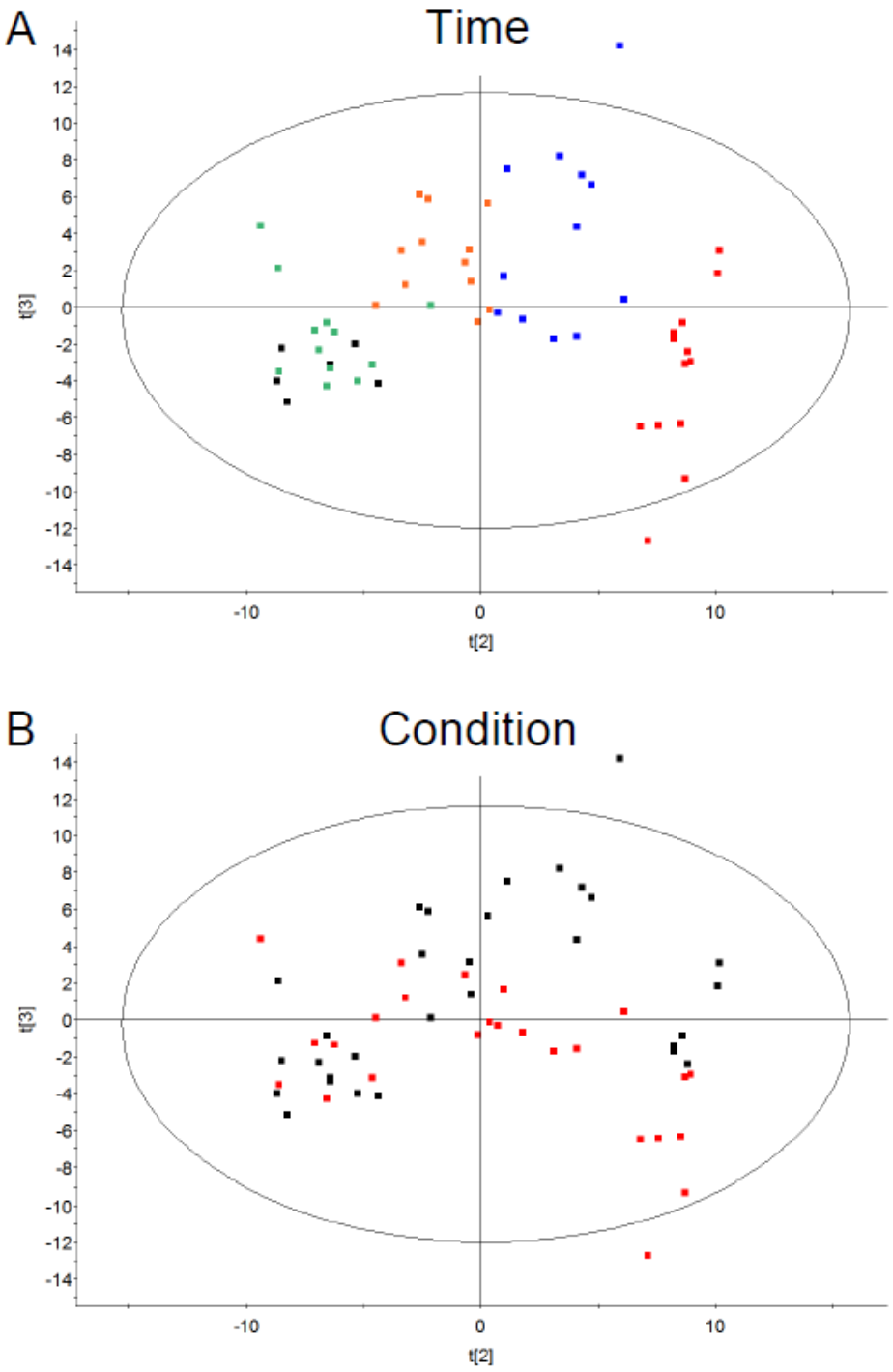

Figure 3.7. Unsupervised principle component analysis (PCA) of control and CKD rat caecum bacterial sequences coloured by (A) day 0 (■) 3 (■), 14 (■), 28 (■) and 42 (■) or by (B) treatment, CKD (■) or control (■). Data is centered without scaling.

Table 3.5. Relative abundances of caecal bacteria. Taxonomy of bacteria with relative abundance effect sizes > 1.5 or < -1.5 and overlap of < 6.5% across days 3, 14, 28 and 42 obtained using R v3.2.3 package ALDEx2 v1.2.0; n ≥ 6 per group.

Phylum	Class	Order	Family	Genus	Effect Size[a]	Overlap (%)	OTU # | % Identity
			Day 3				
Firmicutes	Clostridia	Clostridiales	Lachnospiraceae	Blautia	-1.97744	0.02%	52|73
			Day 14				
Firmicutes	Bacilli	Lactobacillales	Lactobacillaceae	Lactobacillus	1.57949	1.82%	15|96
Firmicutes	Clostridia	Clostridiales	Clostridiaceae_1	Clostridium*	-1.91316	2.86%	7|100
Firmicutes	Clostridia	Clostridiales	Lachnospiraceae	Acetatifactor	-1.28995	5.45%	105|77
Firmicutes	Clostridia	Clostridiales	Lachnospiraceae	unclassified	1.59802	2.86%	1089|100
Firmicutes	Clostridia	Clostridiales	Lachnospiraceae	unclassified	**2.79302**	**0.02%**	5|100
Firmicutes	Erysipelotrichia	Erysipelotrichales	Erysipelotrichaceae	Allobaculum	-1.59115	4.43%	17|100
Firmicutes	Erysipelotrichia	Erysipelotrichales	Erysipelotrichaceae	Turicibacter	-1.62785	2.08%	31|100
			Day 28				
Actinobacteria	Actinobacteria	Bifidobacteriales	Bifidobacteriaceae	Bifidobacterium	**3.33811**	**0.02%**	35|100
Bacteroidetes	Bacteroidia	Bacteroidales	S24-7	unclassified	1.35053	3.65%	37|100
Bacteroidetes	Bacteroidia	Bacteroidales	S24-7	unclassified	1.73352	1.56%	1131|100
Bacteroidetes	Bacteroidia	Bacteroidales	unclassified	unclassified	-1.42179	4.94%	0|86
Bacteroidetes	Bacteroidia	Bacteroidales	Porphyromonadaceae	Parabacteroides	-1.64147	6.23%	38|100
Firmicutes	Clostridia	Clostridiales	Lachnospiraceae	unclassified	**2.67131**	**0.02%**	95|99
Firmicutes	Clostridia	Clostridiales	Ruminococcaceae	unclassified	1.35584	6.25%	33|100
Firmicutes	Erysipelotrichia	Erysipelotrichales	Erysipelotrichaceae	Allobaculum	1.54968	2.34%	71|100
Firmicutes	Erysipelotrichia	Erysipelotrichales	Erysipelotrichaceae	Allobaculum	1.85920	0.26%	42|100
Firmicutes	Erysipelotrichia	Erysipelotrichales	Erysipelotrichaceae	Allobaculum	1.89318	0.02%	81|100
Firmicutes	Erysipelotrichia	Erysipelotrichales	Erysipelotrichaceae	Allobaculum	**3.59784**	**0.02%**	17|100
Firmicutes	Erysipelotrichia	Erysipelotrichales	Erysipelotrichaceae	Turicibacter	-1.87746	1.04%	31|100
			Day 42				
Bacteroidetes	Bacteroidia	Bacteroidales	Porphyromonadaceae	Parabacteroides	**-2.04878**	**0.02%**	38|100
Bacteroidetes	Bacteroidia	Bacteroidales	Porphyromonadaceae	Parabacteroides	-1.77505	5.73%	32|100
Bacteroidetes	Bacteroidia	Bacteroidales	Bacteroidaceae	Bacteroides	-1.54895	5.45%	48|100
Bacteroidetes	Bacteroidia	Bacteroidales	S24-7	unclassified	1.40509	4.16%	134|100
Bacteroidetes	Bacteroidia	Bacteroidales	S24-7	unclassified	1.63886	3.38%	50|100
Bacteroidetes	Bacteroidia	Bacteroidales	S24-7	unclassified	1.85022	3.38%	8|100
Firmicutes	Bacilli	Lactobacillales	Lactobacillaceae	Lactobacillus	-2.02905	3.38%	30|100
Firmicutes	Clostridia	Clostridiales	Ruminococcaceae	Ruminococcus	-1.56150	4.69%	83|100
Firmicutes	Clostridia	Clostridiales	Ruminococcaceae	Oscillibacter	1.31799	5.71%	20|100
Firmicutes	Clostridia	Clostridiales	Lachnospiraceae	Blautia	1.31819	4.16%	139|98
Firmicutes	Erysipelotrichia	Erysipelotrichales	Erysipelotrichaceae	Allobaculum	1.40698	4.94%	81|100
Firmicutes	Erysipelotrichia	Erysipelotrichales	Erysipelotrichaceae	Turicibacter	**-2.17912**	**0.26%**	31|100
unclassified	unclassified	unclassified	unclassified	unclassified	-1.86555	5.45%	54|100

[a]Positive effect sizes indicate bacteria with higher relative abundance in control while negative values indicate bacteria with a higher relative abundance in CKD. Bolded values indicate bacteria with -2 > effect size > 2 and overlap < 0.03%. *Clostridium_sensu_stricto_1.

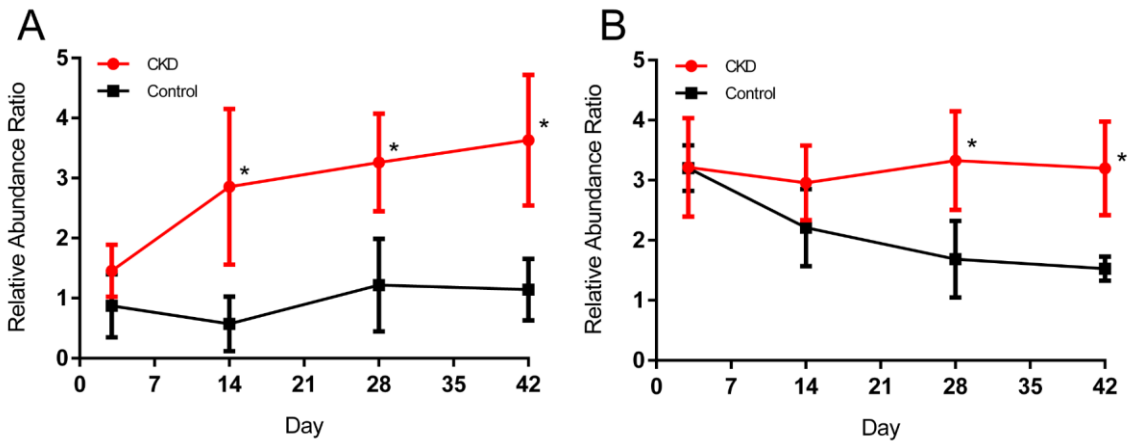

Figure 3.8. Average relative abundance of genus Turicibacter (A) and genus Parabacteroides (B) displayed as an average relative abundance ratio of all OTUs ± 95% confidence interval using R v3.2.3 package ALDEx2 v1.2.0. *Effect size < -1.5 and overlap < 6.5% compared to same day control; $n \geq 6$.

Chapter 4

4 Discussion

The pharmacokinetics of many drugs are unpredictably altered in CKD and these patients are susceptible to ADEs (Corsonello *et al.*, 2005; Manley *et al.*, 2005). Hepatic DMEs such as CYP3A4 and CYP2C9 are responsible for the non-renal drug clearance of nearly half of all marketed pharmaceuticals. It is therefore suggested that DMEs play a role in the altered pharmacokinetics of CKD. Although studies on the downregulation of CYPs in CKD patients are ongoing, animal models clearly identify downregulation associated with loss of renal clearance and subsequent retention of uremic toxins where mechanistic studies currently suggest a wide array of pathways from pre-transcriptional regulation through to direct inhibition of DMEs by uremic toxins, inflammatory factors and hormones (Guévin *et al.*, 2002; Sun *et al.*, 2004; Michaud *et al.*, 2006, 2008; Barnes *et al.*, 2014; Velenosi *et al.*, 2014; Volpe *et al.*, 2014; Yeung *et al.*, 2014). Uremic toxins are also suggested to change the environment of the gut, altering the relative abundance of gut bacteria favouring uremic-toxin producing microbes and creating a state of dysbiosis in CKD patients (Wong *et al.*, 2014; Felizardo *et al.*, 2016; Vaziri, 2016). Further, metabolites or toxins produced by the altered microbiota may fuel the cycle of CKD progression and potentially DME downregulation. However, the pathophysiological factors of uremia and dysbiosis had yet to be tested temporally. In this thesis, uremia and dysbiosis have been characterized over CKD progression to identify potential causes of DME downregulation. Metabolite and bacterial profiles were compared to the expression and activity of CYP3A2 and CYP2C11 in an attempt to support my hypothesis that uremic toxins and/or bacterial alterations are temporally associated with changes in DME regulation.

4.1 Conclusions

4.1.1 CKD Characterization

As expected, urea and creatinine levels increased non-linearly in response to adenine-induced CKD (Kobayashi *et al.*, 2014; Feere *et al.*, 2015). Both disease markers urea and

creatinine confirmed CKD induction by day 14 which increased in severity through to the end of the study and matched with kidney histology (Figure 3.1). Pathohistological features including enlarged nephron tubules, areas of fluid retention, inflammation, atrophy and adenine deposits were seen in diseased kidneys after day 14 as observed in previous studies using this model (Ali *et al.*, 2013). Body weights were unchanged between groups, due to the validity of the pair-feeding method (Figure 3.2).

4.1.2 DMEs over CKD Progression

CYP3A2 and CYP2C11 DMEs were both negatively impacted by CKD on all three levels of detection as previously observed (Hashimoto *et al.*, 1997; Velenosi *et al.*, 2012). The enzymatic activity and protein levels mirror what is seen in mRNA expression suggesting that DMEs are influenced at a transcriptional level, influencing the production of protein and ultimately enzyme activity. CYP3A2 has stable expression in control rats while in CKD, levels decrease starting on day 14. These observations suggest a constitutive factor required for expression is being removed, inhibited or downregulated. Although further studies are required, this could be mediated by the increase in uremic toxins discussed in section 4.1.4 (Wright *et al.*, 1997). In contrast, CYP2C11 shows an increase in control rats as early as day 7 but a failure to increase in CKD rats. The increase in control CYP2C11 has been noted previously in healthy male rat juveniles where it is suspected to reflect the increase of endogenous substrate testosterone during puberty (Wright *et al.*, 1997; Yun *et al.*, 2010). The testosterone levels in male Wistar rats are known to increase starting at 25 days of age and peaking at 60 days of age (Ghanadian *et al.*, 1975). The estimated age of our rats is 60 days of age on day 28 of the study which aligns with our observed peak in CYP2C11 mRNA on day 28 (Figure 3.2.B). This may suggest we are capturing the end of puberty and testosterone peak where CKD may be inhibiting the testosterone peak in these adolescent rats. Additionally, CKD is known to impact male patients by causing hypogonadism associated with decreased levels of testosterone further suggesting a hormonal role in CYP regulation (Carrero *et al.*, 2011). CYP2C11 is also influenced by alterations in the normally cyclic levels of growth hormone (GH) where continuous GH release or complete loss of GH production will both downregulate CYP2C11 (Kaufhold *et al.*, 2002). Interestingly, one-third of pediatric CKD patients experience GH insensitivity

and stunted stature (Cayir & Kosan, 2015; Akchurin *et al.*, 2017). It is therefore possible that the rat CYP2C11 downregulation is due to insufficient levels of substrate testosterone or irregular production of GH. However, testosterone was not identified as a correlated metabolite and GH was not targeted for analysis.

Perhaps the differing trends seen between CYP3A2 and CYP2C11 are attributed to nuclear receptor differences. CYP2C11 is shown to be less dependent on HNF-4α induction, and CKD-induced receptor binding inhibition is less extensive for CYP2C11 than it is CYP3A2 (Honkakoski & Negishi, 2000; Velenosi *et al.*, 2014; Feere *et al.*, 2015). Alternatively, it is possible that the inactivation of shared nuclear receptor PXR or reduced receptor binding capacity of RNA polymerase II is more severe for CYP2C11; however, this has yet to be tested (Mikamo *et al.*, 2003; Velenosi *et al.*, 2014; Feere *et al.*, 2015).

Enzymatic activity effectively produced the same trend as mRNA and protein results for both enzymes. However, CYP3A2 K_m showed a significant increase between CKD and control on days 28 and 42. The increased K_m suggests the concentration of substrate testosterone required to obtain the same half-maximal velocity ($V_{max}/2$) has increased. This could be explained by i) the upregulation of another enzyme with substrate specificity for testosterone, or more likely, ii) an alternate CYP3A2 substrate associated with CKD days 28 and 42 was bound to CYP3A2 prior to microsome isolation and had a stronger binding affinity than testosterone (Berg *et al.*, 2012). This occurred in another study using 4-hydroxylation of triazolam (Toda *et al.*, 2009) although the reason was unexplained. Overall, we can conclude that both CYPs studied herein are negatively regulated in CKD at the transcriptional and expression levels, and CYP2C11 changes occur earlier than those of CYP3A2.

4.1.3 Metabolome over CKD Progression

Untargeted metabolomics analyzed by PCA showed that plasma RPLC allowed for the greatest magnitude of separation between control and CKD rats when compared to plasma HILIC separation. By PCA visualization, plasma samples showed greater separation in earlier stages of disease (days 3-14) than the liver samples. Unlike the plasma samples, liver metabolites were better differentiated with the HILIC column. This suggests CKD

first inflicts a uremic environment in the plasma before infiltrating the liver, which is the physiological expectation since the reduced GFR in CKD directly increases uremic toxin concentration at the glomerulus before the blood is cycled through the liver. This also tells us that uremic changes overlap with the early changes in CYP3A2 and CYP2C11, supporting the hypothesis that uremic toxins are involved with DME regulation.

4.1.4 Uremic Toxins Correlated with DMEs

Metabolites from each run were subjected to correlation analysis with CYP3A2 or CYP2C11 mRNA, protein or enzymatic activity levels. Of the 204 *m/z* ratios retrieved, 8 of the 9 identified at level 1 classification were seen to increase with CKD progression [allantoin, creatinine, 2,8-dihydroxyadenine, pantothenic acid (vitamin B_5), IS, PS, equol-4/7-O-glucuronide and 4-ethylphenyl sulfate]. L-carnitine was the only level 1 metabolite that showed a positive correlation with CYP downregulation and thus decreased over CKD progression.

Allantoin and creatinine are non-protein bound metabolites successfully eliminated by dialysis (Meyer & Hostetter, 2007). This makes them potentially less harmful than their protein-bound counterparts, and in general, the implications of non-protein bound uremic toxins with relation to drug metabolism or altered pharmacokinetics has largely been overlooked. Allantoin is an expected component of uremia because it is the primary elimination product of uric acid and increases are observed in the plasma and urine of CKD rats induced by 5/6th nephrectomy or adenine (Akiyama *et al.*, 2012; Zhao *et al.*, 2013*a*, 2013*b*). Here we also find allantoin in rat liver, suggesting further infiltration due to advanced uremia. Allantoin is generally not produced by humans because we lack uricase activity although allantoin has been detected in CKD patients (Toyohara *et al.*, 2010; Niwa, 2013). Allantoin in humans is suggested to reflect the presence of uric acid-converting reactive oxygen species; however, it could provide evidence for uric acid translocation into the gut. Bacteria in our gut possess uricase activity and are capable of producing allantoin, although studies are needed to confirm this hypothesis (Zhao *et al.*, 2013*a*; Wong *et al.*, 2014).

As discussed (see section 1.3.3), creatinine is a product of creatine and the most common marker of glomerular function used as a clinical tool to calculate eGFR. CYP3A2 and CYP2C11 both correlate with creatinine and urea, the two disease markers defining CKD in this model. Since creatinine increases with respect to CKD and DMEs correlate with CKD onset, creatinine by default will correlate with DME downregulation. However, creatinine involvement with DME regulation has been overlooked and little is known about its pathophysiological impact in CKD. Studies have established that of all creatinine in a patient experiencing renal failure, a variable 16-66% undergoes metabolic clearance (Wyss & Kaddurah-Daouk, 2000). Interestingly, up to 68% of creatinine cleared by metabolism is hypothesized to be converted back to creatine by creatininase-possessing bacteria of the gut, suggesting creatinine translocation across the gut lumen (Wyss & Kaddurah-Daouk, 2000). The creatine can then i) return to the plasma via enteric cycling explaining raised levels of creatine in CKD patients, ii) or continue to be metabolized by gut bacteria to end-products 3,1-methylhydantoin or glycolate (Wyss & Kaddurah-Daouk, 2000). Alternatively, creatinine can undergo oxidation to methylguanidine or methylurea of which methylguanidine has been identified as a harmful uremic toxin, progressing CKD when administered to rats (Wyss & Kaddurah-Daouk, 2000). Ultimately, more information on the toxic or adverse effects of creatinine and its degradation products need to be established with respect to DME regulation in CKD (Storm *et al.*, 2013).

2,8-Dihydroxyadenine, the adenine metabolite responsible for the induction of CKD, is also associated with CYP3A2 and CYP2C11. 2,8-Dihydroxyadenine induces CKD in a mechanistic, concentration-dependent manor and thus, DMEs correlating with CKD onset are expected to correlate with 2,8-dihydroxyadenine (Terai *et al.*, 2008). Since DMEs are downregulated in other models of CKD, it is unlikely that 2,8-dihydroxyadenine is impacting DME regulation directly (Leblond *et al.*, 2002; Velenosi *et al.*, 2014; Feere *et al.*, 2015).

Pantothenic acid (vitamin B_5) is an essential nutrient found in many foods, including the provided rat chow, that is metabolized into coenzyme A, a molecule necessary for healthy biochemical synthesis and energy metabolism (Berg *et al.*, 2012). However, pantothenic acid has rarely been associated with toxic effects nor has any tolerable upper dosage been

established (Institute of Medicine, 1998; Kelly, 2011). An elegant study of organic anion transporter 1 (Oat1) suggests pantothenic acid requires Oat1 transport since it is accumulated in the plasma of Oat1 knockout mice (Wikoff *et al.*, 2011). Additionally, administration of probenecid, a drug known to inhibit Oat transporters, increases plasma pantothenic acid levels (Kelley, 1975; Niwa, 2013). The proposed inhibition of OATs in CKD is associated with high-affinity uremic substrates, effectively incapacitating OAT function and likely causing the increase of pantothenic acid by inhibiting its movement though excretory pathways (Nigam *et al.*, 2015). Pantothenic acid has not been studied as a modulator of DMEs possibly because it is considered non-toxic. However, studies are required to confirm the presence of seemingly non-toxic endogenous metabolites like pantothenic acid are not modulating DMEs.

Gut derived uremic toxins that have prospect for being involved in DME downregulation from this study include IS, PS, 4-ethylphenyl sulfate, equol-4/7-O-glucournide and products of L-carnitine metabolism. IS and PS are two highly retained gut-derived uremic toxins (Wikoff *et al.*, 2011; Leong & Sirich, 2016) both found in CKD patients and animal models (Itoh *et al.*, 2012; Zhao *et al.*, 2013*a*; Velenosi *et al.*, 2016). IS and PS are linked to CKD comorbidities such as CVD (Hung *et al.*, 2017) and have been associated with uremic influences of drug metabolism both through transcriptional regulation (Guévin *et al.*, 2002), and IS as a direct inhibitor of CYP activity (Volpe *et al.*, 2014). Thus, IS and PS found in this study support previously described roles in modifying CYP regulation in CKD.

Equol-4/7-O-glucouronide (EOG) and 4-ethylphenyl sulfate (EPS) are both soy-derived uremic toxins seen in animal models fed a soy-based chow (Kikuchi *et al.*, 2010; Velenosi *et al.*, 2016). The rat chow in this experiment used 22% crude protein content of which daidzein and genistein aglycone equivalents (ranging from 350 to 650 mg/kg) were present. These isoflavones undergo bacterial transformation into equol derivatives such as EOG and EPS in the gut. EOG has only been found in animal models of CKD (Velenosi *et al.*, 2016) where EPS has been detected in dialysis patients, although without significant changes compared to healthy individuals (Itoh *et al.*, 2012). Interestingly, EPS has a similar structure to p-cresyl sulfate, a metabolite usually found concomitant with IS and repeatedly

found in CKD (Itoh *et al.*, 2013; Zhang & Davies, 2016). Due to the similar structure, the function of EPS is suspected to act similarly to p-cresyl sulfate which has been associated with deleterious human liver microsomal CYP3A4 regulation by direct inhibition (Barnes *et al.*, 2014; Zhang & Davies, 2016; Gryp *et al.*, 2017). It has yet to be assessed whether EPS can also directly inhibit the regulation of CYP3A2 or CYP2C11 in rats.

L-Carnitine is a required nutrient primarily obtained through the diet in meat, eggs and protein-rich foods including soy (Klaassen & Cui, 2015). In contrast to an increase in L-carnitine observed in the heart and kidney of adenine-induced CKD rats (Velenosi *et al.*, 2016), here we see a decrease in L-carnitine in the plasma in conjunction with downregulated CYPs in the liver. This could suggest a removal of L-carnitine as it is transformed into TMAO as seen previously (Koeth *et al.*, 2013). L-Carnitine and choline are the precursors to TMA, a bacteria by-product that is converted to TMAO in the liver by flavin-containing monooxygenases (FMO) (Koeth *et al.*, 2013). TMAO is associated with increased risk of developing atherosclerosis and thus, of increasing interest as a harmful uremic toxin in CKD and CVD (Koeth *et al.*, 2013; Aron-Wisnewsky & Clément, 2015). TMAO detection needs a sensitive MS method sometimes referred to as target enhancement, usually utilizing a triple quadropole MS rather than a QTof which is better for sensitivity (Heaney *et al.*, 2016). Therefore, TMAO was missed by our untargeted methods because the sensitivity was insufficient (Heaney *et al.*, 2016). Neither L-carnitine nor TMAO have been tested as DME regulatory factors but have been mentioned in relation to drug metabolism and provide potential candidates for future studies (Selwyn *et al.*, 2015).

The identification and correlation of these uremic toxins support their involvement in DME regulation. However, as discussed in section 1.7.1, administration of AST-120 in CKD, reduces uremic toxin levels (Kikuchi *et al.*, 2010), but CYP3A2 expression is not recovered (Velenosi, 2015). This protection by AST-120 suggests factors other than uremic toxins may be involved. The quantified IS, PS and EPS concentrations over CKD progression observed in this thesis adds support to this idea (Figure 3.6). Severe concentrations (over 150μM for IS) are not observed until following day 28, well after we observe a decrease in CYPs. Preliminary studies using Huh7 human hepatoma cells show that protein-bound

IS at concentrations of 180±20µM were required to reduce CYP3A4 expression by 50% (Velenosi, 2015). In addition, a similar study found that concentrations of IS required to downregulate CYP3A4 activity were above the abnormal range seen in CKD patients, which was defined as the highest ever recorded IS level in a CKD patient at >940µM (Vanholder *et al.*, 2003; Volpe *et al.*, 2014). Although the studies differ dramatically, collectively they suggest that other hypotheses such as immunological factors, PTH or undiscovered pathways might be initiating DME downregulation, and it is not until severe stages of CKD that uremic toxins contribute to the dramatic reduction in CYP expression seen here and by others (Velenosi *et al.*, 2012). In conclusion, it is temporally plausible that uremic toxins contribute to DME downregulation, but other factors may be involved prior to uremic toxin influences.

Interestingly, of the metabolites found by correlation to CYP3A2 or CYP2C11, the five metabolites that are potentially associated to DME downregulation in the literature are all gut-derived uremic toxins. This supports the need to understand the changes in the gut microbial environment and assess if bacterial alterations are impacting the presence of these toxins.

4.1.5 Microbiome over CKD Progression

The gut microbiota, sampled by caecum swab, was phylogenetically analyzed using 16S sequencing. Multivariate analysis showed the microbiota was most significantly influenced by time and secondarily by disease state. This correlation suggests that the microbiota changes caused by CKD induction are less profound than age-associated bacterial changes. Additionally, in comparison to the metabolomic PCA, microbial clustering with respect to disease state was poor and showed little to no separation before day 14. This observation suggests the uremic environment in the plasma and the liver are altered well before dysbiosis occurs. Interestingly however, the metabolite concentrations of IS, PS and EPS all dramatically increase after day 28 when changes are simultaneously observed in the gut microbiota. This lends support to the idea that uremia may be driving the change in gut microbial abundance through a damaged gut wall (Figure 4.1) (Magnusson *et al.*, 1991; Felizardo *et al.*, 2016; Vaziri, 2016). The late and dramatic increase in gut-derived uremic toxins also suggests dysbiosis contributes in the cycle of worsening uremia, likely adding

to the uremic milieu by increasing bacteria capable of uremic toxin production (Wong *et al.*, 2014; Vanholder & Glorieux, 2015; Felizardo *et al.*, 2016). Referencing the KEGG results of Wong and colleagues, all bacterial families significantly changed on days 28 and 42 contained strains capable of producing at least one of the following genes: urease, tryptophanase, phosphotransbutyrylase or butyrate kinase, although the bacteria are inconsistently characteristic of control or CKD rats (Wong *et al.*, 2014). The sole bacterial genus significantly changed due to disease state prior to day 14 resided in the bacterial order Clostridiales, which matched the findings of Barrios and colleagues who sequenced the gut microbiota of 855 people and correlated only bacteria from the Clostridiales order with eGFR in early renal decline (Barrios *et al.*, 2015).

Although interesting to examine the individual days for OTUs differing due to CKD, only two bacterial genera, Turicibacter and Parabacteroides, were significant on two or more consecutive days, best correlating with DME trends. Turicibacter was the most consistently changed bacteria, changing as early as day 14 through to day 42 with an increasing trend as CKD progressed. Identifying the genus Turicibacter in CKD animals is a novel finding. All Turicibacter are gram-positive, strictly anaerobic, rod-shaped bacteria of which very little is known. Turicibacter was first identified and named in 2002 by the University of Zürich, Switzerland where the bacteria were found in the blood of a febrile 35-year-old male with acute appendicitis (Bosshard *et al.*, 2002). Shortly thereafter, another febrile patient diagnosed with acute appendicitis had Turicibacter cultured from their blood; this time a 79-year-old female in Sweden (Bosshard *et al.*, 2002). In 2007, Turicibacter was associated with pouchitis in ulcerative colitis patients which is a complication of proctocolectomy (Falk *et al.*, 2007). We also know Turicibacter *sp.* are found in healthy human feces from a FMT study where human feces were transplanted into colons of germ-free rats to ascertain whether rats should be used as a transplantation model (Licht *et al.*, 2007). Turicibacter was one such bacteria that survived two weeks after transplantation via stool gavage.

Only 4 strains, all within the same species *sanguinis,* have been published to date: MOL361 (Bosshard *et al.*, 2002), PC909 (Cuív *et al.*, 2011), ZCY83 (Cao *et al.*, 2015), H121 (Auchtung *et al.*, 2016). A BLASTn search of our Turicibacter sequence matched the

MOL361 species with 100% identity (NR_028816.1). Turicibacter is anaerobic and therefore, considerably difficult to culture. Of the strains successfully cultured, none have tryptophanase activity suggesting these bacteria are not involved in producing indole derivatives such as IS (Bosshard *et al.*, 2002). The Erysipelotrichaceae family of which Turicibacter belongs does contain strains capable of butyrate and phosphotransbutyrylase activity, although this has yet to be confirmed in the Turicibacter genus (Wong *et al.*, 2014). Assuming all rats were exposed to Turicibacter for the study duration, we suggest our findings indicate CKD animals are more susceptible to gut colonization by Turicibacter.

The BLASTn results for the Parabacteroides genus OTU suggested 99% sequence identity to two stains of the species *distasonis*: strain ATCC 8503 (NR_074376.1) and JCM 5825 (NR_041342.1). In 2006, Bacteroides *distasonis* was reclassified as Parabacteroides *distasonis* and thus, all subsequent information pertains to either classification (Sakamoto & Benno, 2006). Parabacteroides is a gram-negative, anaerobic, non-spore-forming genus. *P. distasonis* is present in the human gut and has been identified via PCR in fecal samples long before the existence of next-generation sequencing methods (Franks *et al.*, 1998). *P. distasonis* is classified in the KEGG pathway database as an opportunistic pathogen capable of anaerobic infection (Xu *et al.*, 2007). In a study of gut microbiota in Crohn's disease, *P. distasonis* was more abundant in the control group, contradictory to expected findings (Mondot *et al.*, 2011). More recently, components of *P. distasonis* have shown improvement of irritable bowel disease (IBD) in mice and have been suggested as a potential therapeutic for reduction of inflammation in IBD (Kverka *et al.*, 2011). However, analysis of bacteria capable of generating phenol and indole compounds found *P. distasonis* proficient at producing p-cresol (Gryp *et al.*, 2017) and IS (Zhang & Davies, 2016). In general, it seems *P. distasonis* is potentially both harmful or beneficial depending on translocation, relative abundance and physiological state of the host. Our results show a unique trend where CKD rats have a stable level of Parabacteroides and controls slowly reduce the abundance of this genus after 28 days. Given the multitude of associations with disease, Parabacteroides may be taking advantage of the dysbiotic state in CKD when it is normally removed in controls by other healthy bacteria as a part of the progression in age-associated microbial changes.

This data shows that DME regulation in CKD is initially mediated by changes independent of an altered gut microbiota; however, late and dramatic increases in both uremic toxins and the bacterial environment suggest the gut microbiota may influence DMEs in severe CKD. It also remains possible that in this late stage CKD, gut microbes are influencing DMEs through uremic-independent methods such as inflammatory factor production as suggested by germ-free studies that also see downregulation of CYPs (Toda *et al.*, 2009; Claus *et al.*, 2011; Selwyn *et al.*, 2015).

4.1.6 Summary

In conclusion, global plasma and liver alterations of the metabolome over disease progression provide support for uremic toxins playing a role in DME downregulation. Alternatively, the early detection of DME downregulation and late surge of gut-derived uremic toxin concentrations suggest other factors are involved in DME regulation in early stages of CKD (Figure 4.1). A temporal association was established between severe CKD, caecal dysbiosis and increase in gut-derived uremic toxins IS, PS and EPS. This association supports the positive-feedback loop of uremia and dysbiosis suspected to drive severe CKD (Figure 4.1).

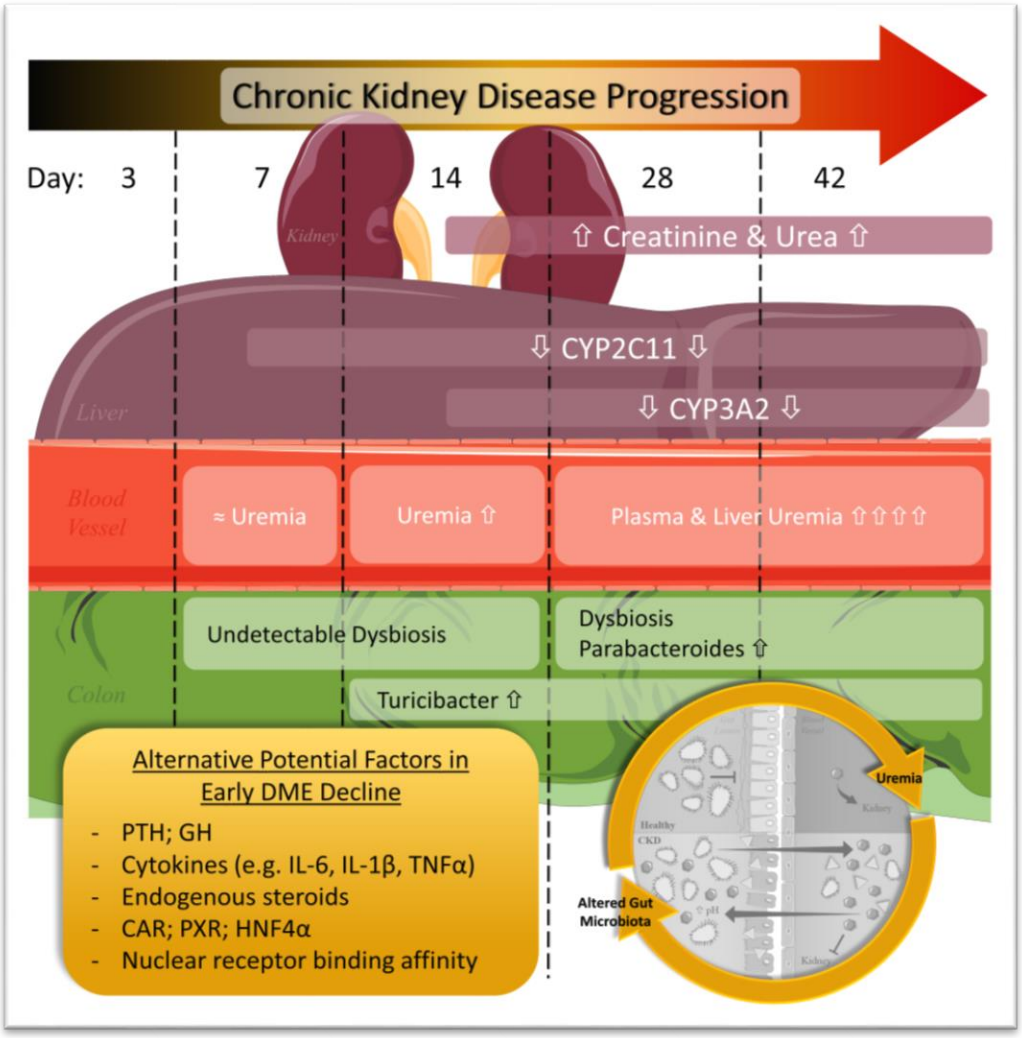

Figure 4.1. Temporal associations of uremia and dysbiosis with CYP3A2 and CYP2C11 expression over CKD progression. Days (3 through 42) refer to rat study time points carried out in this thesis. CKD was characterized by urea and creatinine beginning on day 14 and correlating with the decrease in CYP3A2 expression. CYP2C11 expression decreased as early as day 7. Although plasma uremia may be involved as early as day 7 indicated by untargeted multivariate analysis, quantified uremic toxins were significantly increased only on days 28 and 42. Similarly, gut bacterial dysbiosis was detectable on days 28 and 42 supporting the hypothesis of a positive-feedback cycle involving uremia and the gut microbiota. This study suggests there are likely other factors influencing DMEs in early stages of CKD. Images were modified from Servier Medical Art (http://www.servier.co.uk/medical-art-gallery).

4.2 Limitations

The greatest limitation of this study is that causative conclusions cannot be made from vast cross-sectional data such as those obtained from sequencing or metabolomics. Results from these discovery-based methods instead provide whole-system comprehension of complex mechanistic processes and allows for discovery of previously unknown biological factors that drive future experiments assessing causation.

4.2.1 Animal Model & Study Design

Utilizing *in vivo* animal models is accompanied with limitations when used to understand human physiology. Human CYP expression is comparable to rat and mouse CYP expression through orthologous enzymes that largely perform the same tasks, yet some substrates are species-specific indicating the enzyme activities are not identical to their human orthologs (Nelson *et al.*, 2004; Pan *et al.*, 2016). Secondly, the induction of CKD is achievable through different methods. Adenine-induced CKD is a less invasive orally administered model in comparison to the more common 5/6th nephrectomy model and although not linear, it is suggested to provide a more consistent rate of CKD onset than 5/6th nephrectomy (Terai *et al.*, 2008). Applying a steady rate of CKD onset was important for our temporal study design. Conceptually however, the adenine model has been questioned as a CKD model because it could also represent an acute kidney injury (AKI) model. Adenine metabolites precipitate when concentrated, mechanically damaging the kidney tubules comparable to kidney stones (Engle *et al.*, 1996; Morishita *et al.*, 2011; Succar *et al.*, 2017). Though separately defined in nephrology for clinical diagnosis, AKI is a risk factor for CKD and CKD is a risk factor for AKI, and thus, the adenine model continues to be used for either condition (Chawla *et al.*, 2014). The adenine model also reduces the amount of food ingested during the first days of adenine-induction, requiring that pair-feeding be established. This is especially important for CYP expression analysis since CYPs are influenced by short-term fasting (Lammers *et al.*, 2015). Lastly, it is unknown how adenine and its metabolites will affect the gut microbial environment apart from CKD. When ingested, adenine absorption is proposed to occur within the small intestine, earlier in the intestinal tract than the caecal sampling site (Salati *et al.*, 1984). It

is noteworthy that the adenine metabolite 2,8-dihydroxyadenine was only detected in the plasma and not in the liver of CKD rats suggesting 2,8-dihydroxyadenine is unlikely to be impacting the liver.

4.2.2 Time Point Inclusion

Initial results from this study evaluated only rats sacrificed on day 0, 3, 14, 28 and 42 and suggested CYP expression and uremic toxin levels were changing between days 3 and 14. In the attempt to obtain as much information about the transition between early and late CKD, a second study included rats subjected to identical conditions for 7 days. Upon completion of the second study, preliminary CYP3A2 mRNA expression results showed day 0 control rats had decreased expression in comparison with the other control groups and essentially increased after 3 days (Figure 4.2). It was later identified that DME expression is impacted by short-term fasting (Lammers *et al.*, 2015). Thus, a third study compared only control *ad libitum* fed animals with animals receiving the CKD pair-fed amount of control food. After 72 hours, it was found that DME levels of animals receiving reduced feed were equivalent to levels observed in day 3 control rats. Therefore, day 0 rats from the final study were carried onward as the control day 0 group for the remainder of the investigation (Figure 4.2).

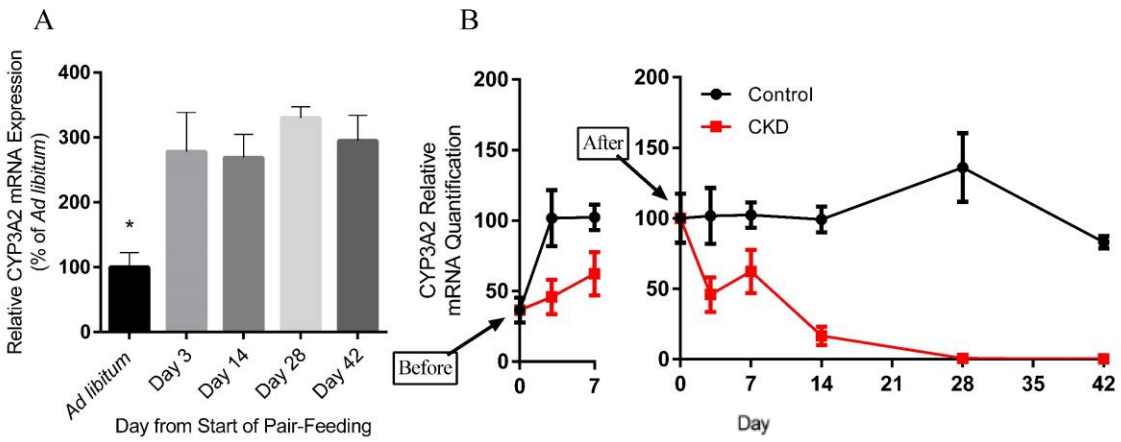

Figure 4.2. Short-term fasting effects on CYP3A2 mRNA expression. A) Preliminary CYP3A2 mRNA expression data comparing rats fed *ad libitum* to rats pair-fed lower food volumes matching those consumed by CKD rats. Values are expressed as the mean ± SEM relative to housekeeping gene β-actin and normalized to the *ad libitum* group. *$p<0.05$ using a one-way ANOVA with Holm-Sidak's multiple comparisons test. B) CYP3A2 mRNA expression results before and after accounting for short-term fasting effects by waiting to sacrifice 72 hours after pair-feeding is initiated.

However, this time sensitivity impacted bacterial sampling. All animals from which bacteria are sampled, ideally must eat and live in the same area and be exposed to all experiences that may introduce foreign bacteria to the same extent if the sample size is small and bacterial differences are expected to be detectable. Ideally, particularly in animal studies, this means the animals should all be bought at the same time in one shipment if being compared together. Since the animals from day 7 and day 0 were obtained from the supplier at different times than the original study, the gut microbiota variability was too large to assess as a whole and therefore removed from bacterial analysis, reducing the number of time points available for evaluation.

4.2.3 "Omics" Method Limitations

Although broadly encompassing, both the Illumina sequencing and untargeted metabolomics methods are limited. Even though the 16S rRNA gene is currently the gene of preference, it is highly conserved, limiting its resolution and accuracy to the genus level (Poretsky *et al.*, 2014). Also, the development of short, overlapping pair-end reads enabled the use of 16S gene sequencing on the MiSeq platform given only a small section of the 16S gene required sequencing (Poretsky *et al.*, 2014). However, this requires that out of the nine variable regions (V1-V9), only a select few can be covered by the read length capabilities of the MiSeq (Caporaso *et al.*, 2012). It has been identified that using different variable regions (V1 through V6) results in different subsets of identifiable bacteria (Chakravorty *et al.*, 2007; Youssef *et al.*, 2009). Therefore, the V4 variable region was chosen based on the most bacteria that could be detected and likely present within a caecal sample (Caporaso *et al.*, 2011).

Similarly, untargeted metabolomics can identify a vast number of metabolites in a single sample, but each metabolite is only detectable if the combination of sample preparation, UPLC column, chromatography and MS configuration are satisfactory for that metabolite. As an example, TMAO is likely present in our rat plasma samples, but is not detected because the MS method needs to be adjusted for sensitivity (Heaney *et al.*, 2016). To obtain as many metabolite masses as possible, two columns of differing hydrophobicity and both positive and negative ionization modes were used.

4.2.4 Statistics

In addition to method limitations, analysis methods were also limiting. Little continuity in genera abundance across time points was primarily caused by small sample size of <7 per group. The inter-individual variability, in addition to machine and sampling variability, effectively masked small changes caused by condition and required broad shifts in bacterial abundance to prove significance (Poretsky *et al.*, 2014; Gloor *et al.*, 2016*a*). Without increasing sample size, this could be somewhat circumvented by using a sequencing method with less error and greater read depth (e.g. Illumina HiSeq), potentially providing more bacterial associations (Caporaso *et al.*, 2012).

Correlative analysis between metabolites and DME levels was the second-best option after a univariate model capable of acquiring an independent, FDR corrected, 2-way ANOVA with multiple comparisons for each time point between CKD and same day control. Although an independent, FDR corrected 2-way ANOVA is obtainable via MetaboAnalyst v3.0, p-values do not indicate on which days the significance is occurring. To answer the question of when the metabolite is changing over time, multiple comparison analysis using Sidaks multiple comparisons test is generally applied to the 2-way ANOVA. However, MetaboAnalyst v3.0 is incapable of multiple comparison testing and alternative software including GraphPad are unable to hold the vast amount of information present in a metabolomics dataset. It is also possible that a custom R script be written to obtain this same goal. However, for this study, there were limited options for identifying at what day each metabolite was changing and related to CYP3A2 (day 14) and CYP2C11 (day 7) expression. Alternatively, Spearman correlation analysis was used to identify metabolites that exhibit a similar trend to DME changes over CKD progression. Unfortunately, this correlation analysis assumes that metabolite concentrations influencing DMEs are directly proportional to DME levels, potentially limiting the results.

4.3 Future Studies

This thesis has emphasized the need for research around DMEs in early stages of CKD. Specifically, it needs to be elucidated if DMEs are truly changed in humans with CKD, apart from animal models. Alternatives to the erythromycin breath test are essential to

understanding human CYP3A4 regulation. In the meantime, DME studies can improve the rodent-to-human physiological gap by employing humanized mouse models of CYP3A4 or CYP2C9 along with other DMEs or transporters (Becker & Hewitson, 2013; Ladda & Goralski, 2016).

Although it is established that dialysis can effectively change the bioavailability of drugs in humans, it has yet to be determined if dialysis changes DME levels (Atkinson & Umans, 2009). In theory, if only protein-bound uremic toxins are affecting drug pharmacokinetics, dialysis will not improve DME levels. An *in vitro* study looked at CYP expression and activity following the implement of pre-dialysis versus post-dialysis serum in rat hepatocytes and showed a decrease in DMEs after only pre-dialysis serum suggesting uremic toxins involved in DME downregulation can be removed via dialysis (Michaud *et al.*, 2008). Additional information on what metabolites are being removed, perhaps through MS methods, would help researchers identify metabolites worth targeting for causation analysis. *In vivo* models of dialysis have been established and would provide an interesting avenue for studying DME levels before and after dialysis (Mortier *et al.*, 2002; Zareie *et al.*, 2005).

It would also prove helpful if the list of mechanistic causes of DME downregulation were assessed together to understand the extent to which each mechanism is contributing to the entire downregulation of DMEs. For example, one could introduce suspected uremic toxins such as IS, PS, EPS, EOG and TMAO to human cells *in vitro* or human liver microsomes *ex vivo* and subsequently test for direct inhibition of human CYP3A4 or CYP2C9 expression alongside nuclear receptor binding alterations and detection of PTH and inflammatory factors.

Studies are needed to assess the implications of specific bacteria on disease states. It is unclear if Turicibacter is normally found in the gut at very low abundance or a foreign bacterium infiltrating a weak host. It is also unknown if this bacterium is pathological or commensal in nature. It would be beneficial to confirm that CKD is not inducible via bacterial alterations such as infection with Turicibacter. This assessment could be accomplished by FMT to introduce CKD microbiota, potentially from human CKD

patients to germ-free mice to see if i) the mouse acquires CKD regardless of initial kidney damage, and ii) if the presence of CKD-associated bacteria can cause DME downregulation in the absence of uremia. In conjunction, caecal or fecal metabolomics would provide information about what metabolites reach the gut lumen and aid in dysbiosis.

4.4 Relevance & Conclusions

In general, future CKD therapies should be targeted not only to improve disease comorbidities and prolong the progression into ESRD, but also improve drug disposition to ensure the pharmaceuticals received are providing the highest efficacy attainable while avoiding drug toxicity. Emerging therapies still directed towards improving pathophysiology and uremia include uremic toxin removal (e.g. AST-120) and pro- or prebiotics to stimulate the reversal of dysbiosis (Ranganathan *et al.*, 2006; Koppe *et al.*, 2015; Rossi *et al.*, 2016; Yamamoto *et al.*, 2016). Currently there is no prospect for FMT to benefit CKD patients, although it has proved largely successful for *C. difficile* infections and theoretically translatable to CKD (Persky & Brandt, 2000; Al Khodor & Shatat, 2016). Our results suggest that future therapeutic research for DME regulation be targeted in the areas of uremic toxin removal as a priority over the reestablishment of the gut microbiota because our results suggest uremic toxins provide a more likely candidate for early stage DME alteration.

Ultimately, understanding the effects of uremia and bacteria with respect to CKD can help assess whether uremic toxins or the gut microbiota are potential therapeutic targets in DME regulation. Whether it be adsorption of uremic toxins or combating bacterial dysbiosis, providing emphasis for one method may drive future research in the direction of greatest efficacy. On a larger scale, knowledge of how DMEs fluctuate with respect to metabolites and bacteria could lead to improved clinical testing, dosing and prevention of adverse reactions.

References

Abraham G, Varughese S, Thandavan T, Iyengar A, Fernando E, Naqvi SAJ, Sheriff R, Ur-Rashid H, Gopalakrishnan N & Kafle RK (2016). Chronic kidney disease hotspots in developing countries in South Asia. *Clin Kidney J* **9,** 135–141.

Akchurin OM, Kogon AJ, Kumar J, Sethna CB, Hammad HT, Christos PJ, Mahan JD, Greenbaum LA & Woroniecki R (2017). Approach to growth hormone therapy in children with chronic kidney disease varies across North America: the Midwest Pediatric Nephrology Consortium report. *BMC Nephrol* **18,** 1–8.

Akiyama Y, Takeuchi Y, Kikuchi K, Mishima E, Yamamoto Y, Suzuki C, Toyohara T, Suzuki T, Hozawa A, Ito S, Soga T & Abe T (2012). A Metabolomic approach to clarifying the effect of AST-120 on 5/6 nephrectomized rats by capillary electrophoresis with mass spectrometry (CE-MS). *Toxins (Basel)* **4,** 1309–1322.

Ali BH, Al-Salam S, Al Za'abi M, Waly MI, Ramkumar A, Beegam S, Al-Lawati I, Adham S a. & Nemmar A (2013). New model for adenine-induced chronic renal failure in mice, and the effect of gum acacia treatment thereon: Comparison with rats. *J Pharmacol Toxicol Methods* **68,** 384–393.

Aron-Wisnewsky J & Clément K (2015). The gut microbiome, diet, and links to cardiometabolic and chronic disorders. *Nat Rev Nephrol* **12,** 169–181.

Arora P, Vasa P, Brenner D, Iglar K, McFarlane P, Morrison H & Badawi A (2013). Prevalence estimates of chronic kidney disease in Canada: results of a nationally representative survey. *CMAJ* **185,** E417-23.

Arumugam M, Raes J, Pelletier E, Paslier D Le, Yamada T, Mende DR, Fernandes GR, Tap J, Bruls T, Batto J, Bertalan M, Borruel N, Consortium M, Weissenbach J, Ehrlich SD & Bork P (2011). Enterotypes of the human gut microbiome. 1–7.

Atkinson a J & Umans JG (2009). Pharmacokinetic studies in hemodialysis patients. *Clin Pharmacol Ther* **86,** 548–552.

Auchtung TA, Holder ME, Gesell JR, Ajami NJ, Duarte RTD, Itoh K, Caspi RR, Petrosino JF & Horai R (2016). Complete Genome Sequence of Turicibacter sp . Strain H121 , Isolated from the Feces of a Contaminated Germ-Free Mouse. **4,** 2015–2016.

Auslander N, Yizhak K, Weinstock A, Budhu A, Tang W, Wang XW, Ambs S & Ruppin E (2016). A joint analysis of transcriptomic and metabolomic data uncovers enhanced enzyme-metabolite coupling in breast cancer. *Sci Rep* **6,** 29662.

Bailey DG, Malcolm J, Arnold O & Spence JD (1998). Grapefruit juice-drug interactions. *Br J Clin Pharmacol* **46,** 101–110.

Barnes KJ, Rowland A, Polasek TM & Miners JO (2014). Inhibition of human drug-metabolising cytochrome P450 and UDP-glucuronosyltransferase enzyme activities in vitro by uremic toxins. *Eur J Clin Pharmacol* **70,** 1097–1106.

Barreto FC, Barreto D V., Liabeuf S, Drüeke TB & Massy ZA (2009*a*). Effects of uremic toxins on vascular and bone remodeling. *Semin Dial* **22,** 433–437.

Barreto FC, Barreto D V., Liabeuf S, Meert N, Glorieux G, Temmar M, Choukroun G, Vanholder R & Massy ZA (2009*b*). Serum Indoxyl Sulfate Is Associated with Vascular Disease and Mortality in Chronic Kidney Disease Patients. *Clin J Am Soc Nephrol* **4,** 1551–1558.

Barrios C, Beaumont M, Pallister T, Villar J, Goodrich JK, Clark A, Pascual J, Ley RE, Spector TD, Bell JT & Menni C (2015). Gut-Microbiota-Metabolite Axis in Early Renal Function Decline. *PLoS One* **10,** e0134311.

Bartel J, Krumsiek J, Schramm K, Adamski J, Gieger C, Herder C, Carstensen M, Peters A, Rathmann W, Roden M, Strauch K, Suhre K, Kastenmüller G, Prokisch H & Theis FJ (2015). The Human Blood Metabolome-Transcriptome Interface. *PLoS Genet* **11,** 1–32.

Bates DW, Cullen DJ, Laird N, Petersen LA, Small SD, Servi D, Laffel G, Sweitzer BJ, Shea BF & Hallisey R (1995). Incidence of adverse drug events and potential adverse drug events. Implications for prevention. ADE Prevention Study Group. *JAMA* **274,** 29–34.

Becker GJ & Hewitson TD (2013). Animal models of chronic kidney disease: Useful but not perfect. *Nephrol Dial Transplant* **28,** 2432–2438.

Belkaid Y & Hand TW (2014). Role of the Microbiota in Immunity and Inflammation. *Cell* **157,** 121–141.

Berg JM, Tymoczko JL & Stryer L (2012). *Biochemistry*, Seventh.ed. Freeman WH. New York.

den Besten G, van Eunen K, Groen AK, Venema K, Reijngoud D-J & Bakker BM (2013). The role of short-chain fatty acids in the interplay between diet, gut microbiota, and host energy metabolism. *J Lipid Res* **54,** 2325–2340.

Bosshard PP, Zbinden R & Altwegg M (2002). Turicibacter sanguinis gen. nov., sp. nov., a novel anaerobic, Gram-positive bacterium. *Int J Syst Evol Microbiol* **52,** 1263–1266.

Bugnicourt J-M, Godefroy O, Chillon J-M, Choukroun G & Massy ZA (2013). Cognitive Disorders and Dementia in CKD: The Neglected Kidney-Brain Axis. *J Am Soc Nephrol* **24,** 353–363.

Camacho D, de la Fuente A & Mendes P (2005). The origin of correlations in metabolomics data. *Metabolomics* **1,** 53–63.

Cao G, Zhang Y, Chen L, Liu J, Mao K, Li K & Zhou J (2015). Production of a bioflocculant from methanol wastewater and its application in arsenite removal. *Chemosphere* **141,** 274–281.

Caporaso JG, Lauber CL, Walters WA, Berg-Lyons D, Huntley J, Fierer N, Owens SM, Betley J, Fraser L, Bauer M, Gormley N, Gilbert JA, Smith G & Knight R (2012). Ultra-high-throughput microbial community analysis on the Illumina HiSeq and MiSeq platforms. *ISME J* **6,** 1621–1624.

Caporaso JG, Lauber CL, Walters WA, Berg-Lyons D, Lozupone CA, Turnbaugh PJ, Fierer N & Knight R (2011). Global patterns of 16S rRNA diversity at a depth of millions of sequences per sample. *Proc Natl Acad Sci U S A* **108 Suppl,** 4516–4522.

Carding S, Verbeke K, Vipond DT, Corfe BM & Owen LJ (2015). Dysbiosis of the gut microbiota in disease. *Microb Ecol Heal Dis* **26,** 1–10.

Carrero JJ, Qureshi AR, Nakashima A, Arver S, Parini P, Lindholm B, Bárány P, Heimbürger O & Stenvinkel P (2011). Prevalence and clinical implications of testosterone deficiency in men with end-stage renal disease. *Nephrol Dial Transplant* **26,** 184–190.

Cayir A & Kosan C (2015). Growth hormone therapy in children with chronic renal failure. *Eurasian J Med* **47,** 62–65.

Chakravorty S, Helb D, Burday M & Connell N (2007). A detailed analysis of 16S ribosomal RNA gene segments for the diagnosis of pathogenic bacteria. *J Microbiol*

Methods **69,** 330–339.

Chawla LS, Eggers PW, Star RA & Kimmel PL (2014). Acute Kidney Injury and Chronic Kidney Disease as Interconnected Syndromes. *N Engl J Med* **371,** 58–66.

Chen Y, Kissling G, Negishi M & Goldstein JA (2005). The nuclear receptors constitutive androstane receptor and pregnane X receptor cross-talk with hepatic nuclear factor 4alpha to synergistically activate the human CYP2C9 promoter. *J Pharmacol Exp Ther* **314,** 1125–1133.

Cho I & Blaser MJ (2012). The human microbiome: at the interface of health and disease. *Nat Rev Genet*; DOI: 10.1038/nrg3182.

Chovan JP, Ring SC, Yu E & Baldino JP (2007). Cytochrome P450 probe substrate metabolism kinetics in Sprague Dawley rats. *Xenobiotica* **37,** 459–473.

Claus SP et al. (2011). Colonization-Induced Host-Gut Microbial Metabolic Interaction. **2,** 1–8.

Corsonello A, Pedone C, Corica F, Mussi C, Carbonin P & Antonelli Incalzi R (2005). Concealed renal insufficiency and adverse drug reactions in elderly hospitalized patients. *Arch Intern Med* **165,** 790–795.

Cuív PÓ, Klaassens ES, Durkin AS, Harkins DM, Foster L, McCorrison J, Torralba M, Nelson KE & Morrison M (2011). Draft genome sequence of Turicibacter sanguinis PC909, isolated from human feces. *J Bacteriol* **193,** 1288–1289.

David LA, Maurice CF, Carmody RN, Gootenberg DB, Button JE, Wolfe BE, Ling A V, Devlin AS, Varma Y, Fischbach MA, Biddinger SB, Dutton RJ & Turnbaugh PJ (2013). Diet rapidly and reproducibly alters the human gut microbiome. *Nature* **505,** 559–563.

Davies EA & O'Mahony MS (2015). Adverse drug reactions in special populations - The elderly. *Br J Clin Pharmacol* **80,** 796–807.

Dowling TC, Briglia AE, Fink JC, Hanes DS, Light PD, Stackiewicz L, Karyekar CS, Eddington ND, Weir MR & Henrich WL (2003). Characterization of hepatic cytochrome P4503A activity in patients with end-stage renal disease. *Clin Pharmacol Ther* **73,** 427–434.

Duranton F, Cohen G, De Smet R, Rodriguez M, Jankowski J, Vanholder R & Argiles A (2012). Normal and Pathologic Concentrations of Uremic Toxins. *J Am Soc Nephrol*

23, 1258–1270.

Eckburg PB, Bik EM, Bernstein CN, Purdom E, Dethlefsen L, Sargent M, Gill SR, Nelson KE & Relman DA (2005). Diversity of the human intestinal microbial flora. *Science* **308,** 1635–1638.

Edgar RC (2010). Search and clustering orders of magnitude faster than BLAST. *Bioinformatics* **26,** 2460–2461.

Edwards IR & Aronson JK (2000). Adverse drug reactions: definitions, diagnosis, and management. **356,** 1255–1259.

Engle SJ, Stockelman MG, Chen JU, Boivin G, Yum M, Davies PM, Ying MOYIN, Sahota A, Simmonds HA, Stambrook PJ & Tischfield JA (1996). Adenine phosphoribosyltransferase-deficient mice develop 2,8-dihydroxyadenine nephrolithiasis Adenine phosphoribosyltransferase-deficient mice develop 2,8-dihydroxyadenine nephrolithiasis (purine metabolism/gene targeting/mouse model/renal disease). *Genetics* **93,** 5307–5312.

Falk A, Olsson C, Ahrné S, Molin G, Adawi D & Jeppsson B (2007). Ileal pelvic pouch microbiota from two former ulcerative colitis patients, analysed by DNA-based methods, were unstable over time and showed the presence of Clostridium perfringens. *Scand J Gastroenterol* **42,** 973–985.

Falony G et al. (2016). Population-level analysis of gut microbiome variation. *Science (80-)* **352,** 560–564.

Farrés M, Platikanov S, Tsakovski S & Tauler R (2015). Comparison of the variable importance in projection (VIP) and of the selectivity ratio (SR) methods for variable selection and interpretation. *J Chemom* **29,** 528–536.

Feere D a, Velenosi TJ & Urquhart BL (2015). Effect of erythropoietin on hepatic cytochrome P450 expression and function in an adenine-fed rat model of chronic kidney disease. *Br J Pharmacol* **172,** 201–213.

Felizardo RJF, Castoldi A, Andrade-Oliveira V & Câmara NOS (2016). The microbiota and chronic kidney diseases: a double-edged sword. *Clin Transl Immunol* **5,** e86.

Fernandes AD, Reid JN, Macklaim JM, McMurrough TA, Edgell DR & Gloor GB (2014). Unifying the analysis of high-throughput sequencing datasets: characterizing RNA-seq, 16S rRNA gene sequencing and selective growth experiments by

compositional data analysis. *Microbiome* **2,** 15.

Feroze U, Kalantar-Zadeh K, Sterling KA, Molnar MZ, Noori N, Benner D, Shah V, Dwivedi R, Becker K, Kovesdy CP & Raj DS (2012). Examining Associations of Circulating Endotoxin With Nutritional Status, Inflammation, and Mortality in Hemodialysis Patients. *J Ren Nutr* **22,** 317–326.

Fisher CDC, Lickteig AJA, Augustine LML, Ranger-Moore J, Jackson JPJ, Ferguston S, Cherrington NNJ, Ferguson SS & Cherrington NNJ (2009). Hepatic cytochrome P450 enzyme alterations in humans with progressive stages of nonalcoholic fatty liver disease. *Drug Metab Dispos* **37,** 2087–2094.

Franks AH, Harmsen HJM, Gerwin C, Jansen GJ, Schut F & Gjalt W (1998). Variations of Bacterial Populations in Human Feces Measured by Fluorescent In Situ Hybridization with Group-Specific 16S rRNA-Targeted Oligonucleotide Probes Variations of Bacterial Populations in Human Feces Measured by Fluorescent In Situ Hybridization . **64,** 3336–3345.

Frassetto LA, Poon S, Tsourounis C, Valera C & Benet LZ (2007). Effects of Uptake and Efflux Transporter Inhibition on Erythromycin Breath Test Results. *Clin Pharmacol Ther* **81,** 828–832.

Gad SC (2009). *Preclinical Development Handbook; ADME and Biopharmaceutical Propertie*sed. Gad S. John Wiley & Sons, Inc., Hoboken, New Jersey.

Gansevoort RT, Correa-Rotter R, Hemmelgarn BR, Jafar TH, Heerspink HJL, Mann JF, Matsushita K & Wen CP (2013). Chronic kidney disease and cardiovascular risk: Epidemiology, mechanisms, and prevention. *Lancet* **382,** 339–352.

Ghanadian R, Lewis JG & Chisholm GD (1975). Serum testosterone and dihydrotestosterone changes with age in rat. *Steroids* **25,** 753–762.

Gilbert JA, Jansson JK & Knight R (2014). The Earth Microbiome project: successes and aspirations. *BMC Biol* **12,** 69.

Gloor GB, Hummelen R, Macklaim JM, Dickson RJ, Fernandes AD, MacPhee R & Reid G (2010). Microbiome profiling by illumina sequencing of combinatorial sequence-tagged PCR products. *PLoS One*; DOI: 10.1371/journal.pone.0015406.

Gloor GB, Macklaim JM & Fernandes AD (2016*a*). Displaying Variation in Large Datasets: Plotting a Visual Summary of Effect Sizes. *J Comput Graph Stat* **25,** 971–

979.

Gloor GB & Reid G (2016). Compositional analysis: a valid approach to analyze microbiome high throughput sequencing data. *Can J Microbiol* **703,** cjm-2015-0821.

Gloor GB, Wu JR, Pawlowsky-Glahn V & Egozcue JJ (2016*b*). It's all relative: analyzing microbiome data as compositions. *Ann Epidemiol* **26,** 322–329.

Gong IY, Schwarz UI, Crown N, Dresser GK, Lazo-Langner A, Zou G, Roden DM, Stein CM, Rodger M, Wells PS, Kim RB & Tirona RG (2011). Clinical and genetic determinants of warfarin pharmacokinetics and pharmacodynamics during treatment initiation. *PLoS One*; DOI: 10.1371/journal.pone.0027808.

Goodrich JK, Waters JL, Poole AC, Sutter JL, Koren O, Blekhman R, Beaumont M, Van Treuren W, Knight R, Bell JT, Spector TD, Clark AG & Ley RE (2014). Human Genetics Shape the Gut Microbiome. *Cell* **159,** 789–799.

Goodwin B, Hodgson E & Liddle C (1999). The orphan human pregnane X receptor mediates the transcriptional activation of CYP3A4 by rifampicin through a distal enhancer module. *Mol Pharmacol* **56,** 1329–1339.

Gregory JC, Buffa JA, Org E, Wang Z, Levison BS, Zhu W, Wagner MA, Bennett BJ, Li L, DiDonato JA, Lusis AJ & Hazen SL (2015). Transmission of atherosclerosis susceptibility with gut microbial transplantation. *J Biol Chem* **290,** 5647–5660.

Gross JL, De Azevedo MJ, Silveiro SP, Canani H, Caramori ML & Zelmanovitz T (2005). Diabetic Nephropathy: Diagnosis, Prevention, and Treatment. *Diabetes Care* **28,** 176–188.

Gryp T, Vanholder R, Vaneechoutte M & Glorieux G (2017). p-Cresyl Sulfate. *Toxins (Basel)* **9,** 52.

Gu X, Ke S, Liu D, Sheng T, Thomas PE, Rabson AB, Gallo MA, Xie W & Tian Y (2006). Role of NF-κB in regulation of PXR-mediated gene expression: A mechanism for the suppression of cytochrome P-450 3A4 by proinflammatory agents. *J Biol Chem* **281,** 17882–17889.

Guévin C, Michaud J, Naud J, Leblond FA & Pichette V (2002). Down-regulation of hepatic cytochrome P450 in chronic renal failure: role of uremic mediators. *Br J Pharmacol* **137,** 1039–1046.

Hahr AJ & Molitch ME (2015). Management of diabetes mellitus in patients with chronic

kidney disease. *Clin Diabetes Endocrinol* **1,** 2.

Hall ME, Silva AA, Juncos LA, Wang Z & Hall JE (2014). Obesity , hypertension , and chronic kidney disease. 75–88.

Halsey LG, Curran-Everett D, Vowler SL & Drummond GB (2015). The fickle P value generates irreproducible results. *Nat Methods* **12,** 179–185.

Hashimoto M, Kurata N, Nishimura Y, Iwase M, Uchida E & Yasuhara H (1997). Effect of Adenine-Induced Renal Failure on Hepatic Enzymes in Rats Microsomal Activities of hepatic microsomal oxidative drug-metabolizing enzymes and heme-metaboliz- ing enzymes are closely related to liver and renal functions1 , 2). Unexptcted adverse . **9,** 1–5.

Heaney LM, Jones DJL, Mbasu RJ, Ng LL & Suzuki T (2016). High mass accuracy assay for trimethylamine N-oxide using stable-isotope dilution with liquid chromatography coupled to orthogonal acceleration time of flight mass spectrometry with multiple reaction monitoring. *Anal Bioanal Chem* **408,** 797–804.

Hiergeist A, Gläsner J, Reischl U & Gessner A (2015). Analyses of intestinal microbiota: Culture versus sequencing. *ILAR J* **56,** 228–240.

Hill NR, Fatoba ST, Oke JL, Hirst JA, Callaghan AO, Lasserson DS & Hobbs FDR (2016). Global Prevalence of Chronic Kidney Disease – A Systematic Review and Meta-Analysis. *PLoS One*1–18.

Hong Y-S, Hong KS, Park M-H, Ahn Y-T, Lee J-H, Huh C-S, Lee J, Kim I-K, Hwang G-S & Kim JS (2011). Metabonomic understanding of probiotic effects in humans with irritable bowel syndrome. *J Clin Gastroenterol* **45,** 415–425.

Honkakoski P & Negishi M (2000). Regulation of cytochrome P450 (CYP) genes by nuclear receptors. *Biochem J* **347,** 321.

Hu N, Hu M, Duan R, Liu C, Guo H, Zhang M, Yu Y, Wang X, Liu L & Liu X (2014). Increased Levels of Fatty Acids Contributed to Induction of Hepatic CYP3A4 Activity Induced by Diabetes — In Vitro Evidence From HepG2 Cell and Fa2N-4 Cell Lines. *J Pharmacol Sci* **124,** 433–444.

Hung S, Kuo K, Wu C & Tarng D (2017). Indoxyl Sulfate: A Novel Cardiovascular Risk Factor in Chronic Kidney Disease. *J Am Heart Assoc* **6,** e005022.

Huttenhower C et al. (2012). Structure, function and diversity of the healthy human

microbiome. *Nature* **486,** 207–214.

Institute of Medicine (1998). *Dietary reference intakes for thiamin, riboflavin, niacin, vitamin B_6, folate, vitamin B_{12}, pantothenic acid, biotin, and choline*.

Ito S & Yoshida M (2014). Protein-bound Uremic toxins: New culprits of cardiovascular events in chronic kidney disease patients. *Toxins (Basel)* **6,** 665–678.

Itoh Y, Ezawa A, Kikuchi K, Tsuruta Y & Niwa T (2012). Protein-bound uremic toxins in hemodialysis patients measured by liquid chromatography/tandem mass spectrometry and their effects on endothelial ROS production. *Anal Bioanal Chem* **403,** 1841–1850.

Itoh Y, Ezawa A, Kikuchi K, Tsuruta Y & Niwa T (2013). Correlation between Serum Levels of Protein-Bound Uremic Toxins in Hemodialysis Patients Measured by LC/MS/MS. *Mass Spectrom (Tokyo, Japan)* **2,** S0017.

Janda JM & Abbott SL (2007). 16S rRNA gene sequencing for bacterial identification in the diagnostic laboratory: Pluses, perils, and pitfalls. *J Clin Microbiol* **45,** 2761–2764.

Jha V, Garcia-Garcia G, Iseki K, Li Z, Naicker S, Plattner B, Saran R, Wang AYM & Yang CW (2013). Chronic kidney disease: Global dimension and perspectives. *Lancet* **382,** 260–272.

Johnson EF & Stout CD (2005). Structural diversity of human xenobiotic-metabolizing cytochrome P450 monooxygenases. *Biochem Biophys Res Commun* **338,** 331–336.

Jover R, Bort R, Gómez-Lechón MJ & Castell J V. (2002). Down-regulation of human CYP3A4 by the inflammatory signal interleukin-6: molecular mechanism and transcription factors involved. *FASEB J* **16,** 1799–1801.

Jover R, Moya M & Gómez-Lechón MJ (2009). Transcriptional regulation of cytochrome p450 genes by the nuclear receptor hepatocyte nuclear factor 4-alpha. *Curr Drug Metab* **10,** 508–519.

Kaufhold A, Nigam PK, Dhir RN & Shapiro BH (2002). Prevention of latently expressed CYP2C11, CYP3A2, and growth hormone defects in neonatally monosodium glutamate-treated male rats by the N-methyl-D-aspartate receptor antagonist dizocilpine maleate. *J Pharmacol Exp Ther* **302,** 490–496.

KDIGO Work Group (2009). KDIGO clinical practice guideline for the diagnosis,

evaluation, prevention, and treatment of Chronic Kidney Disease-Mineral and Bone Disorder (CKD-MBD). *Kidney Int Suppl* **76,** S1-130.

Kelley WN (1975). Effects of drugs on uric acid in man. *Annu Rev Pharmacol* **15,** 327–350.

Kelly GS (2011). Pantothenic acid. Monograph. *Altern Med Rev* **16,** 263–274.

Al Khodor S & Shatat IF (2016). Gut microbiome and kidney disease: a bidirectional relationship. *Pediatr Nephrol*1–11.

Kikuchi K, Itoh Y, Tateoka R, Ezawa A, Murakami K & Niwa T (2010). Metabolomic search for uremic toxins as indicators of the effect of an oral sorbent AST-120 by liquid chromatography/tandem mass spectrometry. *J Chromatogr B Anal Technol Biomed Life Sci* **878,** 2997–3002.

Kim SK & Novak RF (2007). The role of intracellular signaling in insulin-mediated regulation of drug metabolizing enzyme gene and protein expression. *Pharmacol Ther* **113,** 88–120.

Klaassen CD & Cui JY (2015). Review: Mechanisms of How the Intestinal Microbiota Alters the Effects of Drugs and Bile Acids. *Drug Metab Dispos* **43,** 1505–1521.

Klein K & Zanger UM (2013). Pharmacogenomics of cytochrome P450 3A4: Recent progress toward the "missing heritability" problem. *Front Genet* **4,** 1–15.

Kliewer SA, Goodwin B & Willson TM (2002). The nuclear pregnane X receptor: A key regulator of xenobiotic metabolism. *Endocr Rev* **23,** 687–702.

Knights D, Ward TL, McKinlay CE, Miller H, Gonzalez A, McDonald D & Knight R (2014). Rethinking "Enterotypes." *Cell Host Microbe* **16,** 433–437.

Kobayashi T, Matsumura Y, Ozawa T, Yanai H, Iwasawa A, Kamachi T, Fujiwara K, Tanaka N & Kohno M (2014). Exploration of novel predictive markers in rat plasma of the early stages of chronic renal failure. *Anal Bioanal Chem* **406,** 1365–1376.

Koeth RA et al. (2013). Intestinal microbiota metabolism of l-carnitine, a nutrient in red meat, promotes atherosclerosis. *Nat Med* **19,** 576–585.

Koppe L, Mafra D & Fouque D (2015). Probiotics and chronic kidney disease. *Kidney Int* **88,** 1–9.

Kopple JD (2010). Obesity and Chronic Kidney Disease. *J Ren Nutr* **20,** S29–S30.

Kuhl C, Tautenhahn R, Böttcher C, Larson TR & Neumann S (2012). CAMERA: An

integrated strategy for compound spectra extraction and annotation of liquid chromatography/mass spectrometry data sets. *Anal Chem* **84,** 283–289.

Kverka M, Zakostelska Z, Klimesova K, Sokol D, Hudcovic T, Hrncir T, Rossmann P, Mrazek J, Kopecny J, Verdu EF & Tlaskalova-Hogenova H (2011). Oral administration of Parabacteroides distasonis antigens attenuates experimental murine colitis through modulation of immunity and microbiota composition. *Clin Exp Immunol* **163,** 250–259.

Ladda MA & Goralski KB (2016). The Effects of CKD on Cytochrome P450–Mediated Drug Metabolism. *Adv Chronic Kidney Dis* **23,** 67–75.

Lammers L a., Achterbergh R, de Vries EM, van Nierop FS, Klumpen H-J, Soeters MR, Boelen a., Romijn J a. & Mathot R a. a. (2015). Short-Term Fasting alters Cytochrome P450 mediated Drug Metabolism in Humans. *Drug Metab Dispos*819–828.

Lau WL, Kalantar-zadeh K & Vaziri ND (2016). The gut as a source of inflammation in chronic kidney disease. **6034,** 92–98.

Leblond F a, Petrucci M, Dubé P, Bernier G, Bonnardeaux A & Pichette V (2002). Downregulation of intestinal cytochrome p450 in chronic renal failure. *J Am Soc Nephrol* **13,** 1579–1585.

Leblond F, Guévin C, Demers C, Pellerin I, Gascon-Barré M & Pichette V (2001). Downregulation of hepatic cytochrome P450 in chronic renal failure. *J Am Soc Nephrol* **12,** 326–332.

Leong SC & Sirich TL (2016). Indoxyl sulfate-review of toxicity and therapeutic strategies. *Toxins (Basel)*; DOI: 10.3390/toxins8120358.

Levey A, Coresh J, Ethan B, Kausz A, Levin A, Steffes M, Hogg R, Perrone R, Lau J & Eknoya G (2003). Clinical Guidelines National Kidney Foundation Practice Guidelines for Chronic Kidney. *Ann Intern Med* **139,** 137–147.

Ley RE, Backhed F, Turnbaugh P, Lozupone CA, Knight RD & Gordon JI (2005). Obesity alters gut microbial ecology. *Proc Natl Acad Sci* **102,** 11070–11075.

Licht TR, Madsen B & Wilcks A (2007). Selection of bacteria originating from a human intestinal microbiota in the gut of previously germ-free rats. *FEMS Microbiol Lett* **277,** 205–209.

Lin CJ, Wu V, Wu PC & Wu CJ (2015). Meta-analysis of the associations of p-cresyl sulfate (PCS) and indoxyl sulfate (IS) with cardiovascular events and all-cause mortality in patients with chronic renal failure. *PLoS One* **10,** 1–14.

Lisowska-Myjak B (2014). Uremic toxins and their effects on multiple organ systems. *Nephron - Clin Pract* **128,** 303–311.

Livak KJ & Schmittgen TD (2001). Analysis of Relative Gene Expression Data Using Real-Time Quantitative PCR and the 2−ΔΔCT Method. *Methods* **25,** 402–408.

Lloyd-Price J, Abu-Ali G & Huttenhower C (2016). The healthy human microbiome. *Genome Med* **8,** 51.

Lopez-Giacoman S (2015). Biomarkers in chronic kidney disease, from kidney function to kidney damage. *World J Nephrol* **4,** 57.

Lührs H, Gerke T, Müller JG, Melcher R, Schauber J, Boxberge F, Scheppach W & Menzel T (2002). Butyrate inhibits NF-kappaB activation in lamina propria macrophages of patients with ulcerative colitis. *Scand J Gastroenterol* **37,** 458–466.

Luo J, Wu C, Xu T & Wu Y (2011). Diffusion dialysis-concept, principle and applications. *J Memb Sci* **366,** 1–16.

Lynch TOM, Price AMY & Virginia E (2007). The Effect of Cytochrome P450Metabolism on Drug Response,Interactions, and Adverse Effects. *Am Fam Physicians* **76,** 1–6.

Macfarlane GT & Macfarlane S (2012). Bacteria, colonic fermentation, and gastrointestinal health. *J AOAC Int* **95,** 50–60.

Macklaim JM, Fernandes AD, Di Bella JM, Hammond J-A, Reid G & Gloor GB (2013). Comparative meta-RNA-seq of the vaginal microbiota and differential expression by Lactobacillus iners in health and dysbiosis. *Microbiome* **1,** 12.

Mafra D & Fouque D (2015). Gut microbiota and inflammation in chronic kidney disease patients. *Clin Kidney J* **8,** 332–334.

Magnusson M, Magnusson KE, Sundqvist T & Denneberg T (1991). Impaired intestinal barrier function measured by differently sized polyethylene glycols in patients with chronic renal failure. *Gut* **32,** 754–759.

Majerczyk CD, Dunman PM, Luong TT, Lee CY, Sadykov MR, Somerville GA, Bodi K & Sonenshein AL (2010). Direct targets of CodY in Staphylococcus aureus. *J*

Bacteriol **192,** 2861–2877.

Manichanh C, Reeder J, Gibert P, Varela E, Llopis M, Antolin M, Guigo R, Knight R & Guarner F (2010). Reshaping the gut microbiome with bacterial transplantation and antibiotic intake. *Genome Res* **20,** 1411–1419.

Manley HJ, Cannella CA, Bailie GR & St Peter WL (2005). Medication-related problems in ambulatory hemodialysis patients: a pooled analysis. *Am J Kidney Dis* **46,** 669–680.

Manns BJ, Mendelssohn DC & Taub KJ (2007). The economics of end-stage renal disease care in Canada : incentives and impact on delivery of care. **7,** 149–169.

Martín-Fernández J a., Barcelo-Vidal C & Pavlowsky-Glahn V (2003). Dealing With Zeros and Missing Values in Compositional Data Sets Using Nonparametric. *Math Geol* **35,** 253–278.

Masella AP, Bartram AK, Truszkowski JM, Brown DG & Neufeld JD (2012). PANDAseq: paired-end assembler for illumina sequences. *BMC Bioinformatics* **13,** 31.

Matzke GR, Aronoff GR, Atkinson AJ, Bennett WM, Decker BS, Eckardt K-U, Golper T, Grabe DW, Kasiske B, Keller F, Kielstein JT, Mehta R, Mueller BA, Pasko DA, Schaefer F, Sica DA, Inker LA, Umans JG & Murray P (2011). Drug dosing consideration in patients with acute and chronic kidney disease—a clinical update from Kidney Disease: Improving Global Outcomes (KDIGO). *Kidney Int* **80,** 1122–1137.

McMillan A, Rulisa S, Sumarah M, Macklaim JM, Renaud J, Bisanz JE, Gloor GB & Reid G (2015). A multi-platform metabolomics approach identifies highly specific biomarkers of bacterial diversity in the vagina of pregnant and non-pregnant women. *Sci Rep* **5,** 14174.

Meyer TW & Hostetter TH (2007). Uremia. *N Engl J Med* **357,** 1316–1325.

Meyer TW & Hostetter TH (2012). Uremic solutes from colon microbes. *Kidney Int* **81,** 949–954.

Michaud J, Naud J, Chouinard J, Désy F, Leblond F a, Desbiens K, Bonnardeaux A & Pichette V (2006). Role of parathyroid hormone in the downregulation of liver cytochrome P450 in chronic renal failure. *J Am Soc Nephrol* **17,** 3041–3048.

Michaud J, Nolin TD, Naud J, Dani M, Lafrance J-P, Leblond F a, Himmelfarb J & Pichette V (2008). Effect of hemodialysis on hepatic cytochrome P450 functional expression. *J Pharmacol Sci* **108,** 157–163.

Mikamo E, Harada S, Nishikawa JI & Nishihara T (2003). Endocrine disruptors induce cytochrome P450 by affecting transcriptional regulation via pregnane X receptor. *Toxicol Appl Pharmacol* **193,** 66–72.

Moeller a. H & Ochman H (2014). Microbiomes are true to type. *Proc Natl Acad Sci* **111,** 9372–9373.

Mondot S, Kang S, Furet JP, Aguirre De Carcer D, McSweeney C, Morrison M, Marteau P, Doré J & Leclerc M (2011). Highlighting new phylogenetic specificities of Crohn's disease microbiota. *Inflamm Bowel Dis* **17,** 185–192.

Morgan E (2009). Impact of Infectious and Inflammatory Disease on Cytochrome P450–Mediated Drug Metabolism and Pharmacokinetics. *Clin Pharmacol Ther* **85,** 434–438.

Morishita Y, Ohnishi A, Watanabe M, Ishibashi K & Kusano E (2011). Establishment of Acute Kidney Injury Mouse Model by 0.75% Adenine Ingestion. *Ren Fail* **33,** 1013–1018.

Mortier S, De Vriese AS, Van de Voorde J, Schaub TP, Passlick-Deetjen J & Lameire NH (2002). Hemodynamic effects of peritoneal dialysis solutions on the rat peritoneal membrane: role of acidity, buffer choice, glucose concentration, and glucose degradation products. *J Am Soc Nephrol* **13,** 480–489.

Munar MY & Singh H (2007). Drug dosing adjustments in patients with chronic kidney disease. *Am Fam Physician* **75,** 1487–1496.

Nallu A, Sharma S, Ramezani A, Muralidharan J & Raj D (2016). Gut Microbiome in CKD: challenges and opportunities. *Transl Res*1–14.

Nelson DR, Zeldin DC, Hoffman SMG, Maltais LJ, Wain HM & Nebert DW (2004). Comparison of cytochrome P450 (CYP) genes from the mouse and human genomes, including nomenclature recommendations for genes, pseudogenes and alternative-splice variants. *Pharmacogenetics* **14,** 1–18.

Nicholson JK, Holmes E & Wilson ID (2005). Gut microorganisms, mammalian metabolism and personalized health care. *Nat Rev Microbiol* **3,** 431–438.

Nieuwdorp M, Gilijamse PW, Pai N & Kaplan LM (2014). Role of the microbiome in energy regulation and metabolism. *Gastroenterology* **146,** 1525–1533.

Nigam SK, Bush KT, Martovetsky G, Ahn S-Y, Liu HC, Richard E, Bhatnagar V & Wu W (2015). The organic anion transporter (OAT) family: a systems biology perspective. *Physiol Rev* **95,** 83–123.

Niwa T (2013). Targeting protein-bound uremic toxins in chronic kidney disease. *Expert Opin Ther Targets* **17,** 1287–1301.

Nolin TD (2015). A Synopsis of Clinical Pharmacokinetic Alterations in Advanced CKD. *Semin Dial*n/a-n/a.

Nolin TD, Appiah K, Kendrick SA, Le P, McMonagle E & Himmelfarb J (2006). Hemodialysis acutely improves hepatic CYP3A4 metabolic activity. *J Am Soc Nephrol* **17,** 2363–2367.

Nolin TD, Frye RF, Le P, Sadr H, Naud J, Leblond F a, Pichette V & Himmelfarb J (2009). ESRD impairs nonrenal clearance of fexofenadine but not midazolam. *J Am Soc Nephrol* **20,** 2269–2276.

Nolin TD, Naud J, Leblond F a & Pichette V (2008). Emerging evidence of the impact of kidney disease on drug metabolism and transport. *Clin Pharmacol Ther* **83,** 898–903.

O'Hare AM, Choi AI, Bertenthal D, Bacchetti P, Garg AX, Kaufman JS, Walter LC, Mehta KM, Steinman MA, Allon M, McClellan WM & Landefeld CS (2007). Age Affects Outcomes in Chronic Kidney Disease. *J Am Soc Nephrol* **18,** 2758–2765.

OECD (2011). Health at a glance. *Organ Econ Co-operation Dev*.

Otero J, Le¢n JA & Graesser AC eds. (2014). *The Psychology of Science Text Comprehension*. Routledge, New York.

Pan ST, Xue D, Li ZL, Zhou ZW, He ZX, Yang Y, Yang T, Qiu JX & Zhou SF (2016). *Computational Identification of the Paralogs and Orthologs of Human Cytochrome P450 Superfamily and the Implication in Drug Discovery*.

Pan YZ, Gao W & Yu AM (2009). MicroRNAs regulate CYP3A4 expression via direct and indirect targeting. *Drug Metab Dispos* **37,** 2112–2117.

Persky SE & Brandt LJ (2000). Treatment of recurrent Clostridium difficile-associated diarrhea by administration of donated stool directly through a colonoscope. *Am J*

Gastroenterol **95,** 3283–3285.

Poretsky R, Rodriguez-R LM, Luo C, Tsementzi D & Konstantinidis KT (2014). Strengths and limitations of 16S rRNA gene amplicon sequencing in revealing temporal microbial community dynamics. *PLoS One*; DOI: 10.1371/journal.pone.0093827.

Porth C (2011). *Essentials of Pathophysiology: Concepts of Altered Health States*. Lippincott Williams & Wilkins.

Qin J et al. (2010). A human gut microbial gene catalogue established by metagenomic sequencing. *Nature* **464,** 59–65.

Quast C, Pruesse E, Yilmaz P, Gerken J, Schweer T, Yarza P, Peplies J & Glöckner FO (2013). The SILVA ribosomal RNA gene database project: Improved data processing and web-based tools. *Nucleic Acids Res* **41,** 590–596.

Ramezani A, Massy ZA, Meijers B, Evenepoel P, Vanholder R & Raj DS (2015). Role of the Gut Microbiome in Uremia: A Potential Therapeutic Target. *Am J Kidney Dis*1–16.

Ranganathan N, Patel BG, Ranganathan P, Marczely J, Dheer R, Pechenyak B, Dunn SR, Verstraete W, Decroos K, Mehta R & Friedman E a (2006). In vitro and in vivo assessment of intraintestinal bacteriotherapy in chronic kidney disease. *ASAIO J* **52,** 70–79.

Rao X, Huang X, Zhou Z & Lin X (2013). An improvement of the 2ˆ(-delta delta CT) method for quantitative real-time polymerase chain reaction data analysis. *Biostat Bioinforma Biomath* **3,** 71–85.

Reese JB, Urry LA, Cain ML, Wasserman SA, Minorsky P V. & Jackson RB (2011). *Campbell Biology*, Ninth. Benjamin Cummings, Boston.

Rossi M, Johnson DW, Morrison M, Pascoe EM, Coombes JS, Forbes JM, Szeto CC, McWhinney BC, Ungerer JPJ & Campbell KL (2016). Synbiotics easing renal failure by improving gut microbiology (SYNERGY): A randomized trial. *Clin J Am Soc Nephrol* **11,** 223–231.

Saccenti E, Hoefsloot HCJ, Smilde AK, Westerhuis JA & Hendriks MMWB (2014). Reflections on univariate and multivariate analysis of metabolomics data. *Metabolomics* **10,** 361–374.

Sakamoto M & Benno Y (2006). Reclassification of Bacteroides distasonis, Bacteroides goldsteinii and Bacteroides merdae as Parabacteroides distasonis gen. nov., comb. nov., Parabacteroides goldsteinii comb. nov and Parabacteroides merdae comb. nov. *Int J Syst Evol Microbiol* **56,** 1599–1605.

Salati LM, Gross CJ, Henderson LM & Savaiano DA (1984). Absorption and metabolism of adenine, adenosine-5'-monophosphate, adenosine and hypoxanthine by the isolated vascularly perfused rat small intestine. *J Nutr* **114,** 753–760.

Salek RM, Steinbeck C, Viant MR, Goodacre R & Dunn WB (2013). The role of reporting standards for metabolite annotation and identification in metabolomic studies. *Gigascience* **2,** 13.

Sanger F, Nicklen S & Coulson AR (1977). DNA sequencing with chain-terminating inhibitors. *Proc Natl Acad Sci* **74,** 5463–5467.

Satchell SC & Tooke JE (2008). What is the mechanism of microalbuminuria in diabetes: A role for the glomerular endothelium? *Diabetologia* **51,** 714–725.

Schena FP (2005). Pathogenetic Mechanisms of Diabetic Nephropathy. *J Am Soc Nephrol* **16,** S30–S33.

Schloss PD, Westcott SL, Ryabin T, Hall JR, Hartmann M, Hollister EB, Lesniewski RA, Oakley BB, Parks DH, Robinson CJ, Sahl JW, Stres B, Thallinger GG, Van Horn DJ & Weber CF (2009). Introducing mothur: Open-source, platform-independent, community-supported software for describing and comparing microbial communities. *Appl Environ Microbiol* **75,** 7537–7541.

Schwarz UI, Ritchie MD, Bradford Y, Li C, Dudek SM, Frye-Anderson A, Kim RB, Roden DM & Stein CM (2008). Genetic Determinants of Response to Warfarin during Initial Anticoagulation. *N Engl J Med* **358,** 999–1008.

Selwyn FP, Cheng SL, Bammler TK, Prasad B, Vrana M, Klaassen C & Cui JY (2015). Developmental regulation of drug-processing genes in livers of germ-free mice. *Toxicol Sci* **147,** 84–103.

Sereno PC, Wilson JA, Larsson HCE, Dutheil DB & Sues H (2016). Efficiency of Human Visual Signal Discrimination Author (s): A . E . Burgess , R . F . Wagner , R . J . Jennings and H . B . Barlow Published by : American Association for the Advancement of Science Stable URL : http://www.jstor.org/stable/1687274 Acces.

214, 93–94.

Sharif-Askari FS, Sulaiman SAS, Sharif-Askari NS & Hussain AAS (2014). Development of an adverse drug reaction risk assessment score among hospitalized patients with chronic kidney disease. *PLoS One* **9,** 1–8.

Shemesh O, Golbetz H, Kriss JP & Myers BD (1985). Limitations of creatinine as a filtration marker in glomerulopathic patients. *Kidney Int* **28,** 830–838.

Sheweita SA (2000). Drug-Metabolizing Enzymes : Mechanisms and Functions. 107–132.

Smink PA, Lambers Heerspink HJ, Gansevoort RT, de Jong PE, Hillege HL, Bakker SJL & de Zeeuw D (2012). Albuminuria, estimated GFR, traditional risk factors, and incident cardiovascular disease: the PREVEND (Prevention of Renal and Vascular Endstage Disease) study. *Am J Kidney Dis* **60,** 804–811.

Smith C a, Want EJ, O'Maille G, Abagyan R, Siuzdak G & CA Smith, J Elizabeth, G O'Maille,Ruben Abagyan and GS (2006). XCMS: processing mass spectrometry data for metabolite profiling using Nonlinear Peak Alignment,Matching,and Identification. *ACS Publ* **78,** 779–787.

Sotaniemi EA, Lumme P, Arvela P & Rautio A (1995). Age and CYP3A4 and CYP2A6 activities marked by the metabolism of lignocaine and coumarin in man. *Therapie* **51,** 363–366.

Statistics Canada (2015). Annual Demographic Estimates : Canada, Provinces and Territories. *Stat Canada Cat no 91-215-X*1–179.

Staudinger JL, Goodwin B, Jones S a, Hawkins-Brown D, MacKenzie KI, LaTour a, Liu Y, Klaassen CD, Brown KK, Reinhard J, Willson TM, Koller BH & Kliewer S a (2001). The nuclear receptor PXR is a lithocholic acid sensor that protects against liver toxicity. *Proc Natl Acad Sci U S A* **98,** 3369–3374.

Stevens LA, Schmid CH, Greene T, Zhang Y, Beck GJ, Froissart M, Hamm LL, Lewis JB, Mauer M, Navis GJ, Steffes MW, Eggers PW, Coresh J & Levey AS (2010). Comparative performance of the CKD Epidemiology Collaboration (CKD-EPI) and the Modification of Diet in Renal Disease (MDRD) Study equations for estimating GFR levels above 60 mL/min/1.73 m2. *Am J Kidney Dis* **56,** 486–495.

Stewart CJ, Skeath T, Nelson A, Fernstad SJ, Marrs ECL, Perry JD, Cummings SP,

Berrington JE & Embleton ND (2015). Preterm gut microbiota and metabolome following discharge from intensive care. *Sci Rep* **5,** 17141.

Stewart EJ (2012). Growing unculturable bacteria. *J Bacteriol* **194,** 4151–4160.

Storm AC, Htike NL, Cohen DA, Benz RL & Al ET (2013). A Surviving Patient with Record High Creatinine. **2013,** 217–219.

Succar L, Pianta TJ, Davidson T, Pickering JW & Endre ZH (2017). Subclinical chronic kidney disease modifies the diagnosis of experimental acute kidney injury. *Kidney Int*1–13.

Sugiyama H, Kashihara N, Makino H, Yamasaki Y & Ota Z (1996). Apoptosis in glomerular sclerosis. *Kidney Int* **49,** 103–111.

Sun H, Huang Y, Frassetto L & Benet LZ (2004). Effects of uremic toxins on hepatic uptake and metabolism of erythromycin. *Drug Metab Dispos* **32,** 1239–1246.

Talbert RL (1994). Drug dosing in renal insufficiency. *J Clin Pharmacol* **34,** 99–110.

Tedla FM, Brar A, Browne R & Brown C (2011). Hypertension in Chronic Kidney Disease: Navigating the Evidence. *Int J Hypertens* **2011,** 1–9.

Terai K, Mizukami K & Okada M (2008). Comparison of chronic renal failure rats and modification of the preparation protocol as a hyperphosphataemia model. *Nephrology* **13,** 139–146.

Tervaert TWC, Mooyaart AL, Amann K, Cohen AH, Cook HT, Drachenberg CB, Ferrario F, Fogo AB, Haas M, de Heer E, Joh K, Noel LH, Radhakrishnan J, Seshan S V., Bajema IM & Bruijn JA (2010). Pathologic Classification of Diabetic Nephropathy. *J Am Soc Nephrol* **21,** 556–563.

Theriot CM, Koenigsknecht MJ, Carlson PE, Hatton GE, Nelson AM, Li B, Huffnagle GB, Z Li J & Young VB (2014). Antibiotic-induced shifts in the mouse gut microbiome and metabolome increase susceptibility to Clostridium difficile infection. *Nat Commun* **5,** 3114.

Thomas M, Burk O, Klumpp B, Kandel BA, Damm G, Weiss TS, Klein K, Schwab M & Zanger UM (2013). Direct Transcriptional Regulation of Human Hepatic Cytochrome P450 3A4 (CYP3A4) by Peroxisome Proliferator-Activated Receptor Alpha (PPAR). *Mol Pharmacol* **83,** 709–718.

Thomson BK a., Nolin TD, Velenosi TJ, Feere D a., Knauer MJ, Asher LJ, House A a. &

Urquhart BL (2015). Effect of CKD and Dialysis Modality on Exposure to Drugs Cleared by Nonrenal Mechanisms. *Am J Kidney Dis* **65,** 574–582.

Tirona RG, Lee W, Leake BF, Lan L-B, Cline CB, Lamba V, Parviz F, Duncan SA, Inoue Y, Gonzalez FJ, Schuetz EG & Kim RB (2003). The orphan nuclear receptor HNF4α determines PXR- and CAR-mediated xenobiotic induction of CYP3A4. *Nat Med* **9,** 220–224.

Toda T, Saito N, Ikarashi N, Ito K, Yamamoto M, Ishige a, Watanabe K & Sugiyama K (2009). Intestinal flora induces the expression of Cyp3a in the mouse liver. *Xenobiotica* **39,** 323–334.

Toyohara T, Akiyama Y, Suzuki T, Takeuchi Y, Mishima E, Tanemoto M, Momose A, Toki N, Sato H, Nakayama M, Hozawa A, Tsuji I, Ito S, Soga T & Abe T (2010). Metabolomic profiling of uremic solutes in CKD patients. *Hypertens Res* **33,** 944–952.

Triba MN, Le Moyec L, Amathieu R, Goossens C, Bouchemal N, Nahon P, Rutledge DN & Savarin P (2015). PLS/OPLS models in metabolomics: the impact of permutation of dataset rows on the K-fold cross-validation quality parameters. *Mol BioSyst* **11,** 13–19.

Turnbaugh PJ, Bäckhed F, Fulton L & Gordon JI (2008). Diet-induced obesity is linked to marked but reversible alterations in the mouse distal gut microbiome. *Cell Host Microbe* **3,** 213–223.

Turnbaugh PJ, Ley RE, Hamady M, Fraser-Liggett CM, Knight R & Gordon JI (2007). The Human Microbiome Project. *Nature* **449,** 804–810.

Ursell LK, Clemente JC, Rideout JR, Gevers D, Caporaso JG & Knight R (2012). The interpersonal and intrapersonal diversity of human-associated microbiota in key body sites. *J Allergy Clin Immunol* **129,** 1204–1208.

Ursell LK, Haiser HJ, Van Treuren W, Garg N, Reddivari L, Vanamala J, Dorrestein PC, Turnbaugh PJ & Knight R (2014). The intestinal metabolome: An intersection between microbiota and host. *Gastroenterology* **146,** 1470–1476.

Vanholder R et al. (2003). Review on uremic toxins: classification, concentration, and interindividual variability. *Kidney Int* **63,** 1934–1943.

Vanholder R & Glorieux G (2015). The intestine and the kidneys: a bad marriage can be

hazardous. *Clin Kidney J* **8,** 168–179.

Vanholder R, Schepers E, Pletinck A, Nagler E V & Glorieux G (2014). The Uremic Toxicity of Indoxyl Sulfate and p-Cresyl Sulfate: A Systematic Review. *J Am Soc Nephrol* **25,** 1897–1907.

Vanholder R & De Smet R (1999). Pathophysiologic effects of uremic retention solutes. *J Am Soc Nephrol* **10,** 1815–1823.

Vaziri ND (2016). Effect of synbiotic therapy on gut-derived uremic toxins and the intestinal microbiome in patients with CKD. *Clin J Am Soc Nephrol* **11,** 199–201.

Vaziri ND, Wong J, Pahl M, Piceno YM, Yuan J, DeSantis TZ, Ni Z, Nguyen T-H & Andersen GL (2012). Chronic kidney disease alters intestinal microbial flora. *Kidney Int* **83,** 308–315.

Vaziri ND, Yuan J & Norris K (2013). Role of urea in intestinal barrier dysfunction and disruption of epithelial tight junction in chronic kidney disease. *Am J Nephrol* **37,** 1–6.

Vear SI, Ayers GD, Van Driest SL, Sidonio RF, Stein CM & Ho RH (2014). The impact of age and CYP2C9 and VKORC1 variants on stable warfarin dose in the paediatric population. *Br J Haematol* **165,** 832–835.

Velenosi TJ (2015). *Regulation of Hepatic Drug Metabolizing Enzymes in Chronic Kidney Disease* (thesis). UWO.

Velenosi TJ, Feere D a., Sohi G, Hardy DB & Urquhart BL (2014). Decreased nuclear receptor activity and epigenetic modulation associates with down-regulation of hepatic drug-metabolizing enzymes in chronic kidney disease. *FASEB J* **28,** 5388–5397.

Velenosi TJ, Fu AYN, Luo S, Wang H & Urquhart BL (2012). Down-regulation of hepatic CYP3A and CYP2C mediated metabolism in rats with moderate chronic kidney disease. *Drug Metab Dispos* **40,** 1508–1514.

Velenosi TJ, Hennop A, Feere DA, Tieu A, Kucey AS, Kyriacou P, McCuaig LE, Nevison SE, Kerr MA & Urquhart BL (2016). Untargeted plasma and tissue metabolomics in rats with chronic kidney disease given AST-120. *Sci Rep* **6,** 22526.

Velenosi TJ & Urquhart BL (2014). Pharmacokinetic considerations in chronic kidney disease and patients requiring dialysis. 1131–1143.

Vitetta L & Gobe G (2013). Uremia and chronic kidney disease: the role of the gut microflora and therapies with pro- and prebiotics. *Mol Nutr Food Res* **57,** 824–832.

Volpe D a., Tobin G a., Tavakkoli F, Dowling TC, Light PD & Parker RJ (2014). Effect of uremic serum and uremic toxins on drug metabolism in human microsomes. *Regul Toxicol Pharmacol* **68,** 297–303.

Vrieze A et al. (2012). Transfer of intestinal microbiota from lean donors increases insulin sensitivity in individuals with metabolic syndrome. *Gastroenterology* **143,** 913–916.e7.

Wang Z, Schuetz EG, Xu Y & Thummel KE (2013). Interplay between vitamin D and the drug metabolizing enzyme CYP3A4. *J Steroid Biochem Mol Biol* **136,** 54–58.

Wei Z, Jiang S, Zhang Y, Wang X, Peng X, Meng C, Liu Y, Wang H, Guo L, Qin S, He L, Shao F, Zhang L & Xing Q (2014). The Effect of microRNAs in the Regulation of Human CYP3A4: a Systematic Study using a Mathematical Model. *Sci Rep* **4,** 1–7.

Wienkers LC & Heath TG (2005). Predicting in vivo drug interactions from in vitro drug discovery data. *Nat Rev Drug Discov* **4,** 825–833.

Wiklund S (2008). Multivariate Data Analysis for Omics. 228.

Wikoff WR, Anfora AT, Liu J, Schultz PG, Lesley S a, Peters EC & Siuzdak G (2009). Metabolomics analysis reveals large effects of gut microflora on mammalian blood metabolites. *Proc Natl Acad Sci U S A* **106,** 3698–3703.

Wikoff WR, Nagle MA, Kouznetsova VL, Tsigelny IF & Nigam SK (2011). Untargeted metabolomics identifies enterobiome metabolites and putative uremic toxins as substrates of organic anion transporter 1 (Oat1). *J Proteome Res* **10,** 2842–2851.

Williams JA, Hyland R, Jones BC, Smith DA, Hurst S, Goosen TC, Peterkin V, Koup JR & Ball SE (2004). Drug-Drug Interactions for UDP-Glucoronosyl Transferase Substates: A Pharmacokinetic Explanation for Typically Observed Low Exposure (AUCi/AUC) Ratios. *Drug Metab Dispos* **32,** 1201–1208.

Wishart DS et al. (2013). HMDB 3.0-The Human Metabolome Database in 2013. *Nucleic Acids Res* **41,** 801–807.

Wong J, Piceno YM, DeSantis TZ, Pahl M, Andersen GL & Vaziri ND (2014). Expansion of urease- and uricase-containing, indole- and p-cresol-forming and

contraction of short-chain fatty acid-producing intestinal microbiota in ESRD. *Am J Nephrol* **39,** 230–237.

Wouters OJ, Donoghue DJO, Ritchie J, Kanavos PG, Narva AS & Diseases K (2016). Early chronic kidney disease: diagnosis, management and models of care. *Nat Rev Nephrol* **11,** 491–502.

Wright MC, Edwards RJ, Pimenta M, Ribeiro V, Ratra GS, Lechner MC & Paine AJ (1997). Developmental changes in the constitutive and inducible expression of cytochrome P450 3A2. *Biochem Pharmacol* **54,** 841–846.

Wyss M & Kaddurah-Daouk R (2000). Creatine and Creatinine Metabolism. *Physiol Rev* **80,** 1107–1213.

Xu C, Li CY-T & Kong A-NT (2005). Induction of phase I, II and III drug metabolism/transport by xenobiotics. *Arch Pharm Res* **28,** 249–268.

Xu J, Mahowald MA, Ley RE, Lozupone CA, Hamady M, Martens EC, Henrissat B, Coutinho PM, Minx P, Latreille P, Cordum H, Van Brunt A, Kim K, Fulton RS, Fulton LA, Clifton SW, Wilson RK, Knight RD & Gordon JI (2007). Evolution of Symbiotic Bacteria in the Distal Human Intestine. *PLoS Biol* **5,** 1574–1586.

Yamamoto S, Kazama JJ, Wakamatsu T, Takahashi Y, Kaneko Y, Goto S & Narita I (2016). Removal of uremic toxins by renal replacement therapies: a review of current progress and future perspectives. *Ren Replace Ther* **2,** 43.

Yang X, Zhang B, Molony C, Chudin E, Hao K, Zhu J, Gaedigk A, Suver C, Zhong H, Leeder JS, Guengerich FP, Strom SC, Schuet E, Rushmore TH, Ulrich RG, Slatter JG, Schadt EE, Kasarskis A & Lum PY (2010). Systematic genetic and genomic analysis of cytochrome P450 enzyme activities in human liver. *Genome res* **20,** 1020–1036.

Yeung CK, Shen DD, Thummel KE & Himmelfarb J (2014). Effects of chronic kidney disease and uremia on hepatic drug metabolism and transport. *Kidney Int* **85,** 522–528.

Yilmaz P, Parfrey LW, Yarza P, Gerken J, Pruesse E, Quast C, Schweer T, Peplies J, Ludwig W & Glöckner FO (2014). The SILVA and "all-species Living Tree Project (LTP)" taxonomic frameworks. *Nucleic Acids Res* **42,** 643–648.

Yip LY, Chun E & Chan Y (2015). Special Section on Drug Metabolism and the

Microbiome — Minireview Investigation of Host – Gut Microbiota Modulation of Therapeutic Outcome. 1619–1631.

Yoshida K, Sun B, Zhang L, Zhao P, Abernethy D, Nolin T, Rostami-Hodjegan A, Zineh I & Huang S-M (2016). Systematic and quantitative assessment of the effect of chronic kidney disease on CYP2D6 and CYP3A4/5. *Clin Pharmacol Ther* **100,** 75–87.

Yoshinari K, Takagi S, Yoshimasa T, Sugatani J & Miwa M (2006). Hepatic CYP3A expression is attenuated in obese mice fed a high-fat diet. *Pharm Res* **23,** 1188–1200.

Youssef N, Sheik CS, Krumholz LR, Najar FZ, Roe BA & Elshahed MS (2009). Comparison of species richness estimates obtained using nearly complete fragments and simulated pyrosequencing-generated fragments in 16S rRNA gene-based environmental surveys. *Appl Environ Microbiol* **75,** 5227–5236.

Yun KU, Oh SJ, Oh JM, Kang KW, Myung C-S, Song GY, Kim B-H & Kim SK (2010). Age-related changes in hepatic expression and activity of cytochrome P450 in male rats. *Arch Toxicol* **84,** 939–946.

Zanger UM & Schwab M (2013). Cytochrome P450 enzymes in drug metabolism: Regulation of gene expression, enzyme activities, and impact of genetic variation. *Pharmacol Ther* **138,** 103–141.

Zareie M, De Vriese AS, Hekking LHP, ter Wee PM, Schalkwijk CG, Driesprong BAJ, Schadee-Eestermans IL, Beelen RHJ, Lameire N & van den Born J (2005). Immunopathological changes in a uraemic rat model for peritoneal dialysis. *Nephrol Dial Transplant* **20,** 1350–1361.

Zhang LS & Davies SS (2016). Microbial metabolism of dietary components to bioactive metabolites: opportunities for new therapeutic interventions. *Genome Med* **8,** 46.

Zhao Y-Y (2013). Metabolomics in chronic kidney disease. *Clin Chim Acta* **422,** 59–69.

Zhao YY, Cheng XL, Wei F, Bai X, Tan XJ, Lin RC & Mei Q (2013*a*). Intrarenal metabolomic investigation of chronic kidney disease and its TGF-β1 mechanism in induced-adenine rats using UPLC Q-TOF/HSMS/MS E. *J Proteome Res* **12,** 692–703.

Zhao YY, Lei P, Chen DQ, Feng YL & Bai X (2013*b*). Renal metabolic profiling of early

renal injury and renoprotective effects of Poria cocos epidermis using UPLC Q-TOF/HSMS/MSE. *J Pharm Biomed Anal* **81–82,** 202–209.

Zhou C, Tabb MM, Nelson EL, Grün F, Verma S, Sadatrafiei A, Lin M, Mallick S, Forman BM, Thummel KE & Blumberg B (2006). Mutual repression between steroid and xenobiotic receptor and NF-kappaB signaling pathways links xenobiotic metabolism and inflammation. *J Clin Invest* **116,** 2280–2289.

Zhou XJ, Rakheja D, Yu X, Saxena R, Vaziri ND & Silva FG (2008). The aging kidney. *Kidney Int* **74,** 710–720.

Appendices

Appendix A: Ethics Approval

Western

September 10, 2009

This is the Original Approval for this protocol
A Full Protocol submission will be required in 2013

Dear Dr. Urquhart:

Your Animal Use Protocol form entitled:
The Effect of Kidney Failure and Kidney Transplantation on the Expression and Activity of Drug Metabolizing Enzymes and Drug Transport Proteins
Funding Agency UWO Startup/NSERC Applied For

has been approved by the University Council on Animal Care. This approval is valid from **September 10, 2009 to September 30, 2010.** The protocol number for this project is **#2009-058.**.

1. This number must be indicated when ordering animals for this project.
2. Animals for other projects may not be ordered under this number.
3. If no number appears please contact this office when grant approval is received.
   If the application for funding is not successful and you wish to proceed with the project, request that an internal scientific peer review be performed by the Animal Use Subcommittee office.
4. Purchases of animals other than through this system must be cleared through the ACVS office. Health certificates will be required.

ANIMALS APPROVED FOR 4 Years

SPECIES & SECT D.5.1 GROUP ID#	STRAIN &/or OTHER SPECIES DETAIL For Rodents, Also Provide Vendor Stock #	AGE or WEIGHT & SEX	4-YEAR TOTAL ANIMAL NUMBER
Rat ID# 1-36	Sprague-Dawley	200-300g, male	780
As Above ID# 37	Wistar	200-300g, male	120

REQUIREMENTS/COMMENTS
Please ensure that individual(s) performing procedures on live animals, as described in this protocol, are familiar with the contents of this document.

c.c. Approved Protocol - B. Urquhart, W. Lagerwerf
Approval Letter - B. Urquhart, W. Lagerwerf

***The* University *of* Western Ontario**
Animal Use Subcommittee / University Council on Animal Care
Health Sciences Centre, ● London, Ontario ● CANADA – N6A 5C1
PH: 519-661-2111 ext. 86770 ● FL 519-661-2028 ● www.uwo.ca / animal

Appendix B: Supplementary Information

Supplementary Table 1. Table of barcoded primers used for Illumina sequencing. Refer to excel file (.xlsx) titled "Barcoded Primers for Illumina Sequencing".

Supplementary Table 2. Table of 1199 operational taxonomic units identified from Illumina sequencing. Refer to excel file (.xlsx) titled "Final OTU Table from Illumina Sequencing".

Supplementary Table 3. Table of 204 *m/z* ratios found by untargeted mass spectrometry from CKD and control rat plasma and liver samples and RPLC or HILIC chromatography. Refer to excel file (.xlsx) titled "Final Metabolite Table from UPLC-MS". Metabolites satisfying univariate analysis and Spearman correlation to same-sample CYP3A2 or CYP2C11 mRNA, protein or enzyme activity data. Spearman correlation coefficients (r value) are listed. 2-way independent ANOVA was conducted via MetaboAnalyst v3.0 using FDR<0.05 to correct for multiple comparisons and satisfaction required $p<0.05$ across both *Time* and *Disease*. Multivariate analysis required VIP > 0.8 and 0.4 < p(corr)[1] < -0.4 indicating adequate separation by OPLA-DA and S-plot. Mass error was obtained using the 4th decimal place *m/z* from the Human Metabolome Database (HMDB). Italicized suspected metabolites refer to a group of plausible metabolites of similar structure. For definitions of identification levels refer to section 2.6.4.

Curriculum Vitae

Emily Dee Hartjes

Post-secondary Education and Degrees:	BSc. Honours in Biochemistry and Molecular Biology; Specialization in Medical Sciences Trent University, Peterborough, ON, Canada 2011-2015 MSc. in Physiology & Pharmacology University of Western Ontario, London, ON, Canada 2015-2017
Honours and Awards:	2015 - Ontario Graduate Student Award 2016 - Canadian Institutes of Health Research 2016 – Physiology & Pharmacology Research Day Poster Award Winner Western Graduate Program Funding 2015-2017
Related Work Experience	Teaching Assistant The University of Western Ontario, London, ON Department of Physiology & Pharmacology 2015 *Physiology 3140A - Cell Physiology* 2016 *Physiology 3140A - Cell Physiology*

Manuscript:

Lacerda, A. F., **Hartjes, E**., & Brunetti, C. R. (2014). LITAF mutations associated with Charcot-Marie-tooth disease 1C show mislocalization from the late endosome/lysosome to the mitochondria. *PloS one*, *9*(7), e103454.

Gill, N., Sirizzotti, N., Johnson, D., Joubert, G., Kucey, A. S., Tieu, A., Urquhart, B. L., Columbus, M., Lim, R., Rieder, M., Mehrotra, S., **Hartjes, E.** & Poonai, N. (2017). Endogenous Glucocorticoid Response to Single-Dose Dexamethasone for Croup in Children: A Pharmacodynamic Study. *Pediatric Emergency Care*.

Presentations:

Emily Hartjes. Characterization of the gut microbiota and drug metabolism in chronic kidney disease. St. Joseph's Hospital, London, Ontario, Canada, February 3, 2016. ("Talks on Fridays" Presentation)

Emily D. Hartjes, Thomas Velenosi, Andrew S. Kucey, Kait Al, Gregory B. Gloor, Jeremy P. Burton, Gregor Reid, Brad Urquhart. Characterization of chronic kidney disease progression on gut microbiota, metabolomics and drug metabolism. London Health Research Day, London, Ontario, Canada, March 29, 2016. (Poster)

Emily D. Hartjes, Thomas Velenosi, Andrew S. Kucey, Kait Al, Gregory B. Gloor, Jeremy P. Burton, Gregor Reid, Brad Urquhart. Characterization of the Gut Microbiota, Metabolomics and Drug Metabolism over Chronic Kidney Disease Progression. Canadian Society of Pharmacology and Therapeutics in Vancouver, British Columbia, Canada, September 19–21, 2016. (Poster)

Emily Hartjes. Characterization of the Gut Microbiota, Metabolomics and Drug Metabolism over Chronic Kidney Disease Progression. Canadian Society of Pharmacology and Therapeutics Joint Meeting Trainee Oral Presentation, London, Ontario, Canada, Sept 20th 2016. (Oral Presentation)

Emily Hartjes. Characterization of the Gut Microbiota, Metabolomics and Drug Metabolism over Chronic Kidney Disease Progression. Pre-ASN Meeting, London, Ontario, Canada, Nov 10th 2016. (Oral Presentation)

Emily D. Hartjes, Thomas Velenosi, Andrew S. Kucey, Kait Al, Gregory B. Gloor, Jeremy P. Burton, Gregor Reid, Brad Urquhart. The Gut Microbiota and Drug Metabolism over Chronic Kidney Disease Progression. American Society of Nephrology in Chicago, Illinois, USA, November 16-20, 2016. (Poster)

James (Yong) Lim, **Emily Hartjes**, Brad Urquhart. Metabolomics for the Prediction and Early Diagnosis of Cisplatin Induced Acute Kidney Injury. Canadian Society of Pharmacology and Therapeutics in Vancouver, Nova Scotia,
Canada, June 14–16, 2017. (Poster)

Cheng Fang, James Nugent, **Emily Hartjes**, Thomas Velenosi, Dylan Burger, Brad Urquhart. Expression of Hepatic Cytochrome P450 Enzymes in mouse models of Diabetic Nephropathy. London Health Research Day, London, Ontario, Canada, March 28, 2017. (Poster)

James (Yong) Lim, **Emily Hartjes**, Brad Urquhart. Characterization of the Metabolome and Renal Tubular Cisplatin Disposition in Cisplatin Induced Acute Kidney Injury. American Society of Nephrology, New Orleans, Louisiana, USA, November 2-5, 2017. (Upcoming Poster)

Nicholas Tonial, **Emily Hartjes**, Jean-Francois Thibodeau, Chet Holterman, Eldjonai Kamto, Lyne Gagnon, Brad L. Urquhart. Effect of chronic kidney disease on expression of Cyp3a11, Cyp2c37, Cyp2d22 and Oatp1b2 in C57BL/6 mice. American Society of Nephrology, New Orleans, Louisiana, USA, November 2-5, 2017. (Upcoming Poster)